PROTON SPIN-LATTICE RELAXATION IN SOLID HYDROCARBONS

A Thesis

presented by

James L. Page, B.Sc.

to the

University of St. Andrews

in application for the Degree

of Doctor of Philosophy

DECLARATION

I hereby certify that this thesis has been composed by me, and is a record of work done by me, and has not previously been presented for a Higher Degree.

The research was carried out in the Physical Laboratory of St. Salvator's College, in the University of St. Andrews, under the supervision of Dr. F. A. Rushworth.

(James L. Page)

CERTIFICATE

I certify that James L. Page, B.Sc., has spent nine terms at research work in the Physical Laboratory of St. Salvator's College, University of St. Andrews, under my direction, that he has fulfilled the conditions of Ordinance No. 16 (St. Andrews) and that he is qualified to submit the accompanying thesis in application for the Degree of Doctor of Philosophy.

_____

Research Supervisor

CAREER

I first matriculated in the University of St. Andrews in October 1960. I studied Mathematics and Natural Philosophy, and obtained First Class Honours in Natural Philosophy in 1964.

In October 1964, following the award of an S.R.C. Research Studentship, I was enrolled as a research student under Ordinance 12, and was transferred to Ordinance 16 in October 1965 as a candidate for the degree of Ph.D.

ACKNOWLEDGEMENTS

The author wishes to express his sincere thanks to Dr. F. A. Rushworth for his supervision during this project and to Professor J. F. Allen, F.R.S. for providing the excellent facilities and funds. He is also indebted to Dr. D. P. Tunstall for his stimulating discussions, and to Mr. J. McNab for his help and co-operation in technical matters.

CONTENTS

SECTION PAGE

+++++

1. INTRODUCTION

1. INTRODUCTION

Nuclear Magnetic Resonance (n.m.r.) was first discovered by Bloch, Hansen and Packard[1], and by Purcell, Torrey and Pound[2], in 1946, and was originally used as a means of determining basic nuclear properties such as spin and magnetic moment. It has since developed as a technique whereby the magnetic nuclei can be used as a probe of the matter in which they reside. In liquid the information obtained by the n.m.r. method gives details about molecular structure, molecular association and the distribution of electrons in molecules, while in solids, although the technique has been used as a means of measuring internuclear distances and angles, its principal uses have been in the study of molecular motion, spin thermodynamics and as a probe of electron-nuclear interactions in metals.

This thesis is concerned with the investigation by n.m.r. of molecular motions in solids, and in particular with the information gained from the measurement of n.m.r. relaxation time as a function of temperature. It is known that such measurements can yield information on the rate and type of motion as well as on the magnitude of the energy barrier which hinders molecular reorientation. The standard theory applied to these investigations has been extended for the particular type of motion assumed to occur in the substances studied, namely ethylene and the chlorinated ethylenes, and a

reasonable agreement found with the experimental data from these substances. Because quantum mechanical reorientation or tunnelling has previously been assumed to have an important effect on n.m.r. relaxation in small molecules, this topic is reviewed in detail and conclusions reached which are in agreement with experimental work.

The inherent inaccuracies of relaxation time measurement by the equipment previously existing in this laboratory has been avoided by the construction and use of a pulsed n.m.r. apparatus.

2. REVIEW OF BASIC THEORY

2. REVIEW OF BASIC THEORY

2.1 Introduction

The fundamental process in nuclear magnetic resonance (n.m.r.) absorption is the application of a radiofrequency field which induces transitions between quantised nuclear energy levels.

A nucleus with spin $\underline{I}$ has a magnetic moment $\underline{\mu}$ given by

$$\underline{\mu} = \gamma\hbar\underline{I}$$

where γ is the magnetogyric ratio of the type of nucleus under consideration.

On applying a static magnetic field H_o to the nucleus the nuclear magnetic moment becomes spatially quantised forming $(2I + 1)$ possible energy levels, with energies E given by

$$E = - m\gamma\hbar H_o$$

where m is the magnetic quantum number which can have values I, I-1, I-2 ..., -I.

Magnetic transitions between these discreet levels are subject to the rule that $\Delta m = \pm 1$. It then follows that transitions between levels can be induced by providing a quantum of energy

$$h\nu_o = \mu H_o/I \ .$$

In addition the circularly polarised radiation of frequency ν_o must be applied with its magnetic vector rotating in a plane perpendicular to H_o.

For protons ($I = \frac{1}{2}$) there are two energy levels separated by $2\mu H_o$, hence,

$$h\nu = 2\mu H_o \quad . \qquad 2.1$$

The permanent magnet used in the experiments had a field of 5260 gauss and the corresponding frequency to stimulate transitions was therefore 22.6 MHz.

In the presence of the radiofrequency stimulating field the probability of a transition upwards is equal to the probability of a transition downwards by stimulated emission[3]. Hence if the populations of the energy levels were equal there would be no net effect. However at thermal equilibrium it is assumed that the populations of the levels have a Boltzmann distribution. Thus in the lower energy level there is an excess population which results in a net absorption of energy in the presence of a radiofrequency field which satisfies the conditions discussed previously.

It is possible for the spins which have been heated by the r.f. field to be cooled by giving energy to the lattice of the system. This process has a characteristic time T_1 which depends on the strength of the coupling between the spins and the lattice.

The general theory of n.m.r. has been treated in several books and review articles, notably by Andrew[4], Pake[5], Abragam[6] and Slichter[7]. Hence, in this thesis, only a bare outline of the theory will be given

but with emphasis on spin-lattice relaxation.

The n.m.r. experiments were performed on polycrystalline samples in which protons were effectively the only magnetic nuclei present.

2.2 Hamiltonian of the system

The Hamiltonian of a system of spins, each having total spin angular momentum, $\hbar\underline{I}$ in a large external magnetic field $\underline{H}_o$ whose direction is normally chosen to fix the Z axis, has two parts.

a) The interaction of each spin with the external field leading to the Zeeman Hamiltonian $\mathcal{H}_Z$, given by

$$\mathcal{H}_Z = - \gamma\hbar H_o \sum_{i=1}^{N} I_Z^{\,i} \qquad 2.2$$

where i extends over all the N spins, γ is the gyromagnetic ratio and $\omega_o = \gamma H_o$ is the Larmor frequency of the spins in field H_o.

b) The interaction between spins themselves, giving the dipolar interaction. For a system of spins of a single species, i.e. having the same gyromagnetic ratio and the same angular momentum $\hbar\underline{I}$, the dipolar Hamiltonian $\mathcal{H}_1$ is given by,

$$\mathcal{H}_1 = \gamma^2\hbar^2 \sum_{i<j} [\underline{I}^i.\underline{I}^j\, r_{ij}^{-3} - 3\,(\underline{I}^i.\underline{r}_{ij})(\underline{I}^j.\underline{r}_{ij})\, r_{ij}^{-5}] \qquad 2.3$$

where r_{ij} is the distance between the i^{th} and j^{th} spins. Equation 2.3 can be rewritten in polar coordinates as

$$\mathcal{H}_1 = \gamma^2\hbar^2 \sum_{i<j} r_{ij}^{-3} [A_{ij} + B_{ij} + C_{ij} + D_{ij} + E_{ij} + F_{ij}] \qquad 2.4$$

where

$$A_{ij} = I_Z^{\,i}\, I_Z^{\,j}\,(1 - 3\cos^2\theta_{ij})$$

$$B_{ij} = -\frac{1}{4}\,(I_+^{\,i}\, I_-^{\,j} - I_-^{\,i}\, I_+^{\,j})(1 - 3\cos^2\theta_{ij})$$

$$C_{ij} = -\frac{3}{2}\,(I_+^{\,i}\, I_Z^{\,j} + I_Z^{\,i}\, I_+^{\,j})\,\sin\theta_{ij}\cos\theta_{ij}\exp(-i\Phi_{ij}) \qquad 2.5$$

$$D_{ij} = -\frac{3}{2}\,(I_-^{\,i}\, I_Z^{\,j} + I_Z^{\,i}\, I_-^{\,j})\,\sin\theta_{ij}\cos\theta_{ij}\exp(+i\Phi_{ij})$$

$$= C_{ij}^{*}$$

$$E_{ij} = -\frac{3}{4}\, I_+^{\,i}\, I_+^{\,j}\sin^2\theta_{ij}\exp(-2i\Phi_{ij})$$

$$F_{ij} = -\frac{3}{4}\, I_-^{\,i}\, I_-^{\,j}\sin^2\theta_{ij}\exp(+2i\Phi_{ij})$$

$$= E_{ij}^{*}$$

where $$I_{\pm} = I_X \pm I_Y$$

θ_{ij} is the angle between $\underline{r}_{ij}$, $\underline{H}_o$ (again taken as the Z axis), Φ_{ij} is the azimuthal angle of r_{ij}, and * signifies a complex conjugate.

A detailed discussion of the effects of these terms may be found in the books by Abragam[6] and Slichter[7].

In the case where the Zeeman Hamiltonian $\mathcal{H}_Z$ is the dominant part of the complete Hamiltonian of the system, it is found convenient to separate the dipolar Hamiltonian into two parts

$$\mathcal{H}_1 = \mathcal{H}_1^{\circ} + \mathcal{H}_1' \qquad 2.6$$

where $\mathcal{H}_1^{\circ}$ commutes with the Zeeman Hamiltonian and is thus formed from terms A_{ij} and B_{ij}. $\mathcal{H}_1'$ does not commute with the Zeeman Hamiltonian and is composed of terms C_{ij}, D_{ij}, E_{ij}, F_{ij}.

2.3 Bloch Equations

The behaviour of an idealised many spin system in a magnetic field H_o, along the Z axis, is given by the Bloch[8] phenomenological equations.

It can be proved classically or quantum mechanically[6,7] that the equation of motion of the nuclear magnetization $\underline{M}$ is given by

$$\frac{d\underline{M}}{dt} = \gamma \underline{M} \times \underline{H}_o \,. \qquad 2.7$$

Bloch modified this expression by including damping terms of the form,

$$\frac{dM_Z}{dt} = \frac{M_o - M_Z}{T_1}$$

$$\frac{dM_X}{dt} = -\frac{M_X}{T_2} \qquad 2.8$$

$$\frac{dM_Y}{dt} = -\frac{M_Y}{T_2}$$

where M_o is the thermal equilibrium magnitude of $\underline{M}$, T_1 is the spin-lattice relaxation time and T_2 is the spin-spin relaxation time.

Bloch further assumed that equations 2.7 and 2.8 could be added to give

$$\frac{d\underline{M}}{dt} = \gamma \underline{M} \times \underline{H}_o + \frac{M_o - M_Z}{T_1}\underline{k} + \frac{M_X\underline{i} + M_Y\underline{j}}{T_2} \qquad 2.9$$

These equations are not strictly accurate for solids[9], the deviations being especially pronounced at high r.f. power levels.

2.4 Absorption Spectra

In this thesis some mention will be made of quantities relating to n.m.r. absorption spectra of solids. Hence definitions of these quantities will be given in this section.

The spectra referred to in this thesis were obtained using conventional continuous wave techniques[4] at fixed frequency while sweeping the external magnetic field.

2.4.1 Line Width

In a system of interacting protons i.e. spin 1/2 in an external field H_o the n.m.r. absorption line has a finite width caused by the dipolar interactions discussed in section 2.2. The resonance equation 2.1 can therefore be written as

$$h\nu = 2\mu (H_o + H_{local}) \qquad 2.10$$

where H_{local} is the field, caused by neighbouring nuclei, at the spin under consideration.

The line width of the absorption curve can be defined in terms

of the half width at half intensity, or the width between points of maximum and minimum slope. The latter definition is the more useful when finding line width experimentally, by recording the derivative of the line shape. This is the definition used in this thesis.

The inverse of the spin-spin relaxation time T_2 is found to be proportional to the absorption line width[6].

In the case where H_o is large compared to H_{local} the dipolar interaction can be treated as a perturbation on the Zeeman Hamiltonian. It is then possible in simple models to find the perturbed energy eigenvalues and hence the line shape of the absorption. This has been done for a two spin system[10] and particular arrangements of three spin systems[11,12] and four spin systems[13,14].

When the spatial distribution of the spin system is complex, the method of moments, introduced by Van Vleck[15], must be used to relate the absorption line to the given distribution.

2.4.2 Moments of an Absorption Line

If the absorption line is described by a normalized shape function $f(\omega)$ with its maximum at ω_o, then the n^{th} moment M_n is defined as

$$M_n = \int_o^\infty (\omega - \omega_o)^n f(\omega)\, d\omega \ .$$

If $f(\omega)$ is symmetrical with respect to ω_o the odd moments vanish.

In the theoretical calculations of second moment the method of

diagonal sums is used and it is found that the second moment is given by

$$M_2 = - \frac{\mathrm{Tr}\left[\mathcal{H}_1', I_X \right]^2}{\mathrm{Tr}\left[I_X^2 \right]} . \qquad 2.11$$

Only the secular part of the dipolar Hamiltonian is used as the non-secular terms give rise to satellite lines which are normally too weak to observe.

For a single crystal Van Vleck's formula gives

$$M_2 = \frac{3}{4} I(I + 1) \gamma^2 \hbar^2 N^{-1} \sum_{j,k} (3 \cos^2 \theta_{jk} - 1)^2 r_{jk}^{-6} \qquad 2.12$$

while for a polycrystalline sample

$$M_2 = \frac{3}{5} I(I + 1) \gamma^2 \hbar^2 N^{-1} \sum_{j,k} r_{jk}^{-6} \qquad 2.13$$

where N is the number of spins over which the sums are taken.

2.4.3 Effect of Molecular Motion on Line Width and M_2

Molecular motion in the solid under observation causes a reduction in the line width and experimentally measured second moment providing the frequency of the motion is greater than the rigid lattice line width expressed in frequency units[16].

Theoretically[17] the second moment is invariant to motion in the lattice but the observable part, which is proportional to $\mathrm{Tr}[\mathcal{H}_1', I_X]^2$ where $\mathcal{H}_1'$ is the time independent part of the perturbing Hamiltonian,

will be smaller than in the absence of motion.

In the presence of motion of the spins the angular factor of equation 2.12 must be replaced by an average which is dependent on the type of motion taking place. These averages have been found for various types of motion, including reorientation about a diad axis[18], reorientation about an axis of n-fold symmetry ($n \geq 3$)[16] and torsional oscillation[19,20].

3. SPIN-LATTICE RELAXATION THEORY

3. SPIN-LATTICE RELAXATION THEORY

3.1 Introduction

If a system of spins is placed in a steady magnetic field, H_o, in the Z direction, then an equilibrium magnetization M_o will be obtained. In thermal equilibrium M_o is given by Curie's Law

$$M_o = \frac{CH_o}{T_L} = \frac{CH_o}{T_S} \qquad 3.1$$

where C is the nuclear Curie constant, T_L is the lattice temperature and T_S is the spin temperature.

If this system is disturbed by applying a radio frequency field such that the spin temperature is changed, then the system will relax to equilibrium in the characteristic time T_1, the spin-lattice relaxation time. This relaxation takes place by energy exchange between the spin system and the lattice, the magnetization M_Z relaxing toward M_o following the equation

$$\frac{dM_Z}{dt} = \frac{M_o - M_Z}{T_1} . \qquad 3.2$$

This equation is one of Bloch equations.

The approach to equilibrium is usually exponential and the value of T_1 is related to the internal molecular motions in the system.

It should be noted that the concept of spin temperature can

only be applied after the spin system has gained internal thermal equilibrium. This takes a characteristic time[21], the spin-spin relaxation time T_2. The spin temperature assumption can therefore be used in solids where $T_2 << T_1$ but not in liquids where T_1 is usually of the order of T_2.

3.2 Derivation of T_1 in terms of Dipolar Interactions

3.2.1 Discussion of Method

The treatment used to derive an expression for T_1 as a function of the dipolar interactions follows the methods of Hebel and Slichter[22], and Look and Lowe[23].

Firstly a basic expression 3.17 called the Hebel-Slichter formula, will be derived by the concept of spin-temperature. This equation expresses T_1 in terms of the energies of the nuclear spin levels and the probabilities of transitions between these levels. This equation, although referred to as the Hebel-Slichter relation is a generalisation of a formula derived by Gorter[24].

It is then possible[22,23] to obtain an expression for the relaxation in the form of a diagonal sum. This technique of expressing T_1 as a trace eliminates the need for complicated wave-functions and allows the interactions between all the spins to be taken into account; that is within the approximations of first order perturbation theory the contributions to $1/T_1$ from interactions between different pairs of spins may be added.

Holcomb and Pedersen[25] also use the Hebel-Slichter relation in their calculations on T_1 in gypsum, $CaSO_4.2H_2O$. However they do not express the relaxation in the form of a diagonal sum. Their technique is to consider only the intramolecular effect, in their case, a four spin system, and find the complete set of wavefunctions for the system. Hence they are able to find the various matrix elements of the perturbation. Clearly it would be tedious to extend this type of calculation to a system of more than four spins.

3.2.2 Derivation of Hebel-Slichter T_1 formula

At thermal equilibrium the nuclear spin system has the same temperature T_L as the lattice. This implies that the energy levels of the nuclear spin system are populated according to Boltzmann statistics characterized by the lattice temperature. Thus

$$\frac{p_n^{\,o}}{p_m^{\,o}} = \exp \frac{E_m - E_n}{kT_L} = \exp\left[(E_m - E_n)\beta_L\right] \qquad 3.3$$

where $p_n^{\,o}$ and $p_m^{\,o}$ are the equilibrium occupation probabilities of the n^{th} and m^{th} levels, having energies E_n and E_m.

When the system is not in thermal equilibrium with the lattice we assume that it can be characterized by a spin temperature T_S which will not be equal to T_L. This assumption holds providing $T_2 << T_1$.

The specific heat of the lattice is taken as infinite, thus its temperature is unaffected by the temperature of the spin system. Then,

$$\frac{p_n}{p_m} = \exp \frac{E_m - E_n}{kT_S}$$
$$= \exp \left[(E_m - E_n)\beta_S\right] . \qquad 3.4$$

In the presence of a magnetic field H_o an alternative definition of T_S can be given by Curie's Law

$$T_S = \frac{CH_o}{M} . \qquad 3.5$$

If we compare the equations 3.5, 3.2 and 3.1, we find

$$\frac{d\beta_S}{dt} = \frac{\beta_L - \beta_S}{T_1} . \qquad 3.6$$

The time derivative of the total nuclear spin energy, $\bar{E}$, of the system may be written

$$\frac{d\bar{E}}{dt} = \frac{d}{dt} \sum_n p_n E_n = \sum_n \frac{dp_n}{dt} E_n = \frac{d\bar{E}}{d\beta_S} \frac{d\beta_S}{dt} . \qquad 3.7$$

We now introduce W_{mn} as the probability per second that the lattice induce a transition of the system from state m to n, if the system is in state m. It then follows that

$$\frac{dp_n}{dt} = \sum_m (p_m W_{mn} - p_n W_{nm}) . \qquad 3.8$$

Hence from 3.7,

$$\frac{d\bar{E}}{dt} = \sum_{m,n} (p_m W_{mn} - p_n W_{nm})\, E_n$$

$$= \tfrac{1}{2} \sum_{m,n} (p_m W_{mn} - p_n W_{nm})(E_n - E_m) \,. \qquad 3.9$$

To guarantee equilibrium when $\beta_S = \beta_L$ the principle of detailed balance requires that

$$\frac{W_{nm}}{W_{mn}} = \exp[(E_n - E_m)\,\beta_L]$$

$$\doteq 1 - (E_m - E_n)\,\beta_L \qquad 3.10$$

where the high temperature approximation has been used to expand the exponential.

The spin temperature assumption of equation 3.4, on expansion of the exponential, yields

$$\frac{p_n}{p_m} \doteq 1 - (E_n - E_m)\,\beta_S \,. \qquad 3.11$$

Also p_m is given by

$$p_m = \frac{\exp(-\beta_S E_m)}{\sum_n \exp(-\beta_S E_n)}$$

$$\doteq \frac{1 - \beta_S E_m + \frac{\beta_S^2 E_m^2}{2!} - \ldots}{\sum_n (1 - \beta_S E_m + \frac{\beta_S^2 E_n^2}{2!} - \ldots} \qquad 3.12$$

$$\doteq \frac{1}{\sum_n \delta_{nn}} \cdot$$

Substitution of 3.10, 3.11, 3.12 into 3.6 gives

$$\frac{d\bar{E}}{dt} = \tfrac{1}{2} \sum_{m,n} p_m W_{mn} (E_n - E_m)^2 (\beta_S - \beta_L)$$

$$= \frac{1}{2\Sigma\delta_{nn}} \sum_{m,n} W_{mn} (E_n - E_m)^2 (\beta_S - \beta_L) \cdot \qquad 3.13$$

Now

$$\frac{d\bar{E}}{d\beta_S} = \frac{d}{d\beta_S} \sum_n p_n (\beta_S) E_n$$

$$= \frac{1}{\Sigma\delta_{nn}} \sum_n E_n^2 \exp(-\beta_S E_n) \qquad 3.14$$

$$\doteq - \frac{\sum_n E_n^2}{\sum_n \delta_{nn}} \cdot$$

Using 3.7

$$\frac{d\bar{E}}{dt} = - \frac{d\beta_S}{dt} \frac{\sum_n E_n^2}{\Sigma\delta_{nn}} \cdot \qquad 3.15$$

Equating 3.15 to 3.13 and comparing the result with 3.6

$$\frac{d\beta_S}{dt} = \tfrac{1}{2}(\beta_L - \beta_S)\ \frac{\sum_{m,n} W_{mn}(E_m - E_n)^2}{\sum_n E_n^2} \qquad 3.16$$

where T_1 is given by

$$\frac{1}{T_1} = \tfrac{1}{2}\ \frac{\sum_{m,n} (E_m - E_n)^2}{\sum_n E_n^2} \qquad 3.17$$

This is the Hebel-Slichter relation for T_1.

It should be noted that equation 3.17 predicts a single exponential decay for T_1 whilst the rate equations 3.9 themselves imply multiple time constants. This in effect means that by postulating a spin temperature we have taken into account the effect of spin-spin coupling.

3.2.3 T_1 as a function of Dipolar Interactions

We now assume that the dipolar Hamiltonian of 2.4 is time dependent due to a time dependence of r_{ij}, Θ_{ij}, and Φ_{ij} caused by motions of the nuclei. Scalar spin-spin coupling and quadrupole relaxation mechanisms are not present in the samples to be studied. $\mathcal{H}_1(t)$ can therefore be written as

$$\mathcal{H}_1(t) = \sum_q \mathcal{H}_{1r}^q(t)\ \mathcal{H}_{1S}^q \qquad 3.18$$

where r and S refer respectively to the spatial and spin operators and the sum over q includes $q = A_{ij}, B_{ij}, C_{ij}, D_{ij}, E_{ij}$, and F_{ij}, all i and j.

If $\mathcal{H}_{1r}(t)$ is assumed to be a random function of time, W_{nm} can be obtained by first order perturbation theory[6,26]

$$W_{nm} = \frac{1}{\hbar^2} \int_{-\infty}^{\infty} \exp\left[-\frac{i}{\hbar}(E_m - E_n)\tau\right] x \overline{< n|\mathcal{H}_1(t+\tau)|m >< m|\mathcal{H}_1(t)|n >} \, d\tau \qquad 3.19$$

where the bar means the ensemble average of this product of matrix elements.

Inserting 3.18 into 3.19 gives

$$W_{nm} = \frac{1}{\hbar^2} \sum_{qq'} \int_{-\infty}^{\infty} \exp\left[-\frac{i}{\hbar}(E_m - E_n)\tau\right] G_{1r}^{qq'}(t,\tau)\, d\tau \; x \; < n|\mathcal{H}_{1S}^{q}|m >< m|\mathcal{H}_{1S}^{q'}|n > \qquad 3.20$$

where $G_{1r}^{qq'}(t,\tau)$ has the form of a correlation function[27]

$$G_{1r}^{qq'}(t,\tau) = \overline{< \mathcal{H}_{1r}^{q}(t+\tau)\, \mathcal{H}_{1r}^{q'}(t) >} \quad .$$

For stationary random functions, which are the ones considered here, $G_{1r}^{qq'}(t,\tau)$ is independent of t and is therefore a function only

of τ . Hence

$$G_{1r}^{qq'}(t,\tau) = G_{1r}^{qq'}(\tau) \ .$$

A further assumption is that the energy difference $E_n - E_m$ depends on $\mathcal{H}_{1S}^{q}$ and not on the states $|n>$ and $|m>$. This assumption holds if the Zeeman energy is much larger than the dipolar energy. If then

$$E_n - E_m = \hbar\omega^q$$

and we define a spectral density function $J_{1r}^{qq'}(\omega^q)$ by

$$J_{1r}^{qq'}(\omega^q) = \int_{-\infty}^{\infty} \exp(-i\omega^q\tau)\ G_{1r}^{qq'}(\tau)\ d\tau \qquad 3.21$$

equation 3.20 then reduces to

$$W_{nm} = \frac{1}{\hbar^2} \sum_{q,q'} J_{1r}^{qq'}(\omega^q) <n|\mathcal{H}_{1S}^{q}|m><m|\mathcal{H}_{1S}^{q'}|n> \ . \qquad 3.22$$

Inserting equation 3.22 into the Hebel and Slichter formula 3.17, and using $<n|\mathcal{H}_o|n> = E_n$, where $\mathcal{H}_o$ is the Zeeman Hamiltonian, gives

$$\frac{1}{T_1} = \left(\frac{1}{2\hbar^2}\right) \left[- \frac{\sum_{q,q'} J_{1r}^{qq'}(\omega^q)\ \mathrm{Tr}([\mathcal{H}_o, \mathcal{H}_{1S}^{q}][\mathcal{H}_o, \mathcal{H}_{1S}^{q'}])}{\mathrm{Tr}(\mathcal{H}_o^{\,2})} \right] 3.23$$

The traces may now be evaluated in a representation consisting

of the product of the individual spin functions of quantum numbers $m_1, m_2, \ldots\ldots\ldots m_N$ where m_i is the quantum number of the i^{th} spin, of a total of N spins, isolated in a static field[28,29].

This then leads to

$$\frac{1}{T_1} = \gamma^4 \hbar^2 \frac{3I(I+1)}{2N} \sum_{\substack{i \neq j \\ i' \neq j'}} \left(K^{(1)}_{iji'j'}(\omega_o) + K^{(2)}_{iji'j'}(2\omega_o) \right) \qquad 3.24$$

where $\omega_o = \gamma H_o$ and,

$$K^{(1)}_{iji'j'}(\omega) = \tfrac{1}{2} \int_{-\infty}^{\infty} \exp(-i\omega\tau) \left[\langle \overline{c^*_{ij}(0) c_{i'j'}(\tau)} \rangle + \text{complex conjugate} \right]$$

$$K^{(2)}_{iji'j'}(\omega) = \tfrac{1}{2} \int_{-\infty}^{\infty} \exp(-i\omega\tau) \left[\langle \overline{e^*_{ij}(0) e_{i'j'}(\tau)} \rangle + \text{complex conjugate} \right] \qquad 3.25$$

$$c_{ij} = r_{ij}^{-3} \sin\theta_{ij} \cos\theta_{ij} \exp(-i\dot{\Phi}_{ij})$$

$$e_{ij} = r_{ij}^{-3} \sin^2\theta_{ij} \exp(-i2\Phi_{ij}) \qquad 3.26$$

The physical significance of 3.24 is that only molecular motions of frequency ω_o and $2\omega_o$ will give a contribution to the n.m.r. spin-lattice relaxation time if this is measured using a r.f. frequency ω_o. $K^{(1)}_{iji'j'}(\omega_o)$ and $K^{(2)}_{iji'j'}(2\omega_o)$ are respectively the spectral intensities of the motion at frequencies ω_o and $2\omega_o$.

For convenience equation 3.24 is best written in the form

$$\frac{1}{T_1} = \gamma^4\hbar^2 \left[\frac{3I(I+1)}{2N}\right]\left\{ \sum_{i\neq j} \left[K^{(1)}_{ijij}(\omega_o) + K^{(2)}_{ijij}(2\omega_o)\right] + \sum_{\substack{i\neq j \\ i'\neq j'}}^{R} \left[K^{(1)}_{iji'j'}(\omega_o) + K^{(2)}_{iji'j'}(2\omega_o)\right]\right\} \qquad 3.27$$

where $\sum^{R}$ represents a restricted sum such that $i \neq i'$ and $j \neq j'$ at the same time i.e. there are no terms of the form given by the first summation, but terms such as $K_{iji'j'}$ are included.

The first type of term leads to averages of the type

$$\overline{< c^{*}_{12}(0) c_{12}(\tau) >}$$

which is an autocorrelation term, while the second type yields terms such as

$$\overline{< c^{*}_{12}(0) c_{34}(\tau) >} \quad \text{and} \quad \overline{< c^{*}_{12}(0) c_{23}(\tau) >}$$

which are cross correlation terms.

The expression 3.27 for $1/T_1$ could also have been derived using the density matrix notation[30,31].

3.2.4 Effect of the Cross Correlation Terms on T_1

If the relative motions of the spin pairs is uncorrelated then there can be no cross correlation terms expressed by the relations

$$\overline{\langle c^{*}_{ij}(0)c_{i'j'}(\tau)\rangle}^{R} = 0$$

where the R has the same significance as in the restricted sum of 3.27. If the relative motions of the spins is correlated then the cross correlation terms are not in general equal to zero.

Runnels[32] has investigated the T_1 of molecules having three identical spin-$\frac{1}{2}$ nuclei in equivalent positions at the corners of an equilateral triangle. He found that the relaxation is in general described by four decaying exponentials. He also showed that for a system initially describable by a spin-temperature the effect of cross correlation is to retard the relaxation.

Hilt and Hubbard[32] have calculated the T_1 of an ensemble of systems each consisting of three identical spin-$\frac{1}{2}$ nuclei at the corners of an equilateral triangle. The calculations are for hindered rotation of each system about an axis perpendicular to the plane of the triangle. They found that the inclusion of cross correlations of different dipole-dipole interactions in the calculations of T_1 resulted in a T_1 which differed significantly from a simple exponential decay.

4. SPIN-LATTICE RELAXATION PROCESSES

4. SPIN-LATTICE RELAXATION PROCESSES

4.1 Introduction

In the previous chapter a relationship (equation 3.27) was established between T_1 and the correlation functions of the dipolar interaction.

In order to estimate a theoretical value of T_1 the type of molecular motion taking place must be specified and the correlation functions computed for that particular motion.

Various types of molecular motions which could contribute to relaxation in the samples studied will be treated in this chapter. We are of course still concerned with the effect of motion on only the nuclear dipolar interaction. Protons ($I = \frac{1}{2}$) have zero quadrupole moments and thus there is no relaxation due to quadrupole effects.

4.2 Random Brownian Motion

In this model we assume that there are two protons, 1 and 2, separated by a fixed distance, b. This proton system undergoes random Brownian rotation (no preferred direction of the internuclear vector) which is characterized by correlation functions of the form

$$\overline{\langle c_{12}^{*}(t)c_{12}(t+\tau)\rangle} = \overline{\langle c_{12}^{*}(t)c_{12}(t)\rangle}\ \exp(-|\tau|/\tau_c)$$

$$\overline{\langle e_{12}^{*}(t)e_{12}(t+\tau)\rangle} = \overline{\langle e_{12}^{*}(t)e_{12}(t)\rangle}\ \exp(-|\tau|/\tau_c) \qquad 4.1$$

where τ_c the correlation time, is a characteristic time of the random motion[33]. τ_c can be considered as the time interval between jumps of the proton pair, and we assume that it is the same for both dipolar interaction terms considered.

The spectral intensities of equation 3.25 are then given by

$$K^{(1)}_{1212}(\omega_o) = \langle \overline{c^*_{12}(t)c_{12}(t)} \rangle \frac{2\tau_c}{1 + \omega_o^2 \tau_c^2}$$

$$K^{(2)}_{1212}(2\omega_o) = \langle \overline{e^*_{12}(t)e_{12}(t)} \rangle \frac{2\tau_c}{1 + 4\omega_o^2 \tau_c^2} \qquad 4.2$$

Using equations 3.26 for c_{12}, c^*_{12}, e_{12} and e^*_{12}, the values of

$$\langle \overline{c^*_{12}(t)c_{12}(t)} \rangle \text{ and } \langle \overline{e^*_{12}(t)e_{12}(t)} \rangle$$

are readily found by averaging the spatial coordinates over a sphere. It is found that

$$K^{(1)}_{1212}(\omega_o) = \frac{2}{15} \frac{1}{b^6} \frac{2\tau_c}{1 + \omega_o^2 \tau_c^2}$$

$$K^{(2)}_{1212}(2\omega_o) = \frac{8}{15} \frac{1}{b^6} \frac{2\tau_c}{1 + 4\omega_o^2 \tau_c^2} \qquad 4.3$$

Substitution of these equations into equation 3.27 gives

$$\frac{1}{T_1} = C_1 \left[\frac{\tau_c}{1 + \omega_o^2 \tau_c^2} + \frac{4\tau_c}{1 + 4\omega_o^2 \tau_c^2} \right] \qquad 4.4$$

where $$C_1 = \frac{3}{10} \frac{\gamma^4 \hbar^2}{b^6} \quad .$$

This equation was derived in this form by Kubo and Tomita[34], and Solomon[35] although it differs only by a factor 2 in the second term from the original formula derived by Bloembergen, Purcell and Pound[36]. Equation 4.4 will be referred to as the B.P.P. equation.

Two extremes of equation 4.4 may be considered. When the correlation time is short and $\omega_o \tau_c \ll 1$ which is normally the case in liquids, or solids with a high degree of internal motion, then equation 4.4 reduces to

$$\frac{1}{T_1} = 5\, C_1 \tau_c \qquad 4.5$$

and T_1 is independent of the resonance frequency.

When τ_c is long and $\omega_o \tau_c \gg 1$, equation 4.4 reduces to

$$\frac{1}{T_1} = \frac{2C_1}{\omega_o^2 \tau_c} \qquad 4.6$$

and T_1 is dependent on the square of the resonance frequency.

Equations 4.5 and 4.6 show that a plot of T_1 against τ_c will

have a minimum. The condition for this minimum can be found by differentiating equation 4.4 with respect to τ_c. $T_{1(min)}$ is thus found to occur when $\omega_o \tau_c \doteqdot 0.61$. It then follows that

$$\frac{1}{T_{1min}} = C_1 \frac{1.42}{\omega_o} \qquad 4.7$$

4.3 Reorientation between two equilibrium positions

4.3.1 Formulation of Spectral Intensities in terms of the Equilibrium Dipolar Interactions

In this section a theory will be developed for a system of proton pairs which can each reorientate randomly in time between two equilibrium positions denoted by α and β. It is not necessary in this model that the interproton vectors have the same magnitude in positions α and β. The assumption is also made that the time required for the spin to jump between sites is negligible compared to the time spent in the equilibrium sites. The distinction between this theory and the B.P.P. theory is that while both processes are random in time the B.P.P. theory is concerned with random orientation of the interproton vector.

Since the interproton vector has two possible orientations there will be two values of each of the components of the dipolar field c_{ij} and e_{ij} for spins i and j. For the present we will confine our attentions to the c_{ij} term which will jump randomly between the values c_{ij}^{α} and c_{ij}^{β}, where c_{ij}^{α} denotes the value of c_{ij} when the

internuclear vector between proton i and j is in its α position. $c^{\alpha}_{i'j'}$, $c^{\beta}_{i'j'}$ where i'j' may or may not be equal to ij, can be similarly defined.

We wish to find (a) the auto correlation functions $\langle \overline{c^{*}_{ij}(0)c_{ij}(\tau)} \rangle$ where the bar represents an ensemble average, and (b) the cross correlation functions $\langle \overline{c^{*}_{ij}(0)c_{i'j'}(\tau)} \rangle_R$ which only occur if the motions of the proton pairs are correlated.

It is sufficient to find the form of the second of these expressions and then to replace i'j' by ij to find the auto correlation functions.

If the value of $c^{*}_{ij}(0)$ is $c^{\alpha *}_{ij}$, it is possible to write for a single member of the ensemble

$$\langle c^{*}_{ij}(0)c_{ij}(\tau) \rangle = c^{\alpha *}_{ij} \left[P_{\alpha}(\tau)c^{\alpha *}_{i'j'} + P_{\beta}(\tau)c^{\beta}_{i'j'} \right] \qquad 4.8$$

where $P_{\alpha}(\tau) = 1$ if $c_{i'j'} = c^{\alpha}_{i'j'}$ at time τ

$= 0$ if $c_{i'j'} = c^{\beta}_{i'j'}$ at time τ

and $P_{\beta}(\tau) = 1$ if $c_{i'j'} = c^{\beta}_{i'j'}$ at time τ

$= 0$ if $c_{i'j'} = c^{\alpha}_{i'j'}$ at time τ

We can now perform an ensemble average. This replaces $P_{\alpha}(\tau)$ and $P_{\beta}(\tau)$ by their ensemble averages $p_{\alpha}(\tau)$ and $p_{\beta}(\tau)$ which are the probabilities that in an ensemble in which $c_{i'j'}$ was $c^{\alpha}_{i'j'}$ at $\tau = 0$,

it will be respectively $c^{\alpha}_{i',j'}$ or $c^{\beta}_{i',j'}$ at time τ.

Thus if $c^{*}_{ij}(0) = c^{\alpha *}_{ij}$,

$$\langle \overline{c^{*}_{ij}(0)c_{i',j'}(\tau)} \rangle = c^{\alpha *}_{ij} \left[c^{\alpha}_{i',j'} p_{\alpha}(\tau) + c^{\beta}_{i',j'} p_{\beta}(\tau) \right]. \qquad 4.9$$

We now assume that the behaviour of p_{α} and p_{β} as a function of τ is given by the rate equations

$$\frac{dp_{\alpha}}{d\tau} = W(p_{\beta} - p_{\alpha})$$

$$\frac{dp_{\beta}}{d\tau} = W(p_{\alpha} - p_{\beta}) \qquad 4.10$$

where $2W = 1/\tau_{c}$ with τ_{c}, the correlation time, as defined previously.

The solutions of equations 4.10 under the appropriate initial conditions are[37]

$$p_{\alpha}(\tau) = \tfrac{1}{2} \left[1 + \exp(-2W|\tau|) \right]$$

$$p_{\beta}(\tau) = \tfrac{1}{2} \left[1 - \exp(-2W|\tau|) \right]. \qquad 4.11$$

Equations 4.11 substituted into equation 4.9 give

$$\langle \overline{c^{*}_{ij}(0)c_{i',j'}(\tau)} \rangle$$

$$= \tfrac{1}{2} \left[c^{\alpha *}_{ij} c^{\alpha}_{i',j'} + c^{\alpha *}_{ij} c^{\beta}_{i',j'} + (c^{\alpha *}_{ij} c^{\alpha}_{i',j'} - c^{\alpha *}_{ij} c^{\beta}_{i',j'}) \exp(-2W|\tau|) \right] \qquad 4.12$$

Up to this point we have assumed that at $\tau = 0$, $c_{ij}(\tau) = c^{\alpha}_{ij}$. It

is of course equally probable that $c_{ij}(\tau) = c_{ij}^{\beta}$ at $\tau = 0$ which would give

$$\langle \overline{c_{ij}^{*}(0)c_{i',j'}(\tau)} \rangle$$

$$= \tfrac{1}{2}\left[c_{ij}^{\beta*}c_{i',j'}^{\beta} + c_{ij}^{\beta*}c_{i',j'}^{\alpha} + (c_{ij}^{\beta*}c_{i',j'}^{\beta} - c_{ij}^{\beta*}c_{i',j'}^{\alpha}) \exp(-2W|\tau|)\right]. \qquad 4.13$$

Using 4.12 and 4.13 to average over all initial positions we find,

$$\langle \overline{c_{ij}^{*}(0)c_{i',j'}(\tau)} \rangle$$

$$= \frac{1}{4}\left[c_{ij}^{\alpha*}c_{i',j'}^{\alpha} + c_{ij}^{\beta*}c_{i',j'}^{\beta} + c_{ij}^{\alpha*}c_{i',j'}^{\beta} + c_{ij}^{\beta*}c_{i',j'}^{\alpha} \right. \qquad 4.14$$

$$\left. + (c_{ij}^{\alpha*}c_{i',j'}^{\alpha} + c_{ij}^{\beta*}c_{i',j'}^{\beta} - c_{ij}^{\alpha*}c_{i',j'}^{\beta} - c_{ij}^{\beta*}c_{i',j'}^{\alpha}) \exp(-2W|\tau|)\right] .$$

When finding the spectral intensities from equation 4.14 the time independent terms of 4.14 lead to a delta function which is zero at non zero resonant frequency. Hence ignoring the time independent terms and replacing $2W$ by $1/\tau_c$, 4.14 becomes

$$\langle \overline{c_{ij}^{*}(0)c_{i',j'}(\tau)} \rangle$$

$$= \frac{1}{4}\left[c_{ij}^{\alpha*}c_{i',j'}^{\alpha} + c_{ij}^{\beta*}c_{ij} - c_{ij}^{\alpha*}c_{i',j'}^{\beta} - c_{ij}^{\beta*}c_{i',j'}^{\alpha}\right] \exp(-|\tau|/\tau_c) \qquad 4.15$$

A similar expression can be found for $\langle \overline{e_{ij}^{*}(0)e_{ij}(\tau)} \rangle$. The spectral intensities are then given by,

$$K^{(1)}_{iji'j'}(\omega_o) = \frac{1}{4}\left[c^{\alpha*}_{ij}c^{\alpha}_{i'j'} + c^{\beta*}_{ij}c^{\beta}_{i'j'} - c^{\alpha*}_{ij}c^{\beta}_{i'j'} - c^{\beta*}_{ij}c^{\alpha}_{i'j'}\right] \times \frac{2\tau_c}{1 + \omega_o^2\tau_c^2}$$

$$K^{(2)}_{iji'j'}(2\omega_o) = \frac{1}{4}\left[e^{\alpha*}_{ij}e^{\alpha}_{i'j'} + e^{\beta*}_{ij}e^{\beta}_{i'j'} - e^{\alpha*}_{ij}e^{\beta}_{i'j'} - e^{\beta*}_{ij}e^{\alpha}_{i'j'}\right] \times \frac{2\tau_c}{1 + 4\omega_o^2\tau_c^2} \quad . \qquad 4.16$$

In particular, if $i = i'$ and $j = j'$ then

$$\overline{\langle c^{*}_{ij}(0)c_{ij}(\tau)\rangle} = \frac{1}{4}\left[c^{\alpha}_{ij} - c^{\beta}_{ij}\right]^2 \exp(-|\tau|/\tau_c)$$

$$\overline{\langle e^{*}_{ij}(0)e_{ij}(\tau)\rangle} = \frac{1}{4}\left[e^{\alpha}_{ij} - e^{\beta}_{ij}\right]^2 \exp(-|\tau|/\tau_c) \quad . \qquad 4.17$$

Equation 4.17 signifies that the auto correlation functions, for the type of motion considered, are simply proportional to the squared difference of the spatial parts of the two equilibrium dipolar interactions.

The spectral intensities are then given by

$$K^{(1)}_{ijij}(\omega_o) = \frac{1}{4}\left[c^{\alpha}_{ij} - c^{\beta}_{ij}\right]^2 \times \frac{2\tau_c}{1 + \omega_o^2\tau_c^2}$$

$$K^{(2)}_{ijij}(2\omega_o) = \frac{1}{4}\left[e^{\alpha}_{ij} - e^{\beta}_{ij}\right]^2 \times \frac{2\tau_c}{1 + 4\omega_o^2\tau_c^2} \qquad 4.18$$

which are the spectral intensities of the auto correlation functions. Throughout this discussion we have assumed that the correlation times of the two types of dipole-dipole terms are equals[38].

4.3.2 Formulation of the Spectral Intensities in terms of Spatial Coordinates

We now wish to express equations 4.16 and 4.18 in terms of the spatial coordinates of the interproton vectors.

From equations 3.26 we find that

$$
\begin{aligned}
c_{ij}^{\alpha} &= (r_{ij}^{\alpha})^{-3} \sin\theta_{ij}^{\alpha} \cos\theta_{ij}^{\alpha} \exp(-i\Phi_{ij}^{\alpha}) \\
c_{ij}^{\beta} &= (r_{ij}^{\beta})^{-3} \sin\theta_{ij}^{\beta} \cos\theta_{ij}^{\beta} \exp(-i\Phi_{ij}^{\beta}) \\
e_{ij}^{\alpha} &= (r_{ij}^{\alpha})^{-3} \sin^2\theta_{ij}^{\alpha} \exp(-2i\Phi_{ij}^{\alpha}) \\
e_{ij}^{\beta} &= (r_{ij}^{\beta})^{-3} \sin^2\theta_{ij}^{\beta} \exp(-2i\Phi_{ij}^{\beta})
\end{aligned}
\qquad 4.19
$$

where the direction of the external field H_o is the Z axis, θ_{ij}^{α} is the polar angle of the internuclear vector between spins i and j in its α position, Φ_{ij}^{α} is the azimuthal angle of this vector and r_{ij}^{α} is its magnitude.

We can then calculate the spectral intensities of the auto correlation functions and of the cross correlation functions.

a) Auto correlation functions. We find that

$$
\left[c_{ij}^{\alpha} - c_{ij}^{\beta}\right]^2 = (c_{ij}^{\alpha} - c_{ij}^{\beta})(c_{ij}^{\alpha} - c_{ij}^{\beta})^*
$$

$$= (r_{ij}^{\alpha})^{-6} \sin^2\theta_{ij}^{\alpha} \cos^2\theta_{ij}^{\alpha} + (r_{ij}^{\beta})^{-6} \sin^2\theta_{ij}^{\beta} \cos^2\theta_{ij}^{\beta} \qquad 4.20$$

$$- 2 (r_{ij}^{\alpha})^{-3} (r_{ij}^{\beta})^{-3} \sin\theta_{ij}^{\alpha} \cos\theta_{ij}^{\alpha} \sin\theta_{ij}^{\beta} \cos\theta_{ij}^{\beta} \cos(\Phi_{ij}^{\alpha} - \Phi_{ij}^{\beta})$$

and

$$\left[e_{ij}^{\alpha} - e_{ij}^{\beta}\right]^2 = (r_{ij}^{\alpha})^{-6} \sin^4\theta_{ij}^{\alpha} + (r_{ij}^{\beta})^{-6} \sin^4\theta_{ij}^{\beta}$$

$$- 2 (r_{ij}^{\alpha})^{-3} (r_{ij}^{\beta})^{-3} \sin^2\theta_{ij}^{\alpha} \sin^2\theta_{ij}^{\beta} \quad (2 \cos^2(\Phi_{ij}^{\alpha} - \Phi_{ij}^{\beta}) - 1) \; . \qquad 4.20$$

These are sufficient to calculate the spectral intensities of the auto correlation functions given by 4.18.

b) Cross correlation functions. It is convenient to adopt the following notation for the cross correlation functions

$$C(^{\alpha}_{ij}|_{i',j'}^{\beta}) = \frac{1}{4} (r_{ij}^{\alpha})^{-3} (r_{i',j'}^{\beta})^{-3} \times$$

$$\sin\theta_{ij}^{\alpha} \cos\theta_{ij}^{\alpha} \sin\theta_{i',j'}^{\beta} \cos\theta_{i',j'}^{\beta} \cos(\Phi_{ij}^{\alpha} - \Phi_{i',j'}^{\beta}) \qquad 4.21$$

$$E(^{\alpha}_{ij}|_{i',j'}^{\beta}) = \frac{1}{4} (r_{ij}^{\alpha})^{-3} (r_{i',j'}^{\beta})^{-3} \times$$

$$\sin^2\theta_{ij}^{\alpha} \sin^2\theta_{i',j'}^{\beta} (2 \cos^2(\Phi_{ij}^{\alpha} - \Phi_{i',j'}^{\beta}) - 1)$$

then in equation 4.16,

$$\frac{1}{4}\left[c_{ij}^{\alpha *} c_{i'j'}^{\alpha} + c_{ij}^{\beta *} c_{i'j'}^{\beta} - c_{ij}^{\alpha *} c_{i'j'}^{\beta} - c_{ij}^{\beta *} c_{i'j'}^{\alpha}\right] \qquad 4.22$$

$$= C(^{\alpha}_{ij}|_{i',j'}^{\alpha}) + C(^{\beta}_{ij}|_{i',j'}^{\beta}) - C(^{\alpha}_{ij}|_{i',j'}^{\beta}) - C(^{\beta}_{ij}|_{i',j'}^{\alpha})$$

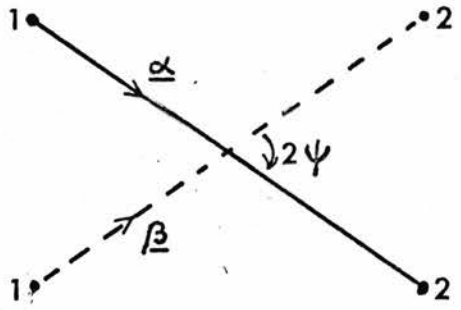

(a)

α represents the direction of the internuclear vector between protons 1 and 2 in its α position.

β represents the direction of the internuclear vector between protons 1 and 2 in its β position

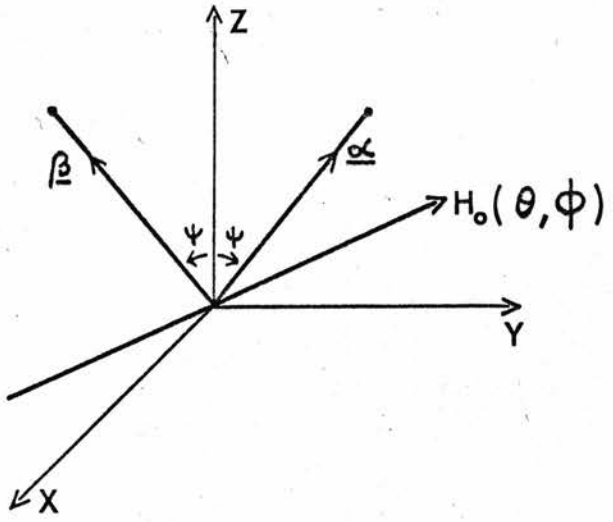

(b)

FIGURE 1

$$\frac{1}{4}\left[e_{ij}^{\alpha*}e_{i'j'}^{\alpha} + e_{ij}^{\beta*}e_{i'j'}^{\beta} - e_{ij}^{\alpha*}e_{i'j'}^{\beta} - e_{ij}^{\beta*}e_{i'j'}^{\alpha}\right]$$

$$= E(^{\alpha}_{ij}|^{\alpha}_{i'j'}) + E(^{\beta}_{ij}|^{\beta}_{i'j'}) - E(^{\alpha}_{ij}|^{\beta}_{i'j'}) - E(^{\beta}_{ij}|^{\alpha}_{i'j'}) \quad . \qquad 4.22$$

These equations are then sufficient to calculate the spectral intensities of the cross correlation functions from equation 3.16.

4.3.3 Calculation of T_{1min} for two protons having two equilibrium positions

For a system of only two protons there will of course be no cross correlation terms. Initially we shall assume that the interproton vector has the same magnitude in its α and β positions. The two directions of the interproton vector are separated by an angle 2ψ. This is shown in figure 1(a). Figure 1(b) shows the coordinate system adopted for this model. The $\underline{\alpha}$ and $\underline{\beta}$ vectors are both in the YZ plane and thus ψ is the angle between $\underline{\alpha}$ or $\underline{\beta}$ and the Z axis. The external magnetic field H_o is specified by the general polar coordinates Θ and Φ. We assume that vectors $\underline{\alpha}$ and $\underline{\beta}$ have unit magnitude. Thus vectors $\underline{\alpha}$, $\underline{\beta}$ and $\underline{H}_o$ can be represented by column matrices,

$$\begin{bmatrix} X_\alpha \\ Y_\alpha \\ Z_\alpha \end{bmatrix} = \begin{bmatrix} 0 \\ \sin\psi \\ \cos\psi \end{bmatrix} \quad \begin{bmatrix} X_\beta \\ Y_\beta \\ Z_\beta \end{bmatrix} = \begin{bmatrix} 0 \\ -\sin\psi \\ \cos\psi \end{bmatrix} \quad \begin{bmatrix} X_{H_o} \\ Y_{H_o} \\ Z_{H_o} \end{bmatrix} = \begin{bmatrix} \sin\Theta\cos\Phi \\ \sin\Theta\sin\Phi \\ \cos\Theta \end{bmatrix}$$

In equation 4.20, 4.21, the external field has the direction of the Z axis. Therefore we must make a coordinate transformation from (X,Y,Z) into (X',Y',Z') where H_o now lies along the Z' axis. The transformation is expressed by

$$\begin{bmatrix} X' \\ Y' \\ Z' \end{bmatrix} = \begin{bmatrix} \cos\Theta\cos\Phi & \cos\Theta\sin\Phi & -\sin\Theta \\ -\sin\Phi & \cos\Phi & 0 \\ \sin\Theta\cos\Phi & \sin\Theta\sin\Phi & \cos\Theta \end{bmatrix} \begin{bmatrix} X \\ Y \\ Z \end{bmatrix}$$

hence $\underline{\alpha}$ and $\underline{\beta}$ can be transformed into this new frame of reference and it is then a simple matter of vector algebra to find Θ_{12}^{α}, Θ_{12}^{β} and $\cos(\Phi_{12}^{\alpha} - \Phi_{12}^{\beta})$ which are required for insertion into 4.20.

At this stage it is possible to select a value of ψ, to select a fixed field direction, compute values for $\overline{\langle c_{12}^{*}(0)c_{12}(\tau)\rangle}$ and $\overline{\langle e_{12}^{*}(0)e_{12}(\tau)\rangle}$ and hence $K_{1212}^{(1)}(\omega_o)$ and $K_{1212}^{(2)}(2\omega_o)$, insert these into equation 3.27 and thus calculate a value for T_1.

The samples investigated were in a polycrystalline state and hence we must average $\overline{\langle c_{ij}^{*}(0)c_{ij}(\tau)\rangle}$ and $\overline{\langle e_{ij}^{*}(0)e_{ij}(\tau)\rangle}$ over all possible field directions i.e. by integrating over a sphere. These new field averaged quantities will be represented by

$$\overline{\langle c_{ij}^{*}(0)c_{ij}(\tau)\rangle}^{H_o} \quad \text{and} \quad \overline{\langle e_{ij}^{*}(0)e_{ij}(\tau)\rangle}^{H_o} .$$

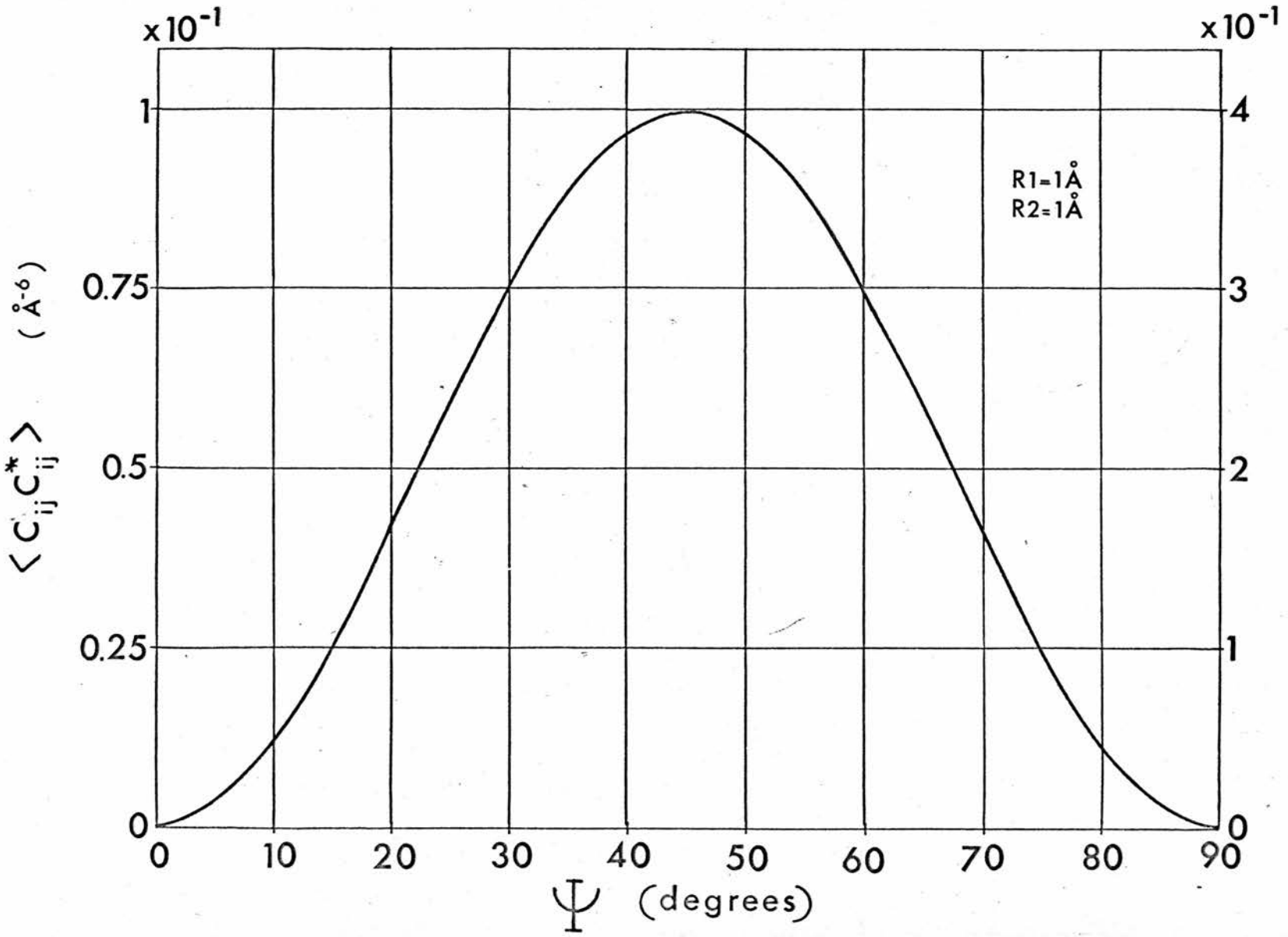
x10⁻¹
x10⁻¹
1
0.75
0.5
0.25
0
4
3
2
1
0
R1=1Å
R2=1Å
0
10
20
30
40
50
60
70
80
90
Ψ (degrees)
< C_ij C*_ij > (Å⁻⁶)
< E_ij E*_ij > (Å⁻⁶)

FIGURE 2

We now adopt the notation

$$\langle C^{*}_{ij}C_{ij}\rangle = \overline{\langle c^{*}_{ij}(0)c_{ij}(\tau)\rangle}^{H_o} \exp(|\tau|/\tau_c)$$

$$\langle E^{*}_{ij}E_{ij}\rangle = \overline{\langle e^{*}_{ij}(0)e_{ij}(\tau)\rangle}^{H_o} \exp(|\tau|/\tau_c) \qquad 4.24$$

Equation 3.27 can then be expressed (including only auto correlation terms) as

$$\frac{1}{T_1} = \gamma^4\hbar^2 \frac{3I(I+1)}{2N} \sum_{i\neq j}\left[\langle C^{*}_{ij}C_{ij}\rangle \frac{2\tau_c}{1+\omega_o^2\tau_c^2} + \langle E^{*}_{ij}E_{ij}\rangle \frac{2\tau_c}{1+4\omega_o^2\tau_c^2}\right] . \qquad 4.25$$

A computer programme for an I.B.M. 1620 digital computer was worked out (see Appendix 1) and was used to compute $\langle C^{*}_{ij}C_{ij}\rangle$ and $\langle E^{*}_{ij}E_{ij}\rangle$ as a function of ψ. These functions are shown in figure 2 for an interproton distance of $1A^{o}$.

The calculations of $\langle C^{*}_{ij}C_{ij}\rangle$ and $\langle E^{*}_{ij}E_{ij}\rangle$ can be checked at two points, namely $\psi = 0^{o}$ and $\psi = 90^{o}$.

a) $\psi = 0^{o}$.

In this case the internuclear vector has not moved hence $C^{\alpha}_{ij} = C^{\beta}_{ij}$ and therefore $\langle C^{*}_{ij}C_{ij}\rangle = 0$ and $\langle E^{*}_{ij}E_{ij}\rangle = 0$ for all H_o field directions.

b) $\psi = 90^{o}$.

The internuclear vector has in this case flipped through 180^{o}.

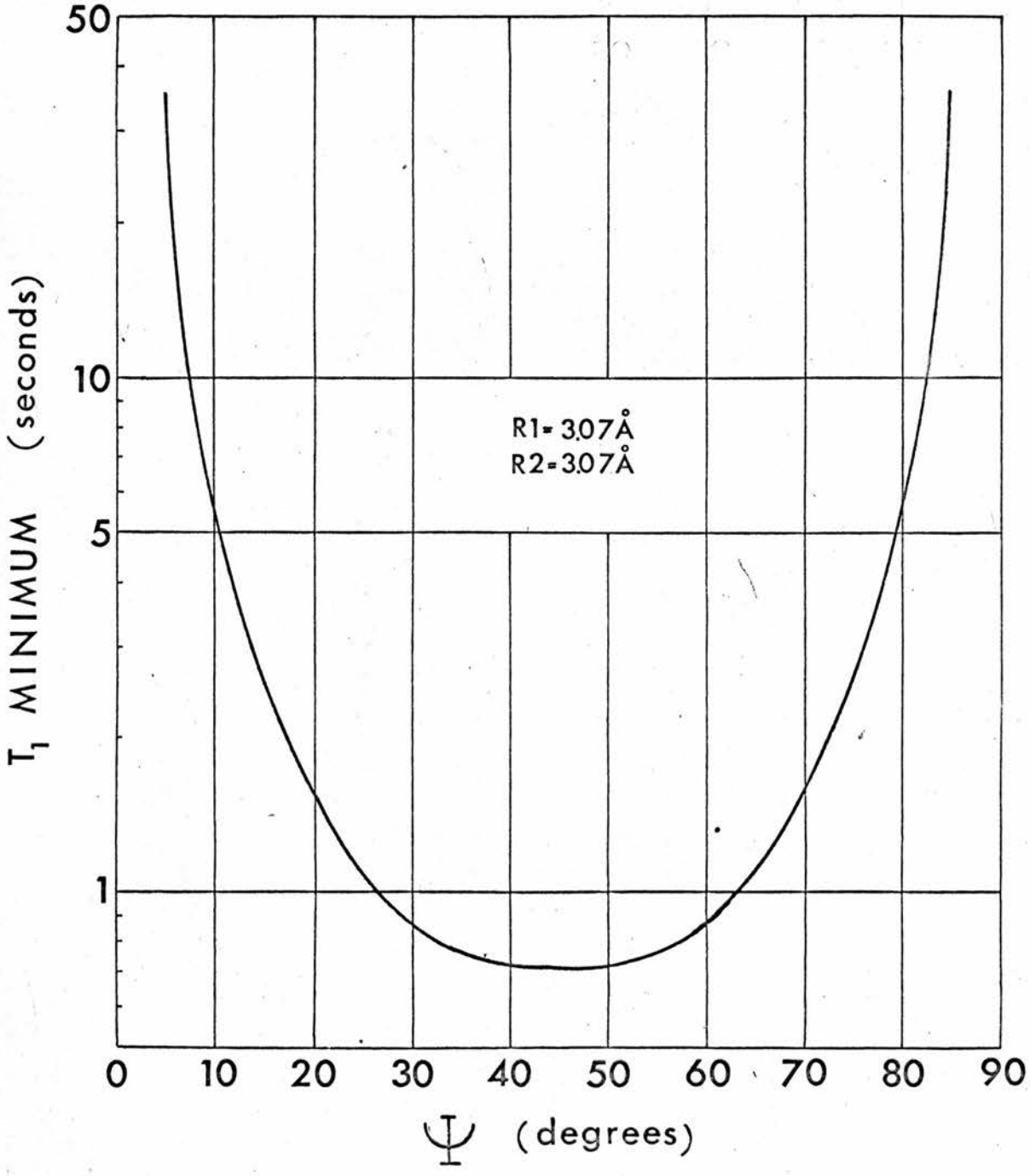
50
10
5
1
T_1 MINIMUM (seconds)
R1= 3.07Å
R2= 3.07Å
0
10
20
30
40
50
60
70
80
90
Ψ (degrees)

FIGURE 3

Thus the two protons have merely interchanged positions, and it is easily seen from equations 4.20 that again $\langle C^{*}_{ij} C_{ij} \rangle = \langle E^{*}_{ij} E_{ij} \rangle = 0$ for all H_o field directions.

It is interesting to note that $\langle E^{*}_{ij} E_{ij} \rangle = 4 \langle C^{*}_{ij} C_{ij} \rangle$ at all values of ψ. This shows a similarity with the result obtained by the B.P.P. Brownian rotation model (equation 4.3).

The digital computer was used to substitute the values of $\langle C^{*}_{ij} C_{ij} \rangle$ and $\langle E^{*}_{ij} E_{ij} \rangle$ into equation 4.25, which is differentiated with respect to τ_c, to find $T_{1(min)}$ as a function of ψ. A plot of $T_{1(min)}$ against ψ is shown in figure 3 for an internuclear distance of 3.07A°. From the reasoning which has gone before it follows that for this model $T_{1(min)} \to \infty$ as $\psi \to 0^{o}$ or 90^{o}.

The direct application of this theory to the samples investigated will be postponed to later chapters.

4.4 Quantum Mechanical Tunnelling Effects

Quantum mechanical tunnelling of an ethylene molecule through its two fold hindering potential barrier has been suggested as a mechanism for spin-lattice relaxation in this substance[39,40]. Although the effect of tunnelling on n.m.r. absorption is quite well understood, its role in spin-lattice relaxation has not yet been conclusively determined. In order to help clarify the present situation regarding tunnelling effects in n.m.r., a brief review of the existing theory and some relevant experimental results will be given.

4.4.1 Theory:- Powles and Gutowsky[41], Stejskal and Gutowsky[42] and Das[43,20] considered methyl group reorientation in a three fold hindering barrier. These theories are easily modified for tunnelling of the ethylene molecule through its two fold barrier. Only tunnelling of the whole molecule need be considered as the barrier hindering torsion of the CH_2 groups, with respect to one another, is approximately 25 kcal/mole[44].

Certain assumptions must be made as to the form of the hindering barrier. These are:-

(A) the potential function is two nodal and is of the shape

$$V(\Phi) = (V_o/2)(1 + \cos 2\Phi) \qquad 4.26$$

where V_o is the barrier height and Φ is the angular coordinate which describes the reorientation of the molecule.

(B) the barrier to reorientation is time independent.

(C) the barrier is temperature independent.

Assumption (A) is reasonable if we choose to ignore a small correction term[45]. Although assumptions (B) and (C) are not strictly correct for ethylene, where the barrier to reorientation must be intermolecular, they do not alter the main conclusions of the theory.

Substituting the potential function 4.26 into the Schrödinger equation we obtain the two nodal Mathieu equation

$$\frac{d^2M(\Phi)}{d\Phi^2} + [a - \frac{S}{2}\cos 2\Phi]M(\Phi) = 0 \qquad 4.27$$

where $M(\Phi)$ is the wave function describing the position of the molecule and

$$a = \frac{2I}{\hbar^2}\left[E - V_o/2\right]$$

$$S = \frac{2I}{\hbar^2} V_o$$

where E is the energy of the molecule and I is its moment of inertia about the rotation axis. General solutions of equation 4.27 may be obtained using tables 46, 47. These tables give solutions for equations of the form

$$\frac{d^2M(\Phi)}{d^2\Phi} + (b - S\cos^2\Phi)\, M(\Phi) = 0 \qquad 4.28$$

which may be obtained from equation 4.27 by placing $\cos 2\Phi = 2\cos^2\Phi - 1$ and $a = b - S/2$.

If the barrier potential is two nodal the torsional levels below the top of the barrier occur in pairs. The amount of splitting of each pair is small compared to the energy difference between pairs of levels. It is also found that the wave function of the lower energy level in each pair is antisymmetric with respect to inversion in the origin, while the upper one is symmetric[44,48]. It is easily shown[48,49], from the symmetries of the levels, that the tunnelling frequency ν_m for the m^{th} level, is given by

$$\nu_m = \frac{2\,\Delta E_m}{h}$$

where ΔE_m is the energy separation of the m^{th} pair of torsional levels. In the terms of the quantities found in the tables[47]

$$\nu_m = \frac{\hbar}{2\pi I}\,\Delta b_m$$

$$= \frac{\hbar}{2\pi I}\,(b_{o_{m+1}}(S) - b_{e_m}(S)) \qquad 4.29$$

where $b_{e_m}(S)$ and $b_{o_m}(S)$ are respectively the even and odd solutions of the Mathieu equation for the m^{th} torsional state. The tables are available for m = 0 to 15. The accuracy of the tables is insufficient to give splittings for the m = 0, 1, 2, 3 levels. For these levels the following expression of Goldstein[49] must be used:-

$$\Delta b_m = \frac{2^{3m+4}}{\pi^{\frac{1}{2}} m!}\, S^{(\frac{2m+3}{4})}\, \exp(-2S^{\frac{1}{2}})(1 + \frac{C_1}{S^{\frac{1}{2}}} + \frac{C_2}{S} + ..) \qquad 4.30$$

where C_1 and C_2 are constants for which values have been quoted by Das[43].

The average tunnelling frequency is then given by

$$\bar{\nu}_t = \frac{\sum_{m=0}^{\infty} \nu_m \exp(-\bar{E}_m/kT)}{Q} \qquad 4.31$$

where $\bar{E}_m$ is the average energy of the m^{th} state and Q is the partition

function given by

$$Q = \sum_{m=0}^{\infty} \exp(-\bar{E}_m/kT) \ .$$

The numerator of this expression is simply the tunnelling frequency of a molecule in the m^{th} torsional state times the Boltzmann probability of its being there.

At higher temperatures it is also possible for the molecule to reorientate by going over the top of the barrier. The transition probability for this type of motion is given by

$$W = \frac{1}{\pi} \left(\frac{2V_o}{I}\right)^{\frac{1}{2}} \exp(-V_o/kT) \ . \qquad 4.32$$

This expression is slightly different from that given by Das[43] which contained an error.

It is now necessary to relate this average tunnelling or reorientation frequency to the spin-lattice relaxation time T_1. Stejskal and Gutowsky[41] do this by relating the tunnelling frequency to the correlation time by

$$\tau_c = \frac{1}{2\pi\nu_t} \ . \qquad 4.33$$

This relationship was proposed by Powles and Gutowsky[41] from theoretical work on second moments. It is then assumed that the form of the correlation function is exponential

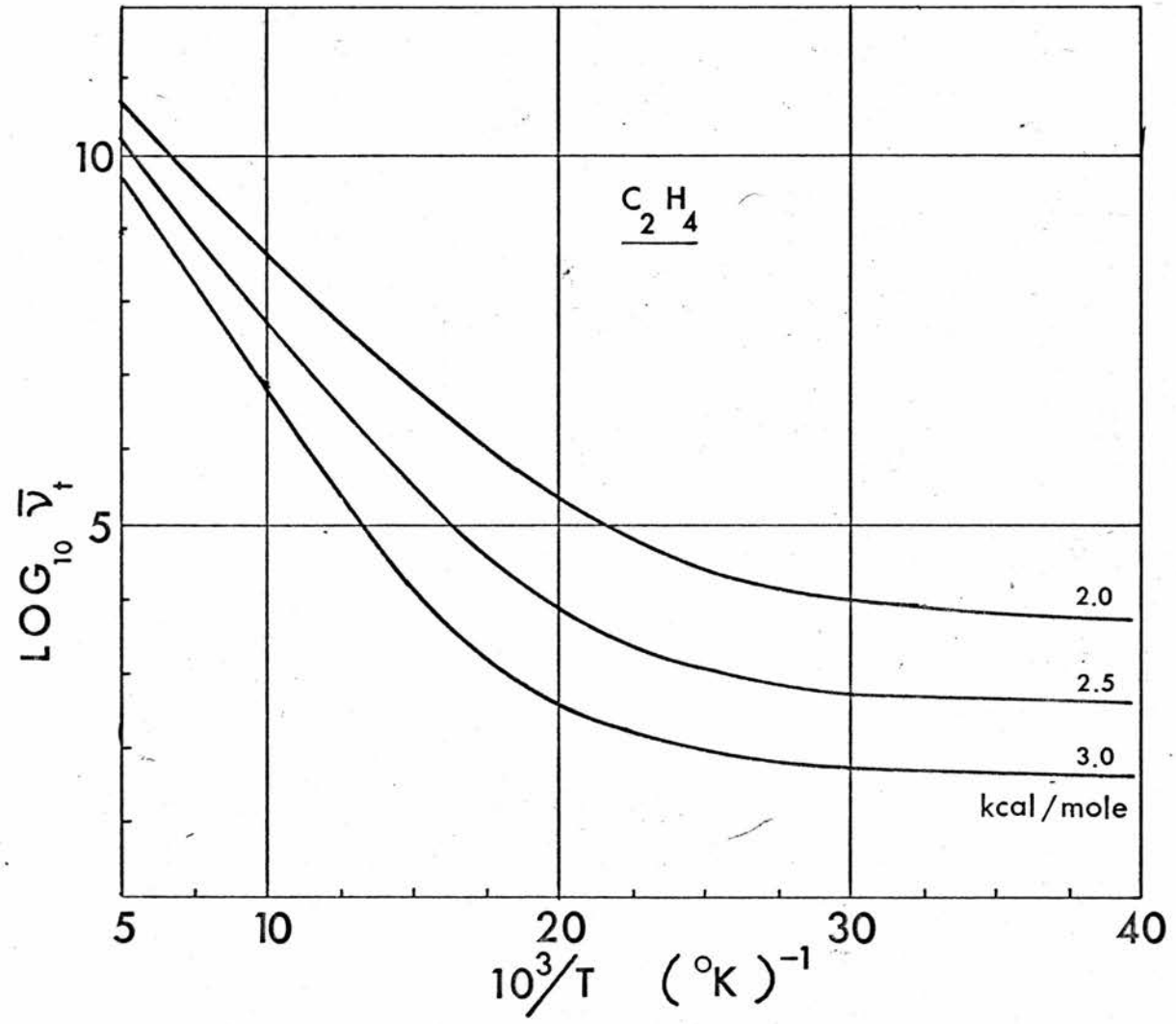

FIGURE 4

$$K(|\tau|) = \langle F^{*}(0)F(t)\rangle \exp(-|\tau|/\tau_c) \quad . \qquad 4.34$$

The spectral density of this correlation function is then given by

$$J(\omega) = \langle 2F^{*}(0)F(t)\rangle \frac{\tau_c}{1 + \omega^2\tau_c^2} \qquad 4.35$$

which when substituted into the modified B.P.P. equation (equation 4.4) gives

$$\frac{1}{T_1} = C\left[\frac{\tau_c}{1 + \omega_o^2\tau_c^2} + \frac{4\tau_c}{1 + 4\omega_o^2\tau_c^2}\right] . \qquad 4.36$$

In the original paper[4.2] equation 4.36 has a slightly different form as it is applied to a CH_3 group tumbling and tunnelling.

Results of this type of calculation for ethylene, where the moment of inertia is 5.64×10^{-40} g cm^2, are shown in figure 4 for values of V_o equal to 2, 2.5 and 3 kcal/mole. Computer programme number 3 in Appendix 1 was used to compute results for these plots.

The most striking prediction of this theory is that as the temperature is decreased, τ_c will converge to a finite non zero limit whose value is dependent on the barrier height. It thus follows from equation 4.36 that T_1 will converge to a finite limit. This contradicts the predictions of theories using the Arhenius relation,

$$\tau_c = \tau_o \exp(E/kT) \qquad 4.37$$

which predicts that, as the temperature is decreased, τ_c will tend to infinity and hence T_1 will tend to infinity.

There are a number of conceptual difficulties in the above theory that have been pointed out in the original papers and by Freed[50]. These difficulties together with a few others will be discussed below.

1) If the tunnelling frequency ν_m in a given state m is to be included in an expression such as 4.31 there must be transitions taking place between the torsional levels at a frequency greater than the tunnelling frequency. This produces in the torsional levels, an uncertainty broadening which is greater than their splitting.

2) In equation 4.35 the factor $(\tau_c/1 + w^2\tau_c^2)$ is the Debye spectral density function. This assumes random motion and requires that the levels be broadened into a continuous Debye-Spectrum with τ_c defined by 4.33. This broadening requires coupling to the other lattice modes.

3) Because of the symmetry of the wave functions of the ethylene molecule if tunnelling implies transitions between the split states of a particular torsional level, then such a transition is nuclear spin forbidden. Coupling with other lattice modes perturbs and mixes the wave functions of the molecule enabling such transitions to take place.

4) If the levels were sharp reorientation could produce relaxation at only discreet Larmor frequencies. These tunnelling resonances have not been observed[16].

5) Tunnelling is basically a coherent process with no energy exchange unless a scattering process is involved. A similar effect occurs in rotating gas molecules which cannot contribute to longitudinal relaxation (take part in energy exchange) until a collision occurs. Again this scattering is a result of coupling to other lattice modes.

Most, if not all, of the difficulties inherent in the tunnelling model can be circumvented if we assume broadening of the torsional levels. In fact, as stated by Stejskal and Gutowsky[42], broadening is such an important feature of the model that it is probably misleading to describe the reorientations as tunnelling. One is therefore led to assume that the temperature dependence of the relaxation would be determined by the temperature dependence, not of the tunnelling process, but of the broadening. On this basis a finite limit for τ_c and hence T_1 is not expected.

The more recent work by Freed[50] is also worth noting although his attempts to analyse the effects that quantised internal rotations can have on magnetic resonance are more closely related to e.s.r. than n.m.r. In the case applicable to n.m.r., that where the rotational motion is strongly coupled to the lattice but loosely coupled

to the spins, he introduces a mean collision frequency and thus introduces the same approximations as previous theories.

4.4.2 Experimental:- The experimental work discussed below will be confined to CH_3 groups, NH_4 groups and ethylene, which all have small moments of inertia and hence a possible tunnelling effect.

Stejskal et al.[51] have reported values of $\bar{\nu}_t$, the tunnelling frequency calculated from T_1 data, as a function of temperature for compounds such as t-butyl chloride $(CH_3)_3Cl$, 2,2-dichloropropane $(CH_3)_2CCl_2$ and methyl chloroform CH_3CCl_3. Although showing reasonable agreement with tunnelling theory at high temperature (i.e. the region where in fact tunnelling theory is in rough agreement with simple activation theory), low temperature agreement is poor. In the case of methyl chloroform they find that the values of $\bar{\nu}_t$, as calculated from experimental second moment results, level off at about 100°K. Unfortunately they have used a formula, relating second moment to correlation time[41], which is valid only when motional narrowing is occurring and in the temperature range of their experiments motional narrowing has ceased in methyl chloroform[52,16].

CH_3 group rotation has also been studied in dimethyl butanes, trimethyl benzenes[53,54,55,56], dimethyl pentane and trimethyl pentanes[57]. The results of these papers show that methyl group rotation by tunnelling causes motional narrowing of the absorption line but that T_1 measurements are insensitive to this motion.

Waugh and Fedin[58] in their paper reviewing the determinations of hindered rotation barriers in solids conclude that for rotation of NH_4 and CH_3 groups, the actual role of the tunnel effect is much smaller than is sometimes suggested.

The tunnelling effect in ethylene which has been reported by Hoch[39,40] will be discussed in a later chapter.

A spurious levelling off of T_1, at low temperatures whilst investigating CH_3 rotations has been recorded by Eades[59]. These measurements of T_1 were made using a C.W. apparatus. The effect was found to be caused by r.f. saturation of the sample.

A similar spurious result was found[60] to have been caused by a temperature gradient over the sample.

4.4.3 Conclusion:- From the above discussion of theory and experiment on CH_3 tunnelling effects, it seems reasonable to conclude that although pure tunnelling can contribute to n.m.r. absorption line narrowing, as in this case no energy transfer is required, it cannot contribute to spin-lattice relaxation. In fact the spin-lattice relaxation will have the temperature dependence, not of the tunnelling process but of the broadening of the torsional levels.

4.5 Relaxation by Paramagnetic Impurities

The first investigation of the effects of paramagnetic impurities, which contain unpaired spins, was carried out by Bloembergen[61]. The

electron spins of the impurity produce time varying fields at neighbouring nuclei and thus cause relaxation of these nuclear spins. It was found that very low concentrations of impurity (1 in 10^6) would be effective in producing relaxation in the sample.

In liquids the large effect of such a small concentration of impurities is easily explained by the high mobility of the impurities. This high mobility allows the impurities to approach sufficiently close to all the nuclear spins and hence relax them by direct relaxation of unlike spins.

In solids the relaxation is by means of two processes occurring serially, namely direct relaxation and spin energy diffusion. Diffusion of Zeeman energy towards an impurity, by means of mutual nuclear spin slips, occurs as a result of the gradient in magnetic energy density created by the direct relaxation of nuclei near the impurity through a dipole-dipole interaction between unlike spins. This spin diffusion of energy is the same process which enabled us to use the spin temperature concept in chapters 3 and 4. It is also of interest to note that the presence of paramagnetic impurities broadens the nuclear resonance at low temperatures[62,63].

4.6 Distribution of Correlation Frequencies

In the derivation of the spin-lattice relaxation formulae 4.4 and 4.25, it was assumed that the motion of the spins could be described by a single correlation time. This assumption has proved

inadequate in interpreting several n.m.r. results[64,65], and so a distribution of correlation frequencies was introduced.

For example, equation 4.4, for a continuous distribution of correlation frequencies, would become[66],

$$\frac{1}{T_1} = \frac{3}{10}\frac{\gamma^4\hbar^2}{b^6}\left[\int_0^\infty \frac{\tau g(\tau)}{1+\omega_o^2\tau^2}\,d\tau + \int_0^\infty \frac{4\tau g(\tau)}{1+4\omega_o^2\tau^2}\,d\tau\right] \qquad 4.38$$

where $g(\tau)$ is a distribution of correlation times.

Several different possible forms of $g(\tau)$ have been investigated by Connor[65]. In general it is found that a distribution of correlation times produces a broadening of the minimum of the curve of $\log T_1$ against temperature. Such a distribution also results in a smaller slope in the limits of $\omega_o\tau_c \ll 1$ and $\omega_o\tau_c \gg 1$ producing an apparent decrease in the activation energy.

5. MEASUREMENT OF SPIN-LATTICE RELAXATION TIME

5. MEASUREMENT OF SPIN-LATTICE RELAXATION TIME

5.1 Pulse Methods

Pulse techniques of measuring T_1 were introduced by Hahn[67]. In this method a large pulse of r.f., at the Larmor frequency ω_o with magnetic amplitude $2H_1$, is applied at right angles to the steady magnetic field H_o. It is well known that a linear polarized field of magnitude $2H_1$ can be considered as a superposition of two fields of amplitude H_1 circularly polarized in opposite senses. Only one of these components has non-negligible effect on the spin system[68].

If the equilibrium magnetization is M_o and is along the Z axis, the axis of H_o, then by appling a r.f. pulse of width t_w, the magnetization precesses to an angle $\theta = \gamma H_1 t_w$ where θ is with respect to the Z axis. The two basic types of pulses are $\pi/2$ pulses, where $t_w = \pi/2\gamma H_1$, and π pulses, where $t_w = \pi/\gamma H_1$.

A $\pi/2$ pulse gives a resultant magnetization along the Y axis, assuming that the r.f. field was applied along the X axis and that $t_w << T_2$. This magnetization then precesses in the XY plane about H_o and induces a r.f. voltage in the receiver coil which is placed along the Y axis. The envelope of the resultant signal, the free precession decay, is the Fourier transform of the steady state line shape[69]. For a viscous liquid the decay time of the free precession signal is simply T_2, the decay of the M_X component in equation 2.8. A π pulse gives a resultant magnetization along the Z axis, which of

course is undetected by the receiver coil. There are three basic pulse sequences, composed of π and $\pi/2$ pulses, which are used for T_1 measurement.

In the first method two $\pi/2$ pulses separated by a time τ, a $\pi/2\tau\pi/2$ sequence, are applied to the sample after the system has reached equilibrium in the H_o field. The maximum magnitude of the induction decay after the first pulse gives a measure of M_o, while that after the second pulse is given by

$$M_Z(\tau) = M_o(1 - \exp(-\tau/T_1)) \quad . \qquad 5.1$$

By comparing the magnitudes of the induction decays at equal times after the initiating pulse, the value of T_1 can be found. After several times T_1 have elapsed, to allow the system to regain equilibrium, another similar sequence with a different value of τ can be applied and T_1 remeasured. T_1 can also be found by finding the value of τ for which the induction decay after the second pulse has a magnitude equal to one half the magnitude of the first decay, in which case $T_1 = \tau/\ln 2$.

A second method is the $\pi\tau\pi/2$ pulse sequence, where the growth of the magnetization as a function of τ is given by

$$M_Z(\tau) = M_o(1 - 2\exp(-\tau/T_1)) \quad . \qquad 5.2$$

Again T_1 can be measured by measuring the relative magnitudes of the induction decays after each $\pi/2$ pulse, or by observing the

null i.e. $M_Z(\tau) = 0$ which occurs when $\tau = T_1 \ln 2$. This method also requires a delay of several times T_1 between pulse sequences.

In the third method T_1 is determined by measuring the recovery of the magnetization component M_Z following a saturating comb of r.f. pulses[70]. This comb has a duration less than T_1 and is composed of 40-80 closely spaced $\pi/2$ pulses. The growth of magnetization, measured at a time τ by a $\pi/2$ observation pulse, is given by

$$M(\tau) = M_o(1 - \exp(-\tau/T_1)) \quad . \qquad 5.3$$

The advantages of this system are that it is unnecessary to wait a time longer than T_1 between sequences and that it is easier to impose a uniform initial Boltzmann distribution ($T = \infty$) on the system, even in the presence of severe inhomogeneous broadening. The importance of a uniform spin temperature for obtaining reliable T_1's has been stressed by Simmons et al.[71].

5.2 Continuous Wave Methods

There are two basic methods of measuring T_1 in solids by continuous wave (C.W.) techniques. The method used depends on the value of T_1; if T_1 is longer than about 15 seconds the method of direct recovery is used, while progressive saturation is utilized for $T_1 < 15$ seconds.

In direct recovery the signal is initially saturated with a

large r.f. field, and the exponential recovery of the absorption signal monitored using the smallest r.f. field H_1 possible. The measured time constant, ignoring apparatus effects, is then strictly T_1Z where[72]

$$Z = 1 + \pi\gamma^2 H_1^2 T_1 f(\omega) \qquad 5.4$$

and where $f(\omega)$ is the line shape function of the absorption curve. A value of T_1 can be determined by measuring T_1Z at different power levels[73] and the data extrapolated to zero power level.

If the absorption line is sufficiently narrow to observe on an oscilloscope, without using lock-in detection, values of T_1 down to about 2 seconds can be measured by monitoring the recovery with a cine camera or storage oscilloscope.

With these methods it must be possible to reduce the r.f. field to very low levels and still maintain a reasonable signal to noise ratio in the receiver. It has generally been found[74] preferable to replace the method of direct recovery by some other technique of measuring T_1.

In progressive saturation[75], as in direct recovery, observations are made at the maximum of the absorption line derivative, but in this case the r.f. field is increased in steps and the reading of the lock-in amplifier output meter noted at each step. A plot of these readings against the logarithm of H_1, or the signal

generator output, yields a saturation curve. The various values of T_1 at different temperatures give a family of curves and it is assumed that corresponding points on two saturation curves A and B are connected by relation 5.4 so that

$$(\pi\gamma^2 H_1^2 T_1 f(\omega))_A = (\pi\gamma^2 H_1^2 T_1 f(\omega))_B \qquad 5.5$$

$$\frac{T_{1A}}{T_{1B}} = \left[\frac{H_{1B}}{H_{1A}}\right]^2 \frac{f_B(\omega)}{f_A(\omega)} \quad . \qquad 5.6$$

The assumption is then made that at the two temperatures producing the saturation curves A and B, $f_A(\omega)$ has the same form as $f_B(\omega)$ and hence $f_A(\omega) = k/\Delta H_A$, while $f_B(\omega) = k/\Delta H_B$ where k is a constant and ΔH_A and ΔH_B are the line widths of the absorption curves at the temperatures A and B. Then

$$\frac{T_{1A}}{T_{1B}} = \left[\frac{H_{1B}}{H_{1A}}\right]^2 \frac{\Delta H_A}{\Delta H_B} \quad . \qquad 5.7$$

Relative values of T_1 are obtained in this way and these are converted into absolute values by comparison with a direct recovery result at a fixed temperature.

An inaccuracy in the measured T_1 can result if this technique is used in a region where the line shape is changing, which can happen in solids where motional narrowing ceases as the temperature is lowered.

Goldman[76] has made an extensive analysis of the use of lock-in detection in T_1 measurements, which are necessarily performed off resonance, and has found this technique unsuitable for reliable results. This conclusion is reached because the absorption signal is found to contain a component which does not saturate as predicted by previous work. An additional effect arises from the shift of the position of the maximum of the derivative curve even at partial saturation.

6. THE PULSE SPECTROMETER

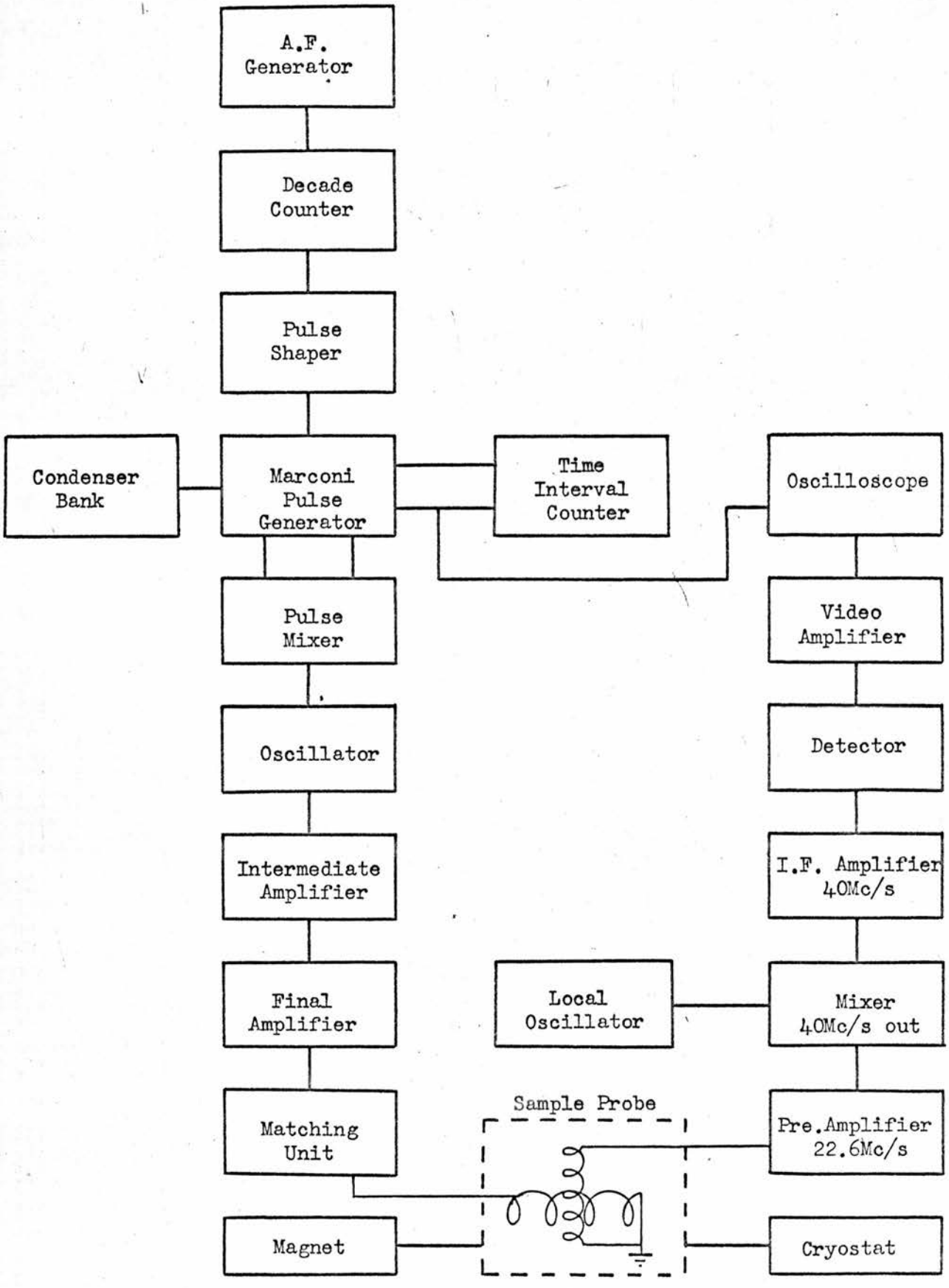
A.F. Generator
Decade Counter
Pulse Shaper
Condenser Bank
Marconi Pulse Generator
Time Interval Counter
Oscilloscope
Pulse Mixer
Video Amplifier
Oscillator
Detector
Intermediate Amplifier
I.F. Amplifier 40Mc/s
Final Amplifier
Local Oscillator
Mixer 40Mc/s out
Sample Probe
Matching Unit
Pre.Amplifier 22.6Mc/s
Magnet
Cryostat

FIGURE 5

6. THE PULSE SPECTROMETER

6.1 Introduction

The pulse n.m.r. spectrometer which was constructed for T_1 measurements was the same basic design as that of Jones[77] with an operating frequency of 22.6 MHz. This design was chosen in preference to those described by Mansfield and Powles[78], Clark[79], and Mazitov and Ionov[80], because it satisfied the specifications required while being of a simpler construction. A block diagram of the spectrometer is given in figure 5.

The spectrometer may be subdivided into four sections:-

(a) the apparatus for the generation and transmission of a specified sequence of r.f. pulses

(b) the method detection and display of the nuclear induction signal

(c) the probe assembly and temperature control

(d) the magnet and field sweep control.

6.2 The Transmitting System

6.2.1 Specifications of the Transmitting System

The requirements for the transmitting section of an n.m.r. pulse apparatus suitable for T_1 measurements in solids are:-

i) r.f. pulse width $t_w \ll T_2$

ii) gating circuits capable of providing the sequences: single 90°, $90^\circ_\tau 90^\circ$, and $180^\circ_\tau 90^\circ$

iii) τ must be variable from several msec upwards

iv) minimum rise and decay times for the r.f. pulses

v) the interval between pulse sequences must be variable from about 1 second to about five times the maximum T_1 measured.

T_2 for a Gaussian line shape for a proton resonance is given by

$$T_2 = \frac{44}{\delta H} \text{ μsec}$$

where δH is the half width in gauss at half the intensity of the absorption line. For a half width of 10 gauss this gives

$$T_2 \doteq 4 \text{ μsec} .$$

To obtain an adiabatic nutation, it is necessary to satisfy condition (i) and hence for a $\pi/2$ pulse a pulse width of approximately 1 μsec is required.

For proton study a $\pi/2$ pulse having a width of 1 μsec requires a r.f. field magnitude H_1 of

$$H_1 = \frac{\theta}{\gamma t_w} = 60 \text{ gauss} .$$

Therefore the amplitude of the linear alternating field is 120 gauss.

The time constant for the rate of decay of excitation following

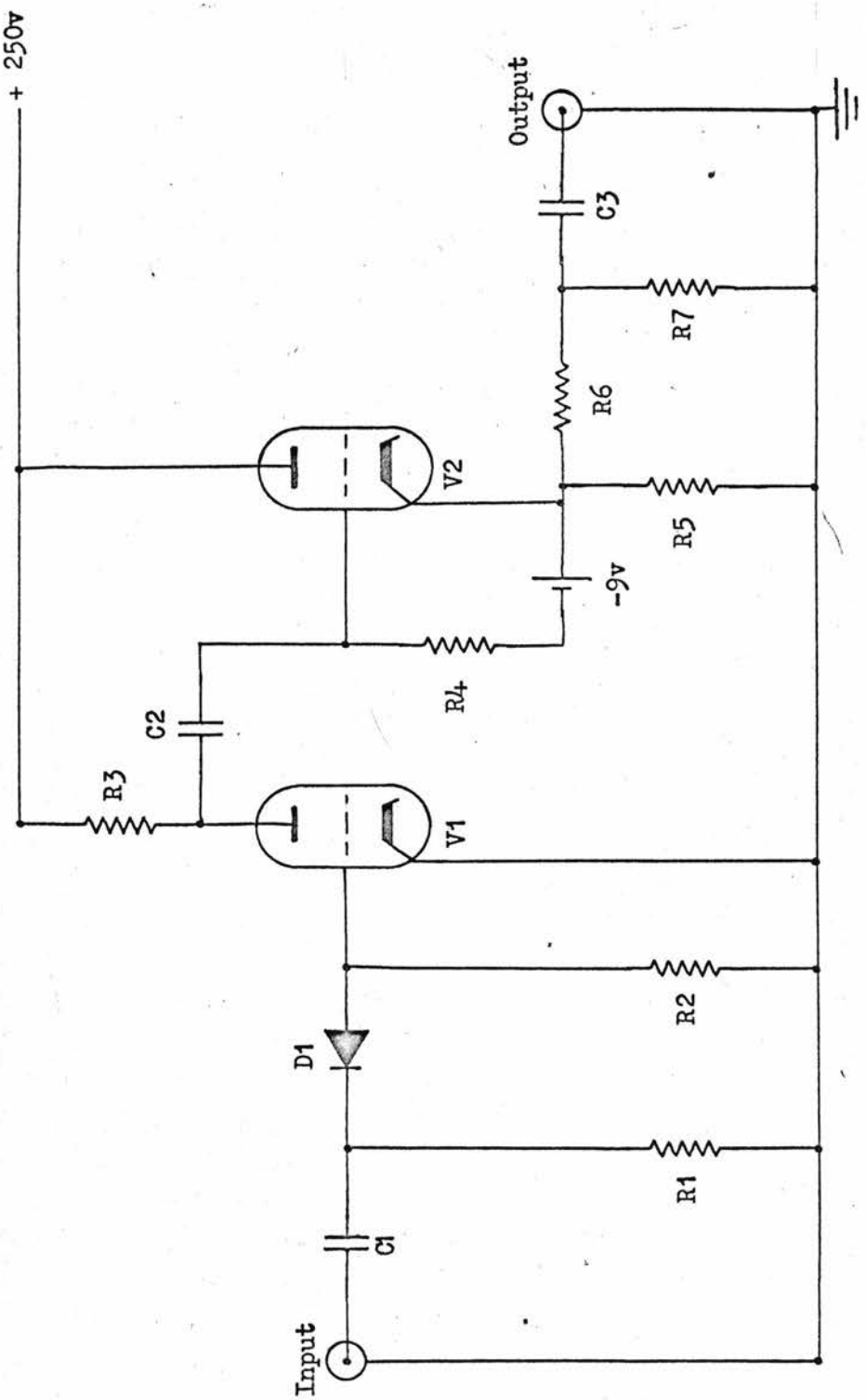

FIGURE 6

an r.f. pulse is given[81] by $Q/\pi f$ where Q is the quality factor and f is the value of the radio frequency. Hence to satisfy (ii) the transmitter coil Q must be low. However for a given transmitter power dissipation in the sample coil, the H_1 value produced is proportional[79] to $Q^{\frac{1}{2}}$, a requirement which indicates a high Q value. These conflicting requirements necessitate an optimisation of the transmitter Q or the use of a switching device to lower the Q of the transmitter coil immediately the pulse has finished.

The use of a "crossed coil" probe instead of a bridge system allows this optimisation of the transmitter coil Q while retaining a high Q for the receiver coil.

6.2.2 Pulse Sequence Triggering System

The Advance a.f. generator H1B, Bendix Dekatron unit 101B, and pulse shaper were used to provide a triggering pulse for a given sequence of r.f. pulses.

The setting of the a.f. generator determined the clocking rate of the Dekatron counter. An output could be selected from any of the four decade counters of the Dekatron unit thus enabling the time between sequences to be varied over a wide range.

The pulse shaper, figure 6, was required because the output of the Dekatron unit was not a single sharp pulse. The input stage of this unit is a differentiating circuit formed by R1, C1. Diode D1 passes only negative pulses on to the grid of valve V1. The output

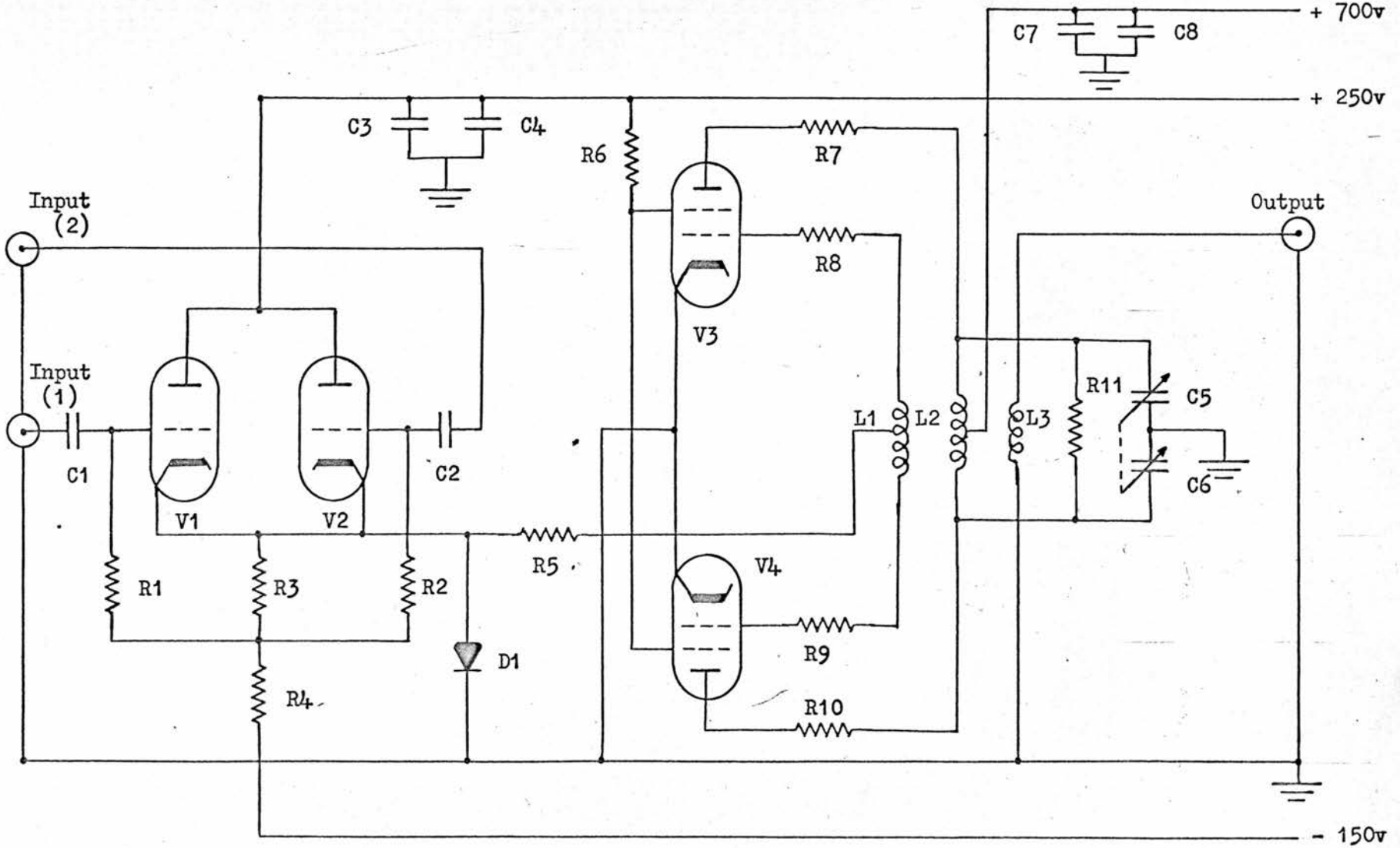
+ 700v
C7
C8
+ 250v
C3
C4
R6
R7
Input
(2)
Output
R8
V3
Input
(1)
R11
C5
L1
L2
L3
C1
C2
C6
V1
V2
R5
V4
R1
R3
R2
R9
D1
R4
R10
- 150v

FIGURE 7

of V1 is fed into V2 which is connected as a cathode follower discriminator with a 9 volt grid bias battery. The resultant sharp output pulses were used to trigger the Marconi pulse generator.

The values of all circuit components are given in Appendix 2.

6.2.3 Marconi Pulse Generator

A Marconi pulse generator TF1400/3 was used to provide the square wave pulses which controlled the r.f. oscillator.

The generator was capable of delivering single or double pulses of variable width and of amplitude +80 volts across the high input resistance of the cathode follower stage. The original delay circuits incorporated allowed the pulse separation to be set to any value between zero and 3 msec. This maximum delay time was expanded to 40 seconds by extending the range of condensers in the feedback circuit of the screen-coupled phantastron, which normally determined the delay time.

6.2.4 Time Interval Counter

The time interval between pulses was measured using a Hewlett Packard 5223L digital frequency meter. This counter has single line or separate start and stop lines, and a minimum time interval measurement of 10 μsec.

6.25 Cathode Follower Mixer

A cathode follower mixer (figure 7) coupled both channels of the Marconi pulse generator to the r.f. oscillator.

In the absence of an input pulse a voltage of -60v exists at the cathodes of V1 and V2 which is sufficient to hold off the oscillator. During an input pulse the cathode voltages rise to zero at which voltage they are clamped by diode D1.

6.2.6 R.F. Oscillator

The r.f. oscillator (figure 7) is a push-pull Hartley circuit with inductive feedback from anode to grid and incorporating grid modulation. Push-pull circuits were used in all the transmitter stages as the power output is thereby doubled for given tubes and voltages while the interelectrode capacitance placed across the anode tank circuit is halved. Parallel operation doubles the capacitance hence requiring a lower inductance in the tank circuit. The valve used was a QQV06-40A a double r.f. beam tetrode having a power output of 90 watts at 600v anode potential. For increased stability the oscillator was operated at voltages suitable for continuous operation.

To keep the rise and decay times of the oscillator as small as possible, the grid resistor R5, which was a non-capacitive type, was by-passed only by the grid-cathode interelectrode capacitance (2 x 10.5 pF) and strays. The time constant of the grid circuit is therefore 10^{-7} sec which was sufficient to give rise and decay times of approximately 0.1 μsec for a step function input.

The Q of the anode tank circuit controls the rise and decay

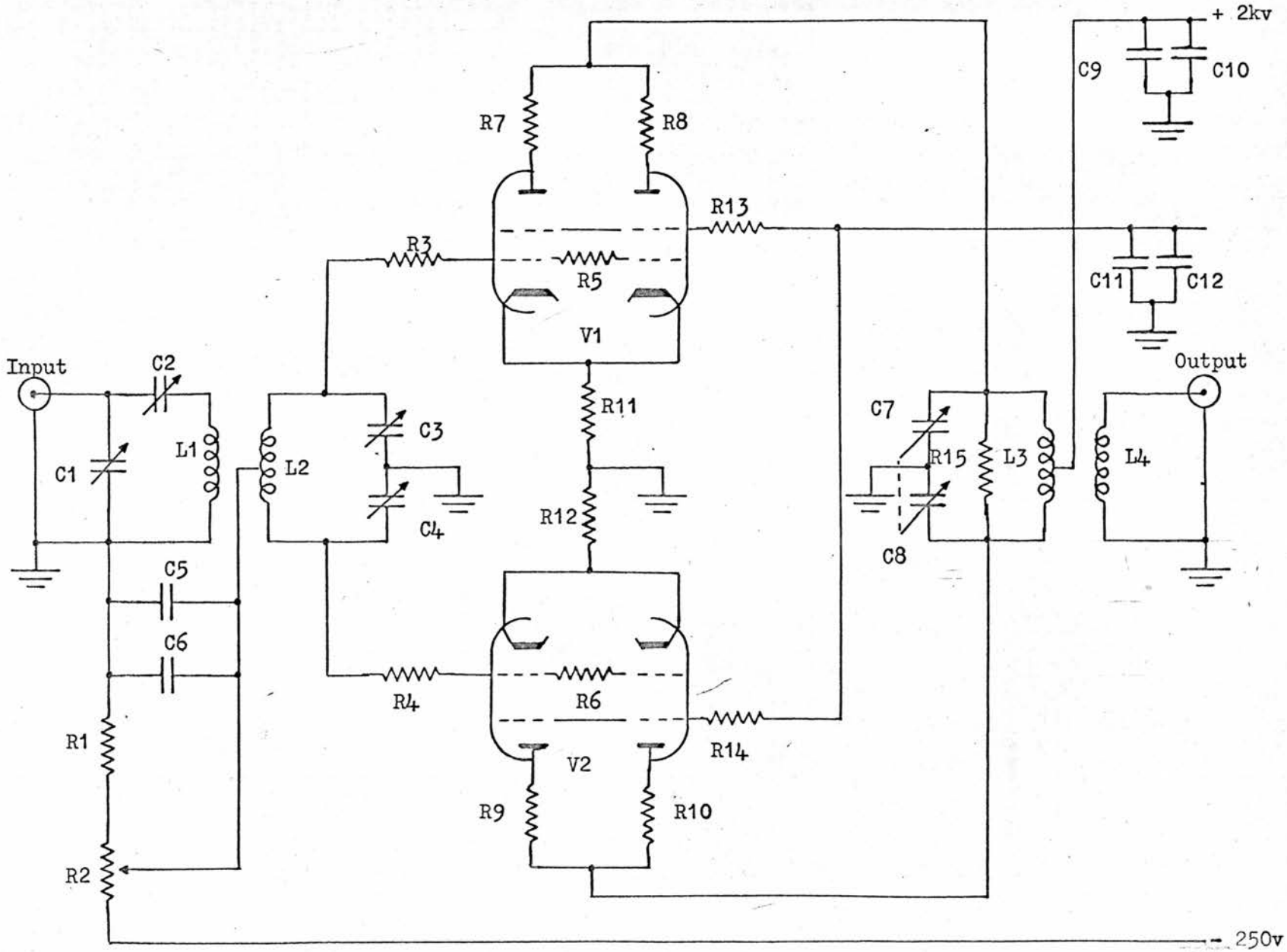
+ 2kv
C9
C10
R7
R8
R13
R3
R5
C11
C12
V1
Input
C2
Output
R11
C7
C1
L1
L2
C3
R15
L3
L4
C4
R12
C8
C5
C6
R4
R6
R14
R1
V2
R9
R10
R2
- 250v

FIGURE 8

times of the oscillator. Although a high Q is desirable for stability this would limit the rise and decay times, as discussed in section 6.2.1, and so a compromise Q value of 14 was chosen.

Resistors R6, R7, R8, R9 and R10 are stoppers to prevent parasitic oscillations. C3 and C7 are bypass condensers, while C4 and C8 are storage condensers.

The oscillator has an output impedance of 5kΩ and a pulse output of 800 volts peak to peak, giving a power output of 15 watts. The rise and decay times were respectively 0.3 μsec and 0.5 μsec.

6.2.7 Intermediate Amplifier

The intermediate amplifier (figure 8) is a fixed bias class C r.f. amplifier using two QQV06-40A valves in parallel push-pull operation. When the r.f. pulse is fed into such a clipping amplifier, well cut off, only the tip of the pulse is allowed to pass through, thus cutting off the trailing edge of the pulse. This type of amplifier is also described by Mansfield and Powles[78].

A π matching network, formed by C1, C2 and L1 was used to match the input to the 75 ohm connecting line.

The control grid voltage, variable from -125v to -250v, is obtained by means of the potentiometer chain R1, R2. The voltage swing on the anodes is limited to 1.5kv peak to peak, and the maximum power output is 1kw. A Q value of 7 was chosen for the anode tank circuit and R15 was set experimentally to 10kΩ. This gave rise and

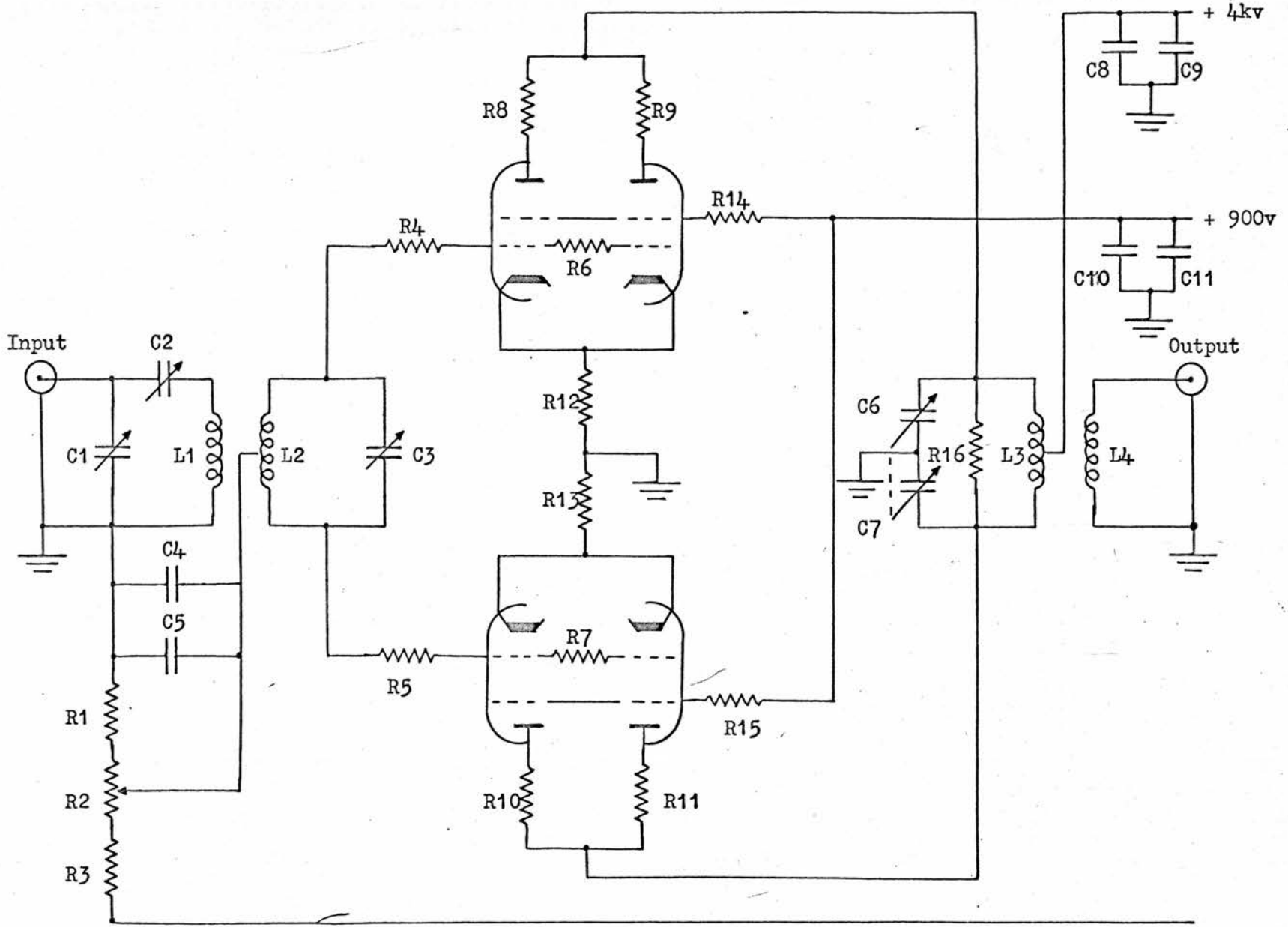
+ 4kv
C8
C9
R8
R9
R14
R4
R6
+ 900v
C10
C11
Input
C2
Output
C1
L1
L2
C3
R12
C6
R16
L3
L4
R13
C7
C4
C5
R7
R5
R15
R1
R2
R10
R11
R3

FIGURE 9

decay times of 0.4 μsec.

Resistors R3 to R14 are all stopper resistors and again all power supply lines have decoupling and bypass capacitors.

The output is fed out by means of an inductive link coupling matched to 75 ohm.

6.2.8 Final Amplifier

The final amplifier (figure 9) has basically the same design as the intermediate amplifier.

A 3E29 tetrode valve was used with 4kv anode voltage, 850 watts on the screen and the control grid bias variable between -18v and -360v. The allowable voltage swing on the anodes is 3kv peak to peak and the maximum obtainable power output is 10kw into a load of 400Ω.

The input to the final amplifier is fed in through a π matching device while the output of amplitude about 2kv r.m.s. is fed out using an inductive link matched to 75Ω.

An unsuccessful attempt was made to reduce the decay time of the r.f. pulse by using a thyraton switching circuit[82].

6.3 The Receiving System

6.3.1 Introduction

The receiving system required for the observation of pulsed n.m.r. signals must be able to

(a) recover from overload conditions in a time of the order of a

few μsec

(b) amplify linearly from approximately 20μv to about 5mv with a voltage gain of about 80db and a low noise figure

(c) amplify signals of the duration of 5 μsec.

The inability of an amplifier to recover quickly from an overload condition is the result of two main effects, namely paralysis and blackout. Paralysis results in loss of gain, following an overload pulse, while the grid bias or interstage coupling condensers charge up, having been discharged during the pulse. To reduce this effect to a minimum, all time constants must be less than the overload pulse width. Blackout[83] can only be eliminated by tube replacement.

To pass a pulse of width t_d the bandwidth B required is given by $B = 2/t_d$. Therefore requirement (c) necessitates an overall bandwidth of 1 MHz if we assume an induction decay with a minimum time constant of 2 μsec. This in turn limits the Q to about 22 as $Q = f/B$ where f is the frequency of operation (22.6 MHz in this case).

A superheterodyne system was chosen because this allowed a commercial I.F. strip to be used. It also allows the use of smaller r.f. bypass capacitors, thus keeping circuit time constants to a minimum.

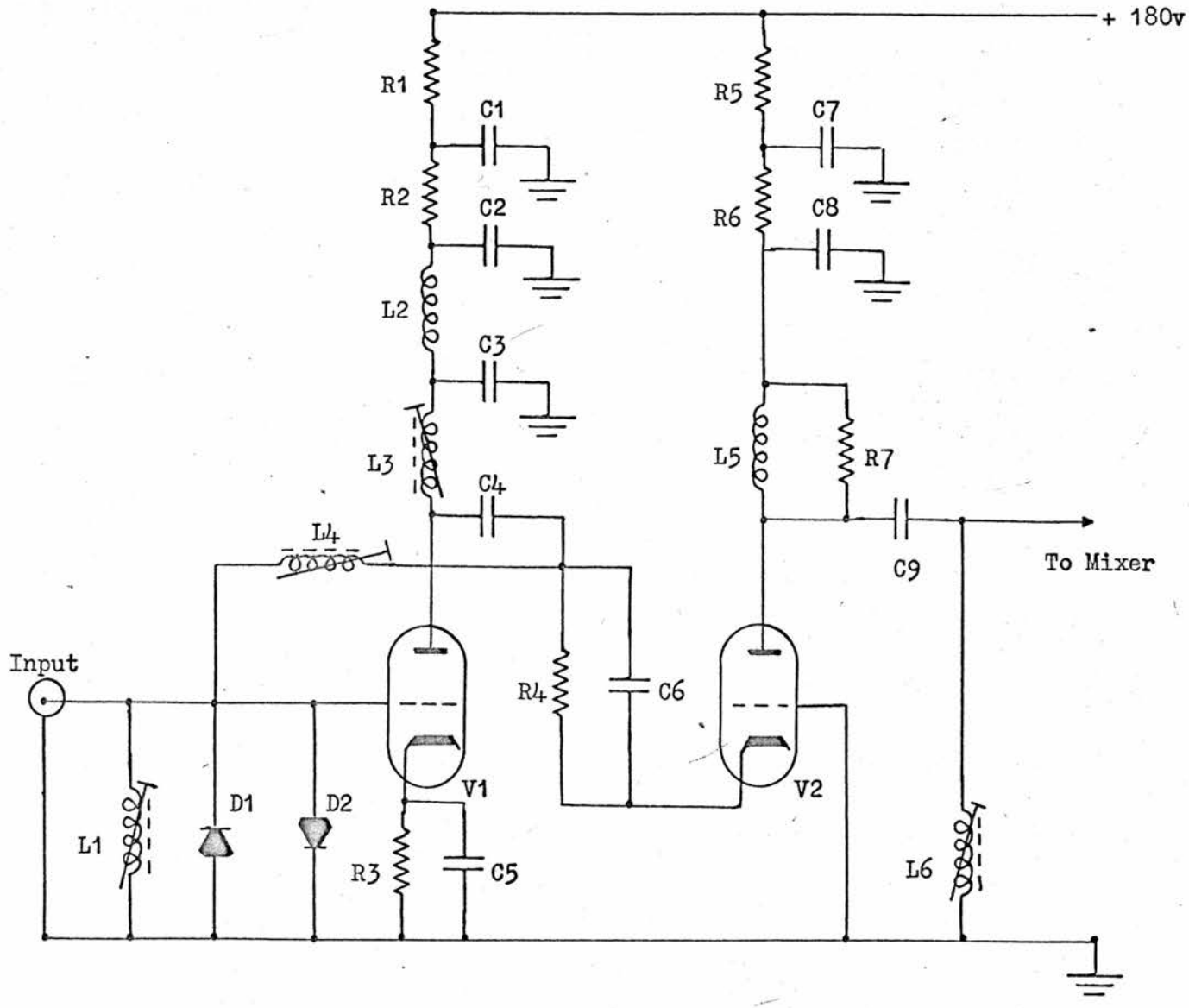
+ 180v
R1
C1
R2
C2
L2
C3
L3
C4
L4
R5
C7
R6
C8
L5
R7
C9
To Mixer
Input
L1
D1
D2
V1
R3
C5
R4
C6
V2
L6

FIGURE 10

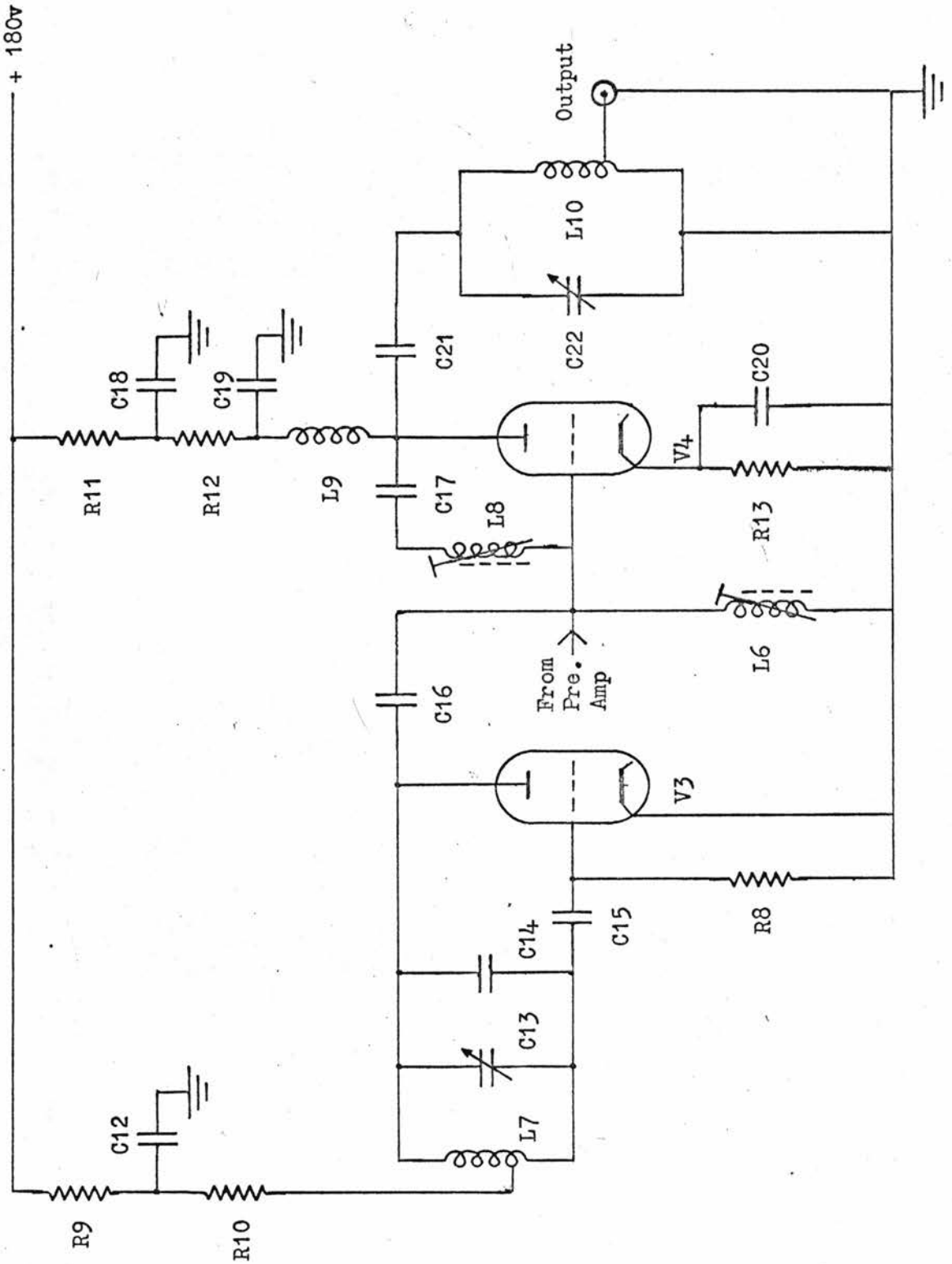
+ 180v
Output
L10
C22
C21
C18
C19
C20
R11
R12
L9
C17
L8
V4
R13
L6
From Pre. Amp
C16
V3
C15
R8
C14
C13
L7
C12
R9
R10

FIGURE 11

6.3.2 The Preamplifier (figure 10)

From low noise considerations it is best to use a cascode amplifier for the first stage of the receiving system. The design used is basically the same as published in a G.E.C. handbook on low noise amplifiers using triodes[84] modified to work at 22.6 MHz.

The crossed diodes, D1 and D2, short circuit the input for the r.f. pulse breakthrough and thus help to prevent saturation in the preamplifier. Little sensitivity is lost when the system is receiving as the diodes then present an impedance of greater than 100kΩ (for signals below 100mv).

The anode supply decoupling resistor and condenser system includes long time constant circuits formed by C_1R_2 and C_7R_6 to eliminate paralysis. Another modification is that the tuning inductance L6 has been moved to the d.c. earth side of the output coupling condenser. This again eliminates paralysis.

The preamplifier gave a power gain of 26db and a linear response for input signals between 2μv and 5mv.

6.3.3 Local Oscillator and Mixer

The local oscillator (figure 11) operating at 62.6 Mc/s uses an EC91 valve in a Hartley oscillator circuit to give an output at the anode of the oscillator of about 15 volts of which only 1.3v are fed through C16 into the mixer. The anode tuned circuit also acts as a tuned r.f. filter between the oscillator and the mixer. The filter

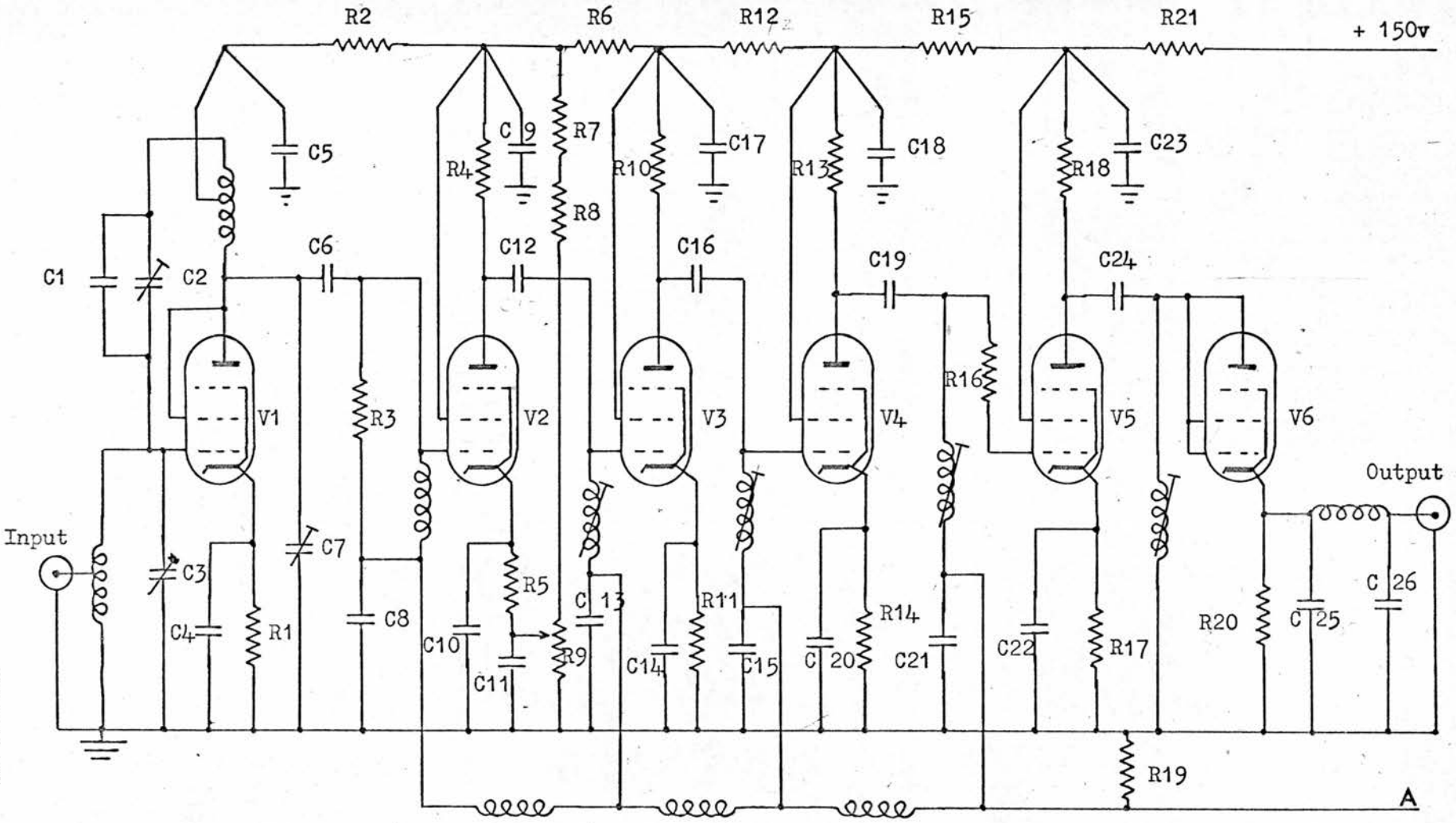
R2
R6
R12
R15
R21
+ 150v
C5
C9
R7
R4
C17
R10
C18
R13
C23
R18
R8
C6
C12
C16
C19
C24
C1
C2
V1
R3
V2
V3
V4
R16
V5
V6
Output
Input
C3
C7
R5
C13
R11
R14
C26
C4
R1
C8
C10
C11
R9
C14
C15
C20
C21
C22
R17
R20
C25
R19
A

FIGURE 12

so formed has a bandwidth small compared with the intermediate frequency and hence no noise side-bands at the intermediate frequency are allowed into the mixer. An exceptionally stable oscillator was not required as the I.F. strip had a bandwidth of 3 MHz.

The mixer cut-off bias is 1.7 volts which is obtained from the cathode resistor R13 using the local oscillator voltage on the grid. Inductance L6 tunes at 22.6 MHz with the output capacitance of V2 in the preamplifier, the input capacitance, and strays while L8 is a neutralisation coil to prevent 22.6 MHz from passing to the anode by means of the grid-anode capacitance.

The cathode bias time constant has again been made small and all power supplies decoupled. The output appears across the tuned circuit formed by C22 and L10, the coil being tapped so that the 75Ω output cable is transformed to an effective load of 10kΩ.

6.3.4 I.F. Strip (figure 12)

The I.F. strip used was a commercial Decca amplifier with a centre frequency of 40 MHz and a bandwidth of 3 MHz. A detector and video amplifier were also included in the unit. This unit had to be modified to improve the paralysis time and the dead time i.e. minimum time between reception of induction decays.

It was found that by moving the gain control from the fourth to the second stage paralysis in the later stages was reduced. The video amplifier (not shown in figure 12) which was part of the

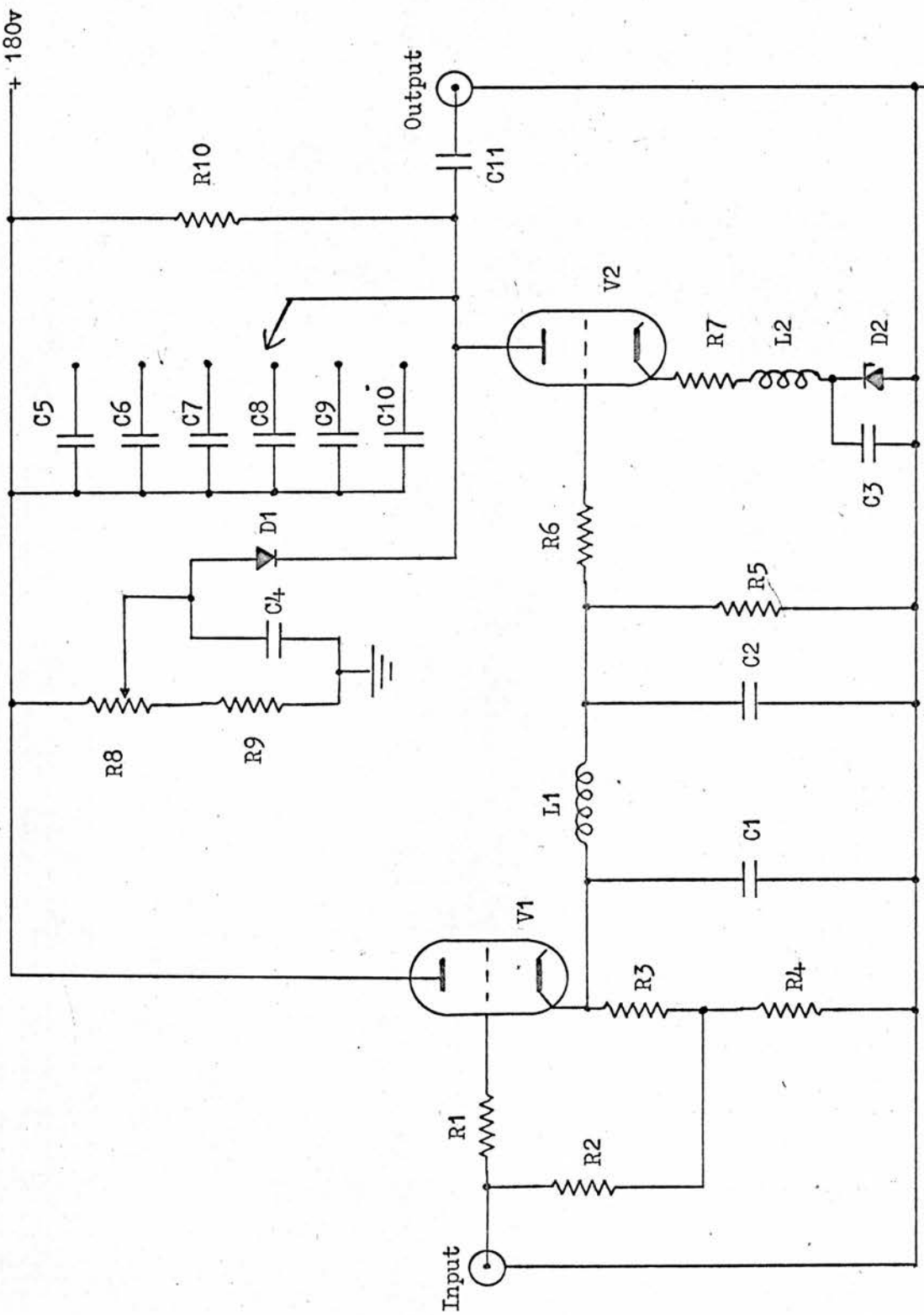
+ 180v
Output
C11
R10
V2
R7
L2
D2
C3
C5
C6
C7
C8
C9
C10
D1
C4
R6
R5
C2
R8
R9
L1
C1
V1
R3
R4
R1
R2
Input

FIGURE 13

original unit proved to have a time constant in the 500ms range, and it was thus impossible to observe two induction decays occurring in a time less than about one second. This stage was therefore replaced by a more suitable unit which is described in the next section.

The I.F. strip was also provided with a means of applying suppression pulses, socket A, to the grids of four of the amplifier valves. However this proved unsuccessful in reducing the decay time because the transients produced by the suppression pulses on the grids had a longer decay time than those produced by saturation.

6.3.5 Video Amplifier

The video amplifier, shown in figure 13, was used to replace the one in the unmodified I.F. strip, and was identical to that described by Clark[79].

Valve V1 is used as a cathode follower feeding into the r.f. filter composed of C1, C2 and L1. The video output stage has a variable bandwidth controlled by the switching of capacitors C5, C6 ..... C10 in the anode load circuit of V2. Large peaks which occur during an r.f. pulse are cut off by the clipper formed by diode D1, whose bias is set by the resistor chain R8 and R9.

6.3.6 Oscilloscope

A Hewlett Packard 175A oscilloscope with delayed time base plug-

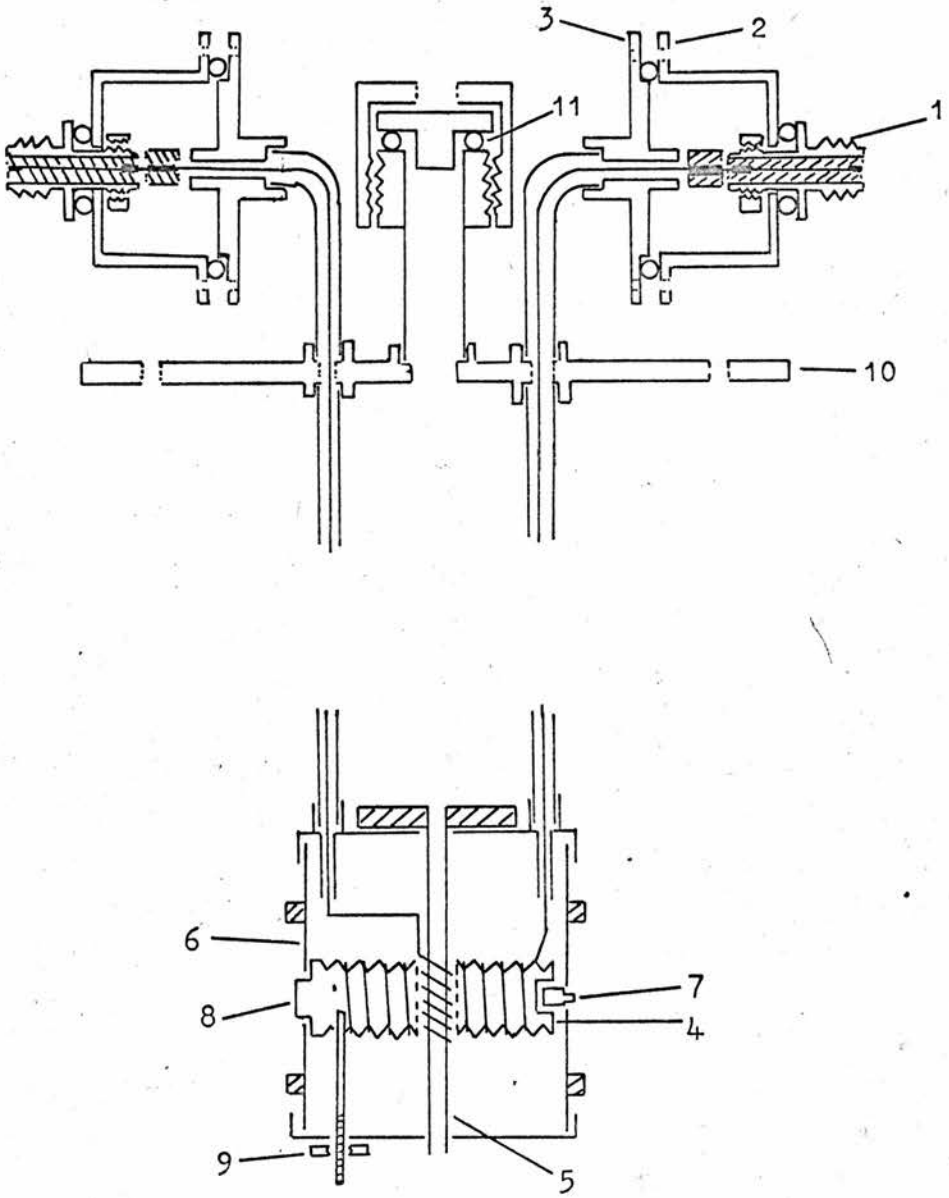

FIGURE 14

in unit 1781B and Y amplifier 1755A (sensitivity 1mv/cm) was used to observe the induction decays and the r.f. pulse from the transmitter. The decays were recorded using a Hewlett Packard 196B Polaroid oscilloscope camera.

A simple form of averaging was performed using a Hewlett Packard 141A storage oscilloscope by photographing the net result of several sequences of induction decays which were stored on the oscilloscope screen. By adjusting the camera settings only the brightest part of the distribution of decays was recorded and a type of average signal was shown on the photograph. An absolute accuracy of 10% is assumed for T_1 measurements by these means.

6.4 Probe and Cryostat Assembly

The probe and cryostat assembly was built for operation from room temperature down to liquid hydrogen temperature 20°K. Figures 14 and 15 show the constructional details.

The r.f. transmitter pulse was fed into the probe via a vacuum tight r.f. socket (1). Kovar to glass vacuum seals proved unsuccessful because of high voltage breakdown. Connection from the vacuum side of the socket was then made to the coaxial minicable (diameter 2.7 mm) which fed the pulse down to the transmitter coil. To enable rapid rewiring of the probe flanges (2) and (3) of the coaxial socket mounting were coupled by an O-ring. The coaxial cable leading down the probe to the transmitter coil was enclosed in a

thin walled stainless steel tube for shielding and rigidity.

A crossed coil arrangement was used in the probe. The transmitter coil (4) had a total of 8 turns of 24 SWG wire wound on a grooved teflon former. A thin walled teflon tube (5) was the former for the 12 turns of 34 SWG enamelled wire of the receiver coil. The receiver coil former fitted through a hole in the transmitter coil former.

The receiver and transmitter coil assembly fitted inside a thin walled isothermal copper shield (6). A simple means of adjusting the orthogonality of the coils was provided. One end of the transmitter coil was fixed in position by a spring loaded pin (7) which fitted into a hole in the shield. The other end of the transmitter had a ridge (8) which could be moved along a vertical slit in the wall of the shield. A piece of 8 BA screwed rod had one end sunk into the transmitter coil former and its other end passed through the cap at the bottom of the shield. By adjusting the nut (9) on the screwed rod, the orthogonality of the coils could be adjusted. Adjustments to the orthogonality were made while observing the breakthrough pulse on the receiver coil.

The coaxial lead from the receiver was taken out by the same method as the transmitter lead entered the probe.

A heater of 32 SWG Eureka wire was non-inductively wound over the outside of the isothermal shield. The leads to this heater and

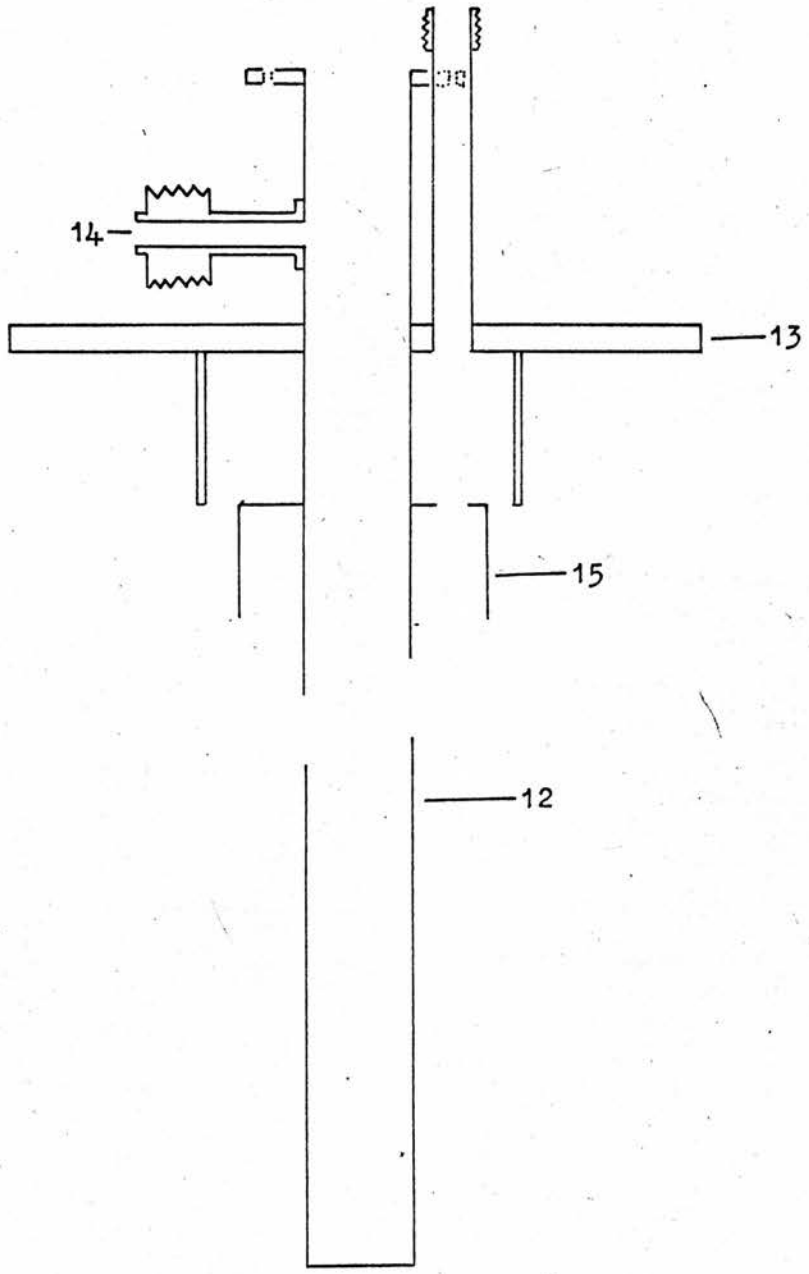

FIGURE 15

the thermocouple which was attached to the sample were led into the probe through vacuum tight Kovar-to-glass seals (not shown in the diagram).

A sample which was gaseous at N.T.P. was contained in a pyrex flask kept above the top flange (10). From the flask a 10 mm pyrex tube led down into the probe through the vacuum O-ring (11) (plug C being removed) and ended in a 4.5 mm tube which fitted into the receiver coil former. A second heater was wound around the sample tube where it narrowed to the 4.5 mm tube. This was to ensure that the sample condensed into the tip of the tube.

The probe assembly then fitted into the thin walled stainless steel jacket (12) of the cryostat assembly (figure 15). Flanges (10) and (13) fitted together with an O-ring.

The probe enclosure could be evacuated through the pumping line (14). The coolant was contained in a 1 litre stepped glass dewar surrounding the steel jacket (12).

Adjustment of the probe position in the magnet gap was by means of the four levelling screws attached to the top plate (13).

A radiation shield (15) was fitted around the stainless steel jacket to reduce heat leak down the cryostat.

A fixed sample temperature was maintained by selecting a suitable exchange gas pressure inside the stainless steel jacket and varying the current through the sample heater. An absolute accuracy

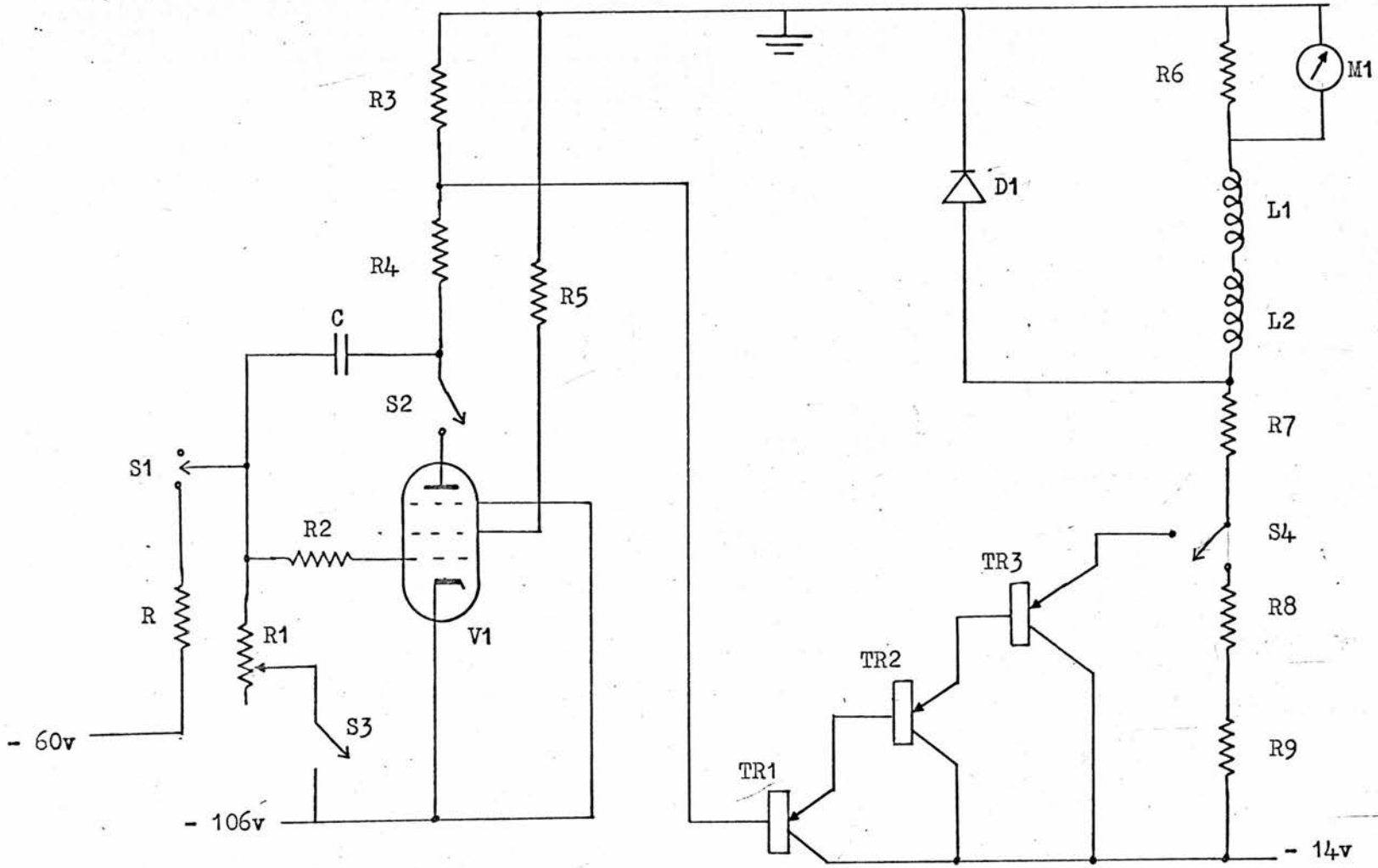
R3
R4
R5
C
S2
S1
R2
R
R1
V1
S3
- 60v
- 106v
D1
R6
M1
L1
L2
R7
S4
TR3
R8
TR2
TR1
R9
- 14v

FIGURE 16

of $\pm$ 1°K was easily obtained by this method.

6.5 Magnet Assembly

6.5.1 Permanent Magnet

The magnet used in the experiments was a permanent magnet having the following specification: field strength 5260 gauss; pole face diameter 8 inches; gap width 2 inches. Special ring-shims designed by Andrew and Rushworth[85,86] were used to increase the field homogeneity to approximately 0.25 gauss/cm^3 which was sufficiently homogeneous for the experiments performed.

By passing a current through the original magnetising coils the field could be swept through approximately 40 gauss.

6.5.2 Field Sweep

The transistorised field sweep, shown in figure 16, was constructed to replace a motor driven potentiometer system which increased the magnetic field by jumps rather than in the required smooth manner.

The closing of switches S1 and S2 allows condenser C to discharge in an approximately linear fashion with a time constant RC. A range of values of R from 20 to 200MΩ was provided. The discharging of C gives a negative ramp voltage at the anode of V1 and hence at the base of transistor TR1. Transistors TR2 and TR3 are both used as emitter followers to increase the current capability of the sweep. The current through the field sweep coils L1 and L2

is measured by the millivoltmeter M1 across the 0.2Ω standard resistor R6.

The sweep can be stopped and held at a fixed position at any time by opening switch S2. Switch S3 and potentiometer R1 were used to set the initial values of the sweep.

It is also possible to sweep the field manually by using switch S4 to disconnect the automatic sweep and then vary the settings of the potentiometers R8 and R9.

7. ETHYLENE

7. ETHYLENE C_2H_4

7.1 Sample

The sample of ethylene was supplied by the National Physical Laboratory, Teddington. The purity was stated to be 99.92 moles per cent, as determined by mass spectrometry, with ethane as the most probable impurity.

The 500ml sample was delivered in a pyrex flask fitted with a break-tip seal and to ensure that the purity of the sample was maintained, the following technique was adopted while transferring the sample. A length of pyrex tubing ending with a thin walled pyrex tip, as described in section 6.4, was sealed to the flask after having inserted a solid glass cylinder. This cylinder of glass, used as a seal breaker, was supported by a constriction designed to prevent glass from the broken seal reaching the bottom of the sample tube. The tube was then evacuated, degassed by torching, and sealed. The break-tip seal was then broken when the sample was required.

The 500ml flask was retained as a storage volume for two reasons. Firstly this allowed the use of a thin walled sample tube tip and hence a good filling factor. Secondly it avoided the risk of explosion and subsequent damage to the n.m.r. probe on heating the sample from its solid to its gaseous state.

7.2 Physical Data

7.2.1 Molecular Structure

The ethylene molecule is planar with D_{2h} symmetry. There are however significant differences between the values of the C-H bond length and ∠HCH as evaluated using the techniques of Raman spectroscopy[87], infrared spectroscopy[88], and electron diffraction[89]. In their second paper[90] Bartell et al. reviewed all the published results and suggested that the variations might be the result of complications in the interpretation of the mean distances measured by the spectroscopic methods. They also discarded their earlier result[89] for the bond length C-H because of errors introduced by the apparatus. After applying corrections to the spectroscopic results to allow for molecular vibrations, they found that the revised values then agreed, within the limit of experimental error, with those found in their electron diffraction experiment. The values of the molecular parameters are as follows

$$\begin{aligned} \text{C-H} \quad & 1.103 \pm 0.001 \text{ Å} \\ \text{C = C} \quad & 1.336 \pm 0.001 \text{ Å} \\ \angle\text{HCH} \quad & 117.2^{\circ} \pm 1.2^{\circ} \end{aligned}$$

7.2.2 Crystal Structure

Although it is impossible to fix the ethylene proton positions using X-ray diffraction, because of the low diffracting power of

C_2H_4

a=4.87 Å
b=6.46 Å
c=4.14 Å

Pnnm (D_{2h}^{12})

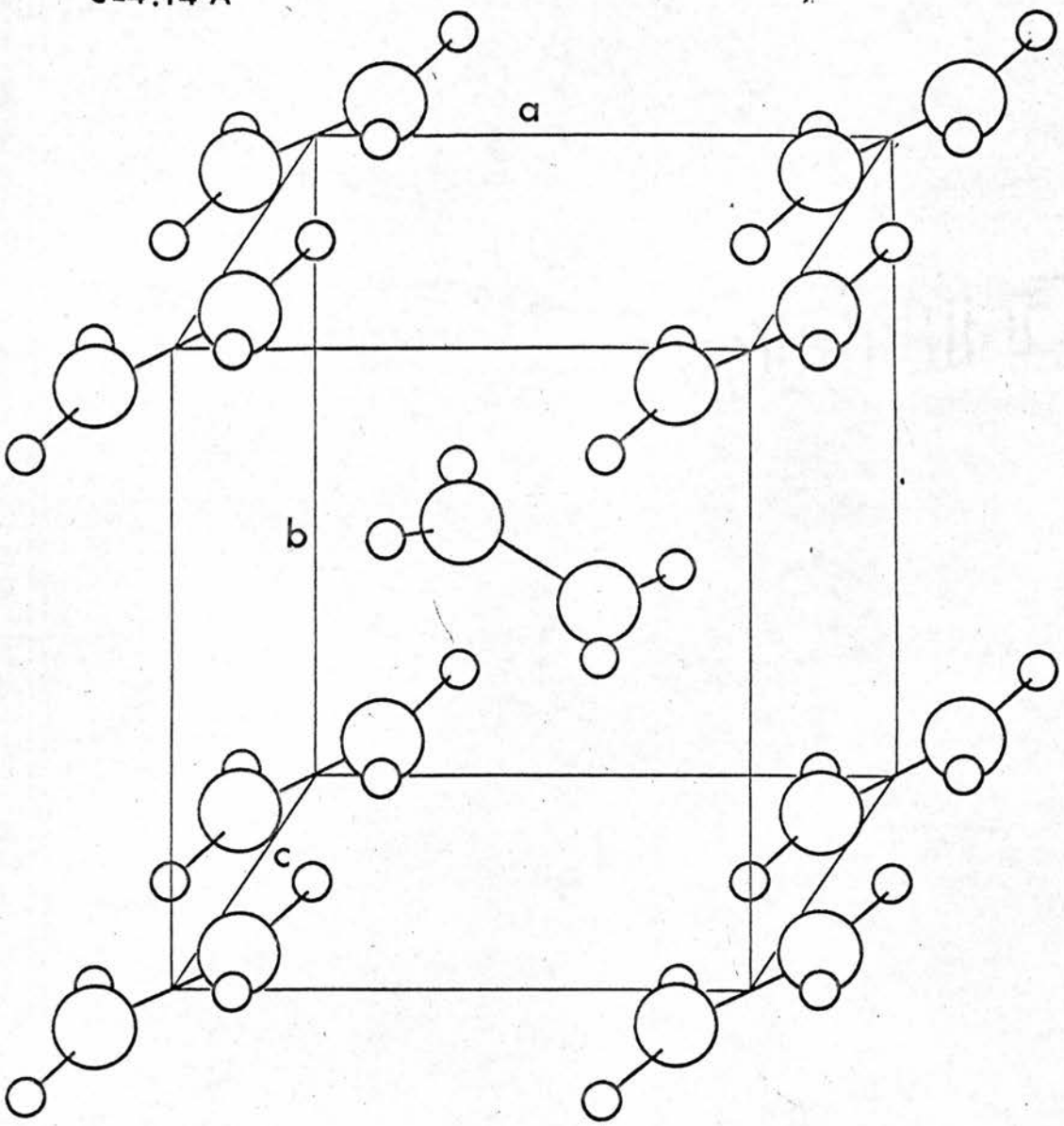

FIGURE 17

$C_2 H_4$

a=4.87 Å
b=6.46 Å
c=4.14 Å

$P2_1 / n \ (C_{2h}^5)$

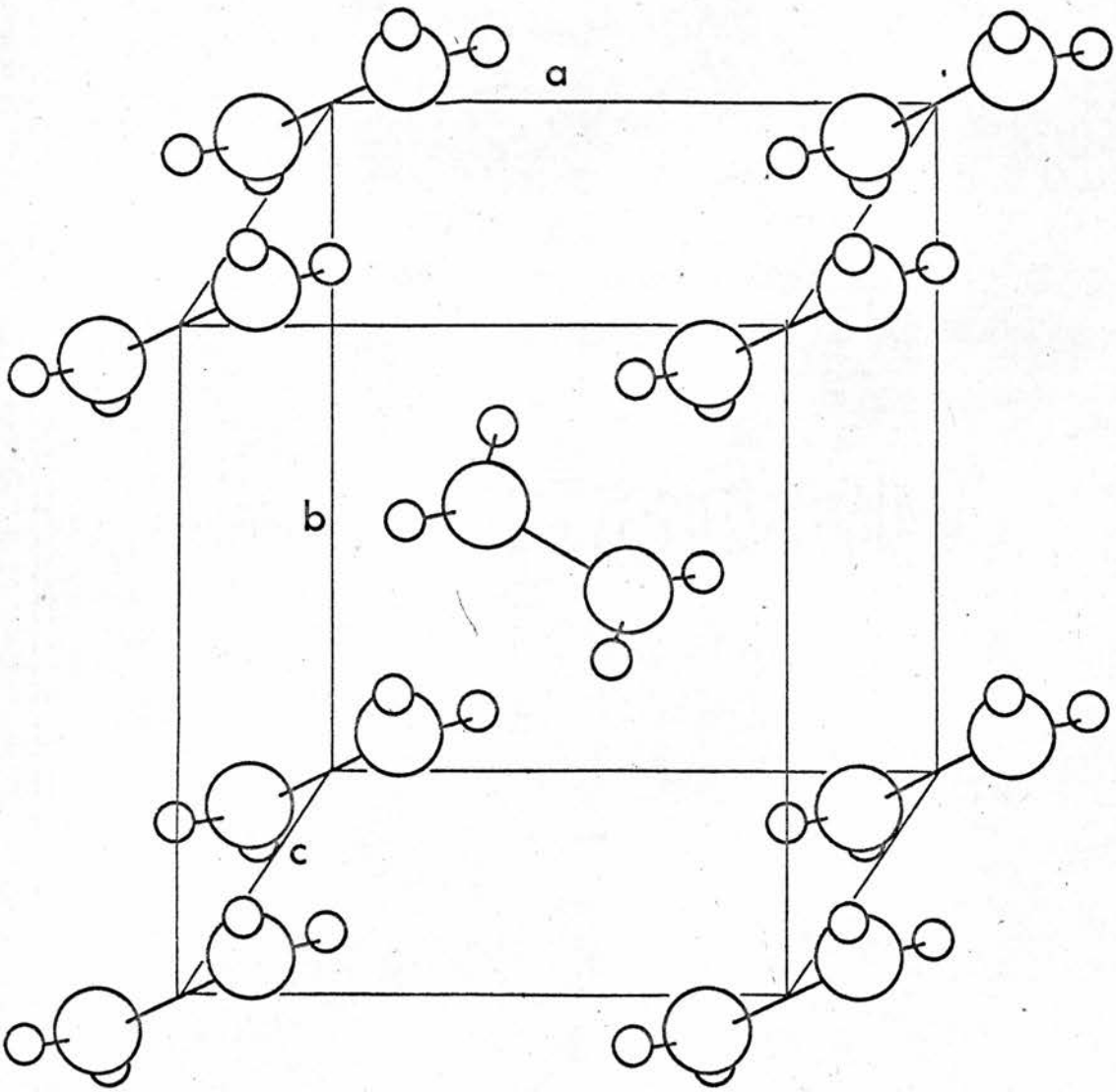

FIGURE 18

protons, Bunn[91] and Keesom and Taconis[92] proposed a $P_{nnm}(D_{2h}^{12})$ space group for the ethylene structure by considering their diffraction results in conjunction with theoretical considerations of the effective radii of the hydrogen and carbon atoms. The $P_{nnm}(D_{2h}^{12})$ structure, shown in figure 17, is orthorhombic with unit cell dimensions: a = 4.87 Å, b = 6.46 Å and c = 4.14 Å, while the C = C bond lies in the ab plane and makes an angle of 36° with the a axis.

Polarised infrared studies by Brecher[93] and by Brecher and Halford[94] on a single crystal of ethylene led to the proposal of a $P_{21}/n(C_{2h}^{5})$ structure. This differs from the previous model by a rotation of the planes of the molecules and could equally well have been predicted from the previous experimental results. In the $P_{21}/n(C_{2h}^{5})$ structure, see figure 18, the molecular planes are perpendicular to the unit cell body diagonals and the two shortest intermolecular H-H distances are equal.

Jacox[95] has obtained high resolution infrared spectra for polycrystalline ethylene at 4°K and 53°K and found that the spectra at 4°K favour the $P_{nnm}(D_{2h}^{12})$ structure while at 53°K the $P_{21}/n(C_{2h}^{5})$ space group is the more probable. There was however a large experimental error in the measured temperature of the sample and to obtain agreement between spectral and specific heat measurements it was concluded that the gradual phase transition between the two space groups occurred somewhere above 53°K.

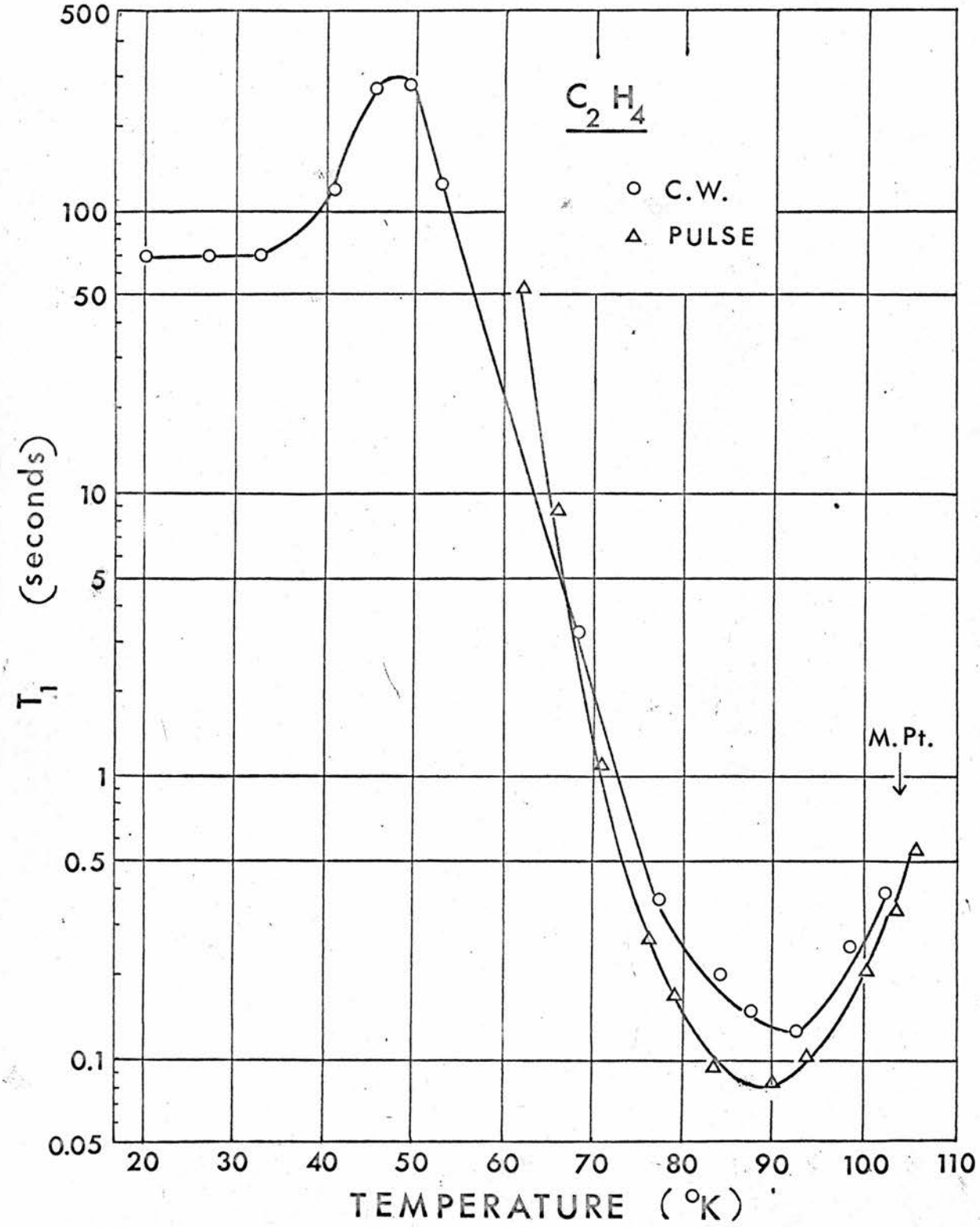
C_2H_4
C.W.
PULSE
M. Pt.
T_1 (seconds)
500
100
50
10
5
1
0.5
0.1
0.05
20
30
40
50
60
70
80
90
100
110
TEMPERATURE (°K)

FIGURE 19

7.2.3 Thermal Data

Measurements of the specific heat of ethylene in the range 15°K to the melting point, 103.95 ± 0.05°K, were made by Egan and Kemp[96]. Up to 90°K the specific heat curve showed no evidence of solid state phase transitions, while at 90°K a small λ-type anomaly occurred.

An attempt to measure the barrier to reorientation about the C = C axis has been made by Todireanu[97] using the scattering of slow neutrons by ethylene adsorbed on activated charcoal at 80°K. He was however only able to estimate a lower limit of 2.2 kcal/mole for the barrier to rotation.

7.3 Results

7.3.1 Spin-lattice Relaxation Time

The variation of T_1 with temperature as measured by C.W. techniques (circular data points) and pulse techniques (triangular data points) is shown in figure 19.

The C.W. measurements from 20°K to the melting point were made by Hoch[40]. These measurements show a minimum T_1 value of 120 msec at about 90°K and a curious anomaly at 50°K and below. The measurements were made during one run using liquid hydrogen (20°K) then liquid nitrogen as coolant. A separate run was then made to check the presence of the low temperature anomaly. Below 60°K the direct recovery method (section 5.2) was used (T_1 > 100S) while at higher temperatures progressive saturation was employed.

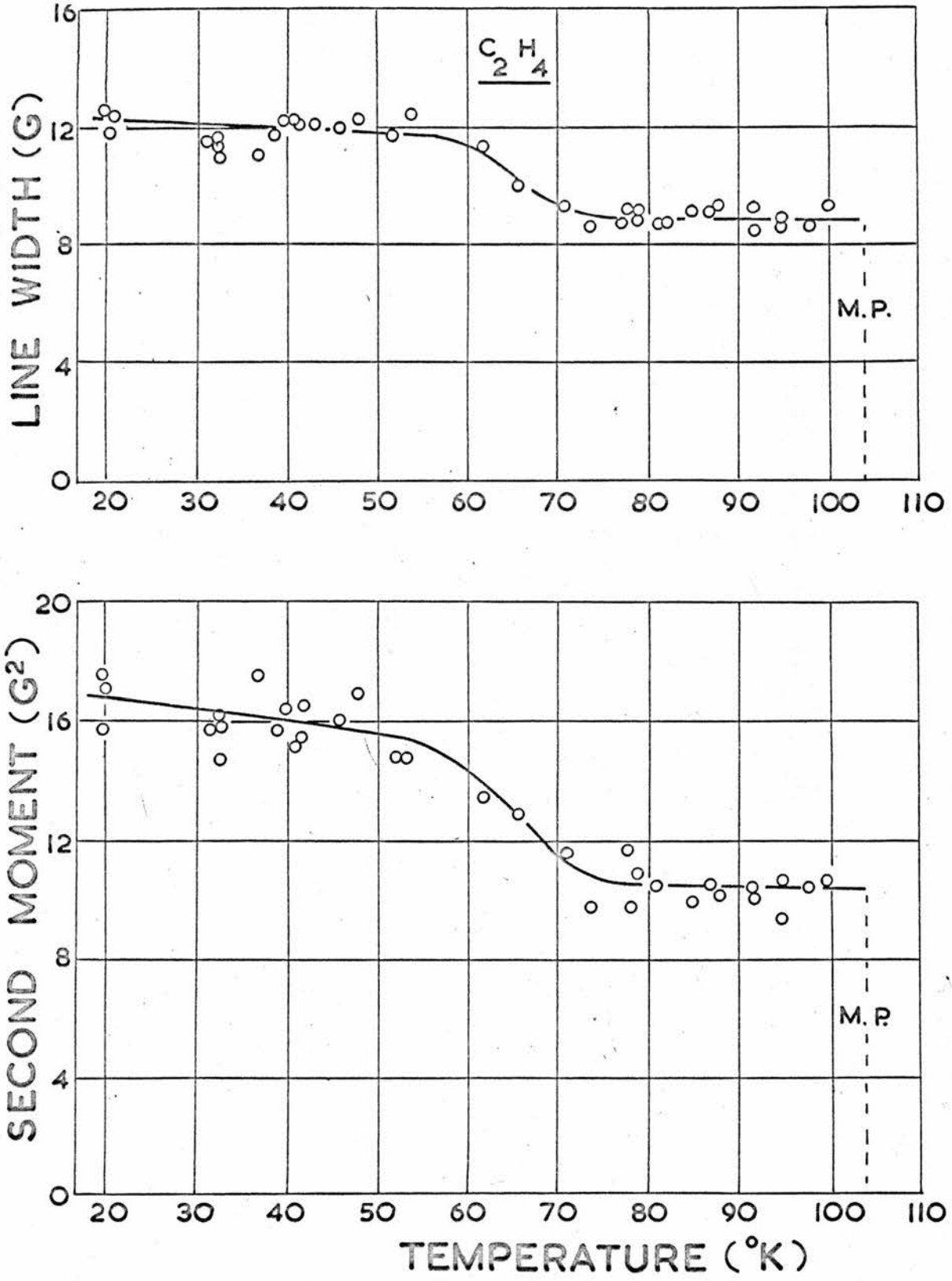
C_2H_4
LINE WIDTH (G)
0
4
8
12
16
M.P.
20
30
40
50
60
70
80
90
100
110
SECOND MOMENT (G^2)
0
4
8
12
16
20
M.P
TEMPERATURE (°K)

FIGURE 20

The pulse techniques described in section 5.1 were used to obtain values of T_1 between 105°K and 62°K (pumped nitrogen). Unfortunately liquid nitrogen was not available when these measurements were made. The value of T_1 minimum obtained by pulse methods was 85 ± 9 msec and again it occurred at 90°K.

7.3.2 Second Moment and Line Width

Line width and second moment measurements (figure 20) were performed on ethylene between 20°K and the melting point by Hoch[40]. No fine structure or excessively narrowed liquid line was observed over the temperature range investigated but a slight narrowing of the line occurred between 55°K and 75°K.

7.4 Discussion

7.4.1 Spin-lattice Relaxation Time

Because of the occurrence of a minimum in the T_1 against temperature curve it is interesting to attempt to find a correlation between the measured value of T_1 minimum and the theories of chapter 4. The random Brownian motion model (B.P.P.) will be used first, and then the theory of reorientation about a two-fold axis will be developed in two ways.

First if we are to use the B.P.P. random motion model of section 4.2 the theory must be generalised for the case of more than two protons. For two protons separated by a distance b, the minimum value of T_1 is given by combining equations 4.4 and 4.7 to give,

$$\frac{1}{T_{1(min)}} = A\, b^{-6} \qquad 7.1$$

where $$A = \frac{0.426}{\omega_o}\gamma^4\hbar^2 \quad .$$

We now assume that the dipolar interaction can be expressed as a sum of pair interactions. This means that if nuclei i, j and k interact then the interactions of i with j and i with k are independent and unaffected by the interaction of j and k i.e. there are no cross correlation terms of the type described in section 4.3.2. Hence for the i^{th} nucleus

$$\frac{1}{T_{1(min)}^{i}} = A \sum_j r_{ij}^{-6} \quad . \qquad 7.2$$

From which it follows that the decay of magnetisation of the i^{th} nucleus is given by $\exp(-t/T_{1(min)}^{i})$.

If all the nuclei are identical the resultant decay for all the nuclei is

$$N^{-1} \sum_i \exp\left[- t\, A \sum_j r_{ij}^{-6}\right] .$$

This is in general non-exponential as it is the sum of exponentials. However this expression is normally used[98] to obtain the best approximate exponential $\exp(-t/T_{1(min)})$ where,

$$\frac{1}{T_{1(\min)}} = N^{-1} A \sum_{i,j} r_{ij}^{-6} . \qquad 7.3$$

In addition, if all the nuclei are equivalent, this can be rewritten as

$$\frac{1}{T_{1(\min)}} = A \sum_{j} r_{ij}^{-6} \qquad 7.4$$

which is simply equation 7.2 for the relaxation of the i^{th} nucleus.

For clarity, the protons of an ethylene molecule are referred to by the numbers shown in the figure below.

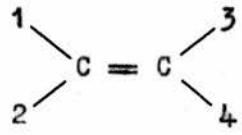

It is now possible to calculate the value of $T_{1(\min)}$, for the intramolecular effect, as predicted by the B.P.P. random reorientation theory. If we assume that in the ethylene molecule one of the protons, say 1, has a dipolar relaxation interaction with all three of the remaining protons, then from 7.4

$$\frac{1}{T_{1(\min)}} = A \left[r_{12}^{-6} + r_{13}^{-6} + r_{14}^{-6} \right] \qquad 7.5$$

which, with the molecular structure of section 7.2.1, gives a $T_{1(\min)}$ value of 21 msec. Even before allowing for the contribution to

$T_{1(min)}$ from vibrational motion, which would lower the value of T_1, this result is a factor of four times less than the measured value. Random Brownian reorientation is therefore not the cause of the relaxation effect in ethylene. It should be noted that because of the relative magnitudes of the interproton distance r_{12} and the distance between proton 1 and a proton on a different molecule, the intermolecular effect contributes only a negligible amount to the total relaxation, as calculated by this method.

Although it is not strictly valid to separate the dipolar interactions, it will be useful, for the purpose of future discussions, to examine the contributions from the individual proton pairs within a molecule. The principal interactions obviously comes from the closest protons i.e. protons 1 and 2. This interaction by itself would produce a $T_{1(min)}$ of 25 msec. The interactions between protons 1 and 3 and 1 and 4 have less effect and would by themselves yield values of $T_{1(min)}$ of 183 msec and 550 msec respectively.

It should be emphasized at this point that the B.P.P. random motion theory is seldom used to estimate $T_{1(min)}$. The normal procedure is to find the value of the constant C_1 in equation 4.7 from the measured value of $T_{1(min)}$, if it is observable, and then to substitute into formula 4.4 to predict the values of T_1 at different temperatures.

The theory of section 4.3 for the relaxation occurring in a system in which the molecules are undergoing reorientation between two equilibrium positions will now be applied to the system of ethylene molecules. Equations 3.25 and 3.27 can be written as

$$\frac{1}{T_1} = \frac{9}{4}\gamma^4\hbar^2\Big[\sum_{i\neq j}\left(<\overline{c^*_{ij}(0)c_{ij}(\tau)}> f(\omega_o) + <\overline{e^*_{ij}(0)e_{ij}(\tau)}> f(2\omega_o)\right)$$

$$+ \sum_{\substack{i\neq j\\ i'\neq j'}}^{R}\left(<\overline{c^*_{ij}(0)c_{i'j'}(\tau)}> f(\omega_o) + <\overline{e^*_{ij}(0)e_{i'j'}(\tau)}> f(2\omega_o)\right)\Big] \qquad 7.6$$

where
$$f(\omega) = \frac{\tau_c}{(1+\omega^2\tau_c^2)} \quad . \qquad 7.7$$

The first summation is over all i and j with $i\neq j$. In the second summation $\sum^R$ has the same meaning as in equation 3.27 i.e. the summation is performed over all i, j, i' and j' with $i\neq j$ and $i'\neq j'$ and with the added restriction that $i\neq i'$ and $j\neq j'$ at the same time. This last restriction merely avoids the repetition of terms already present in the first summation.

Because the nuclei are identical and equivalent 7.6 can be rewritten as

ETHYLENE.

α positions

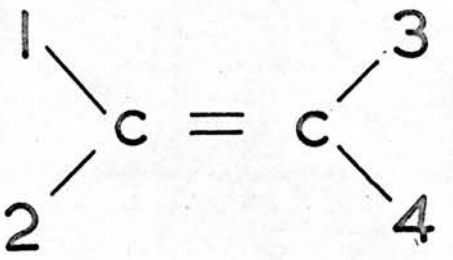

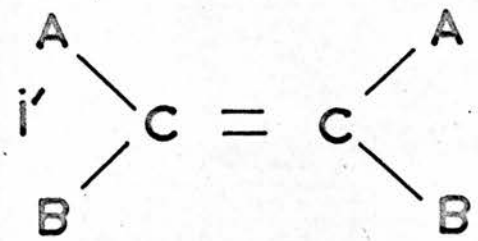

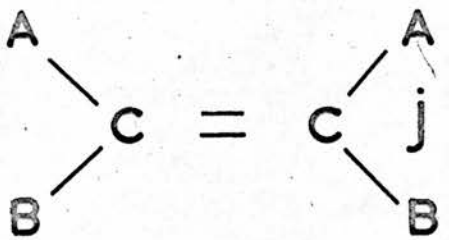

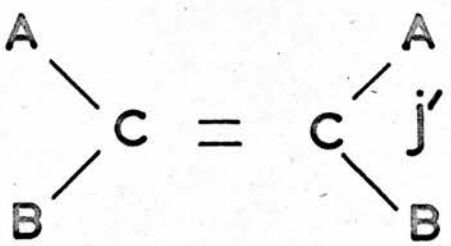

β positions

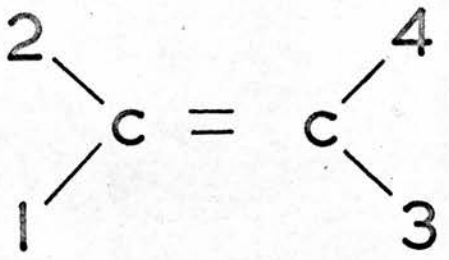

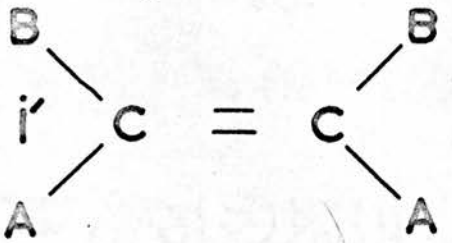

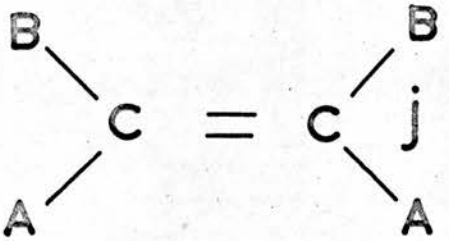

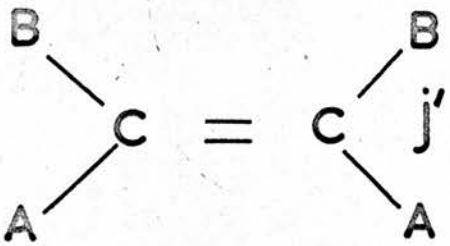

FIGURE 21

$$\frac{1}{T_1} = \frac{9}{4}\gamma^4\hbar^2 \Big[\sum_{j\neq 1} \left(\overline{< c^*_{1j}(0)c_{1j}(\tau) >} f(\omega_o) + \overline{< e^*_{1j}(0)e_{1j}(\tau) >} f(2\omega_o) \right) \qquad 7.8$$

$$+ \sum_{\substack{j\neq 1 \\ i'\neq j'}}^{R} \left(\overline{< c^*_{1j}(0)c_{i'j'}(\tau) >} f(\omega_o) + \overline{< e^*_{1j}(0)e_{i'j'}(\tau) >} f(2\omega_o) \right) \Big]$$

where i does not now appear in the summation because the i^{th} proton has been fixed as proton number 1.

It is convenient to adopt the notation shown in figure 21 for the system of ethylene molecules. The two protons linked to the same carbon atom are denoted by the letters A and B, and form a pair. These proton pairs are referred to by the letters i', j and j'. Note that although the diagram shows proton pairs j and j' on different molecules, it is of course possible for them to be on the same molecule. Also some molecule on the system is chosen as a reference and the protons of this molecule are then labelled 1, 2, 3 and 4. The diagram also shows the two positions of each of the molecules, namely the α and β positions, and it is seen that on moving between these positions i.e. a flip of 180° about the C = C bond, the positions of the protons in any one pair are interchanged e.g. the α position of proton i'A is the same as the β position of proton i'B.

First, because of the convenient result obtained, the cross

correlation terms of equation 4.21 will be evaluated using the theory of section 4.3. It is important to note that these terms only occur if the motions of the molecules are correlated. By correlated we mean that when one molecule flips then the adjacent molecules must flip e.g. if protons A and B on the j^{th} proton pair interchange positions, then protons A and B of the j'^{th} proton pair on an adjacent molecule will interchange positions.

From section 4.3.2 we have for four protons, labelled i, j, i' and j', cross correlation terms of the form

$$\overline{c^{*}_{ij}(0)c_{i',j'}(\tau)} = C(^{\alpha}_{ij}|_{i',j'}^{\alpha}) + C(^{\beta}_{ij}|_{i',j'}^{\beta}) - C(^{\alpha}_{ij}|_{i',j'}^{\beta}) - C(^{\beta}_{ij}|_{i',j'}^{\alpha}) \qquad 7.9$$

where

$$C(^{\alpha}_{ij}|_{i',j'}^{\beta}) = \frac{1}{4}(r^{\alpha}_{ij})^{-3}(r^{\beta}_{i',j'})^{-3} \times \sin\theta^{\alpha}_{ij}\cos\theta^{\alpha}_{ij}\sin\theta^{\beta}_{i',j'}\cos\theta^{\beta}_{i',j'}\cos(\Phi^{\alpha}_{ij} - \Phi^{\beta}_{i',j'}) \qquad 7.10$$

and similar expressions for $\langle \overline{e^{*}_{ij}(0)e_{i',j'}(\tau)} \rangle$. For four protons there would therefore be 20 terms of the type $\langle \overline{c^{*}_{ij}(0)c_{i',j'}(\tau)} \rangle$ and 20 of the type $\langle \overline{e^{*}_{ij}(0)e_{i',j'}(\tau)} \rangle$. In our new notation we are interested in the effect of all protons on a proton labelled 1 and we therefore only have terms of the type

$$\overline{\langle c^{*}_{1,i'A}(0)c_{jB,j'A}(\tau)\rangle} = C(_1\,{}^{\alpha}_{i'A}|_{jB}\,{}^{\alpha}_{j'A}) + C(_1\,{}^{\beta}_{i'A}|_{jB}\,{}^{\beta}_{j'A})$$

$$- C(_1\,{}^{\alpha}_{i'A}|_{jB}\,{}^{\beta}_{j'A}) - C(_1\,{}^{\beta}_{i'A}|_{jB}\,{}^{\alpha}_{j'A}) \quad . \qquad 7.11$$

The commas have been added to the expression on the left hand side of equation 7.11 to separate the proton labels.

Now, because the α positions of protons jA and j'B are the β positions of protons jB and j'A, equation 7.11 becomes

$$\overline{\langle c^{*}_{1,i'A}(0)c_{jB,j'A}(\tau)\rangle} = C(_1\,{}^{\alpha}_{i'A}|_{jA}\,{}^{\beta}_{j'B}) + C(_1\,{}^{\beta}_{i'A}|_{jA}\,{}^{\alpha}_{j'B})$$

$$- C(_1\,{}^{\alpha}_{i'A}|_{jA}\,{}^{\alpha}_{j'B}) - C(_1\,{}^{\beta}_{i'A}|_{jA}\,{}^{\beta}_{j'B}) \qquad 7.12$$

$$= - \overline{\langle c^{*}_{1,i'A}(0)c_{jA,j'B}(\tau)\rangle} \quad .$$

Hence

$$\overline{\langle c^{*}_{1,i'A}(0)c_{jA,j'B}(\tau)\rangle} + \overline{\langle c^{*}_{1,i'A}(0)c_{jB,j'A}(\tau)\rangle} = 0$$

and similarly

$$\overline{\langle c^{*}_{1,i'B}(0)c_{jA,j'B}(\tau)\rangle} + \overline{\langle c^{*}_{1,i'B}(0)c_{jB,j'A}(\tau)\rangle} = 0$$

$$< \overline{c^{*}_{1,i'B}(0)c_{jA,j'A}(\tau)} > + < \overline{c^{*}_{1,i'B}(0)c_{jB,j'B}(\tau)} > = 0$$

$$< \overline{c^{*}_{1,i'B}(0)c_{jB,j'B}(\tau)} > + < \overline{c^{*}_{1,i'B}(0)c_{jA,j'A}(\tau)} > = 0$$

$$< \overline{c^{*}_{1,i'B}(0)c_{jB,j'A}(\tau)} > + < \overline{c^{*}_{1,i'B}(0)c_{jA,j'B}(\tau)} > = 0$$

$$< \overline{c^{*}_{1,i'A}(0)c_{jB,j'B}(\tau)} > + < \overline{c^{*}_{1,i'A}(0)c_{jA,j'A}(\tau)} > = 0$$

$$< \overline{c^{*}_{1,i'A}(0)c_{jB,j'A}(\tau)} > + < \overline{c^{*}_{1,i'A}(0)c_{jA,j'B}(\tau)} > = 0$$

$$< \overline{c^{*}_{1,i'A}(0)c_{jA,j'A}(\tau)} > + < \overline{c^{*}_{1,i'A}(0)c_{jB,j'B}(\tau)} > = 0$$

A similar set of equations can also be formed for terms of the type $< \overline{e^{*}_{ij}(0)e_{i'j'}(\tau)} >$. Because the proton pairs labelled i', j and j' can refer to any proton pair, including the proton pair on the same molecule as that containing proton 1, the set of equations 7.13 is complete. The significance of the equations is that if we choose any cross correlation term formed by any three or four protons in the complete system, it is always possible to find another term of equal magnitude, but opposite sign. There-

fore the net effect of cross correlation terms in ethylene is zero, whether the molecular motion is correlated or uncorrelated.

The next effect to be considered is the pure intramolecular interaction i.e. the effect of protons labelled 2, 3 and 4 on proton 1. From equation 3.27, 4.17 and 4.20, in order to calculate the intramolecular effect, we must find the values of the terms of the form $\overline{\langle c_{1j}^{\alpha}(0)c_{1j}(\tau)\rangle}$ and $\overline{\langle e_{1j}^{\alpha}(0)e_{1j}(\tau)\rangle}$ or rather $\left[c_{1j}^{\alpha} - c_{1j}^{\beta}\right]^2$ and $\left[e_{1j}^{\alpha} - e_{1j}^{\beta}\right]^2$ where j now denotes protons 2, 3 or 4, and α and β are again the two equilibrium positions of the ethylene molecule.

Let us first consider the relaxation effect of proton 2 on proton 1 when the molecule flips from its α position to its β position. This contribution will be related to

$$\left[c_{12}^{\alpha} - c_{12}^{\beta}\right]^2 = (r_{12}^{\alpha})^{-6} \sin^2\theta_{12}^{\alpha} \cos^2\theta_{12}^{\alpha} + (r_{12}^{\beta})^{-6} \sin^2\theta_{12}^{\beta} \cos^2\theta_{12}^{\beta}$$
$$- 2 (r_{12}^{\alpha})^{-3} (r_{12}^{\beta})^{-3} \sin\theta_{12}^{\alpha} \cos\theta_{12}^{\alpha} \sin\theta_{12}^{\beta} \cos\theta_{12}^{\beta} \cos(\Phi_{12}^{\alpha} - \Phi_{12}^{\beta}) \qquad 7.14$$

and

$$\left[e_{12}^{\alpha} - e_{12}^{\beta}\right]^2 = (r_{12}^{\alpha})^{-6} \sin^4\theta_{12}^{\alpha} + (r_{12}^{\beta})^{-6} \sin^4\theta_{12}^{\beta}$$
$$- 2 (r_{12}^{\alpha})^{-3} (r_{12}^{\beta})^{-3} \sin^2\theta_{12}^{\alpha} \sin^2\theta_{12}^{\beta} \cos 2(\Phi_{12}^{\alpha} - \Phi_{12}^{\beta}) \quad . \qquad 7.15$$

When the ethylene molecule flips protons 1 and 2 interchange

position and therefore the internuclear vector between protons 1 and 2 simply reverses its direction.

Hence, $$\theta_{12}^{\beta} = \pi - \theta_{12}^{\alpha}$$

while $$\Phi_{12}^{\alpha} - \Phi_{12}^{\beta} = \pi \qquad 7.16$$

and therefore, $\left[c_{12}^{\alpha} - c_{12}^{\beta}\right]^2 = \left[e_{12}^{\alpha} - e_{12}^{\beta}\right]^2 = 0$ giving

$\overline{< c_{12}^{*}(0)c_{12}(\tau)>} = \overline{< e_{12}^{*}(0)e_{12}(\tau)>} = 0$ which predicts that when the molecule flips, the motion of proton 2 has no relaxation effect on proton 1.

Let us now consider the effect of proton 3 on proton 1. When the molecule flips about its C = C bond, the internuclear vector between protons 1 and 4 maintains its initial direction in space.

Hence, $$\theta_{13}^{\alpha} = \theta_{13}^{\beta}$$

$$\Phi_{13}^{\alpha} = \Phi_{13}^{\beta} \qquad 7.17$$

and therefore from equation 4.20 $\left[c_{13}^{\alpha} - c_{13}^{\beta}\right]^2 = \left[e_{13}^{\alpha} - e_{13}^{\beta}\right]^2 = 0$

and $\overline{< c_{13}^{*}(0)c_{13}(\tau)>} = \overline{< e_{13}^{*}(0)e_{13}(\tau)>} = 0$. Hence the relaxation of proton 1 is unaffected by the interaction with proton 3, and therefore the only contribution to the intramolecular relaxation of proton 1 comes from the interaction between protons 1 and 4.

A value of $T_{1(\min)}^{\text{intra}}$ where the relaxation is caused solely by

protons 1 and 4, can be calculated using the model of section 4.3.3. In this case ψ is the angle between the internuclear vector between protons 1 and 4, and the C = C bond. The molecular structure of section 7.2.1 was used and a value of $T_{1(min)}^{intra}$ of 759 msec was found. When this calculated value of $T_{1(min)}^{intra}$ is compared with the experimental $T_{1(min)}$ of 85 msec, it is obvious that the intramolecular interaction by itself is too small to account for the measured relaxation and therefore it is necessary to calculate the effect of protons of neighbouring molecules on the relaxation i.e. the intermolecular effect.

In the calculation of the intermolecular interaction, because the sample is polycrystalline, averages of the correlation functions over all H_o magnetic field directions are involved and it is important to perform this averaging at the correct point in the calculations. The two methods which will be considered are

(A) Averaging separately the individual correlation functions over all possible magnetic field direction, then summing the averages and using the totals to obtain a single value of $T_{1(min)}$.

(B) Calculating total value of the correlation functions for a fixed field direction, using this to find $T_{1(min)}$ for a fixed field direction, repeating the calculations for different field directions, then averaging the values.

In method (A) the coordinates were calculated of all protons up

to a distance of 10 Å from the proton selected to be denoted as proton 1. Again using the model which has two equilibrium positions there are two positions of the internuclear vector $\underline{r}_{1j}$ between protons 1 and j, denoted by $\underline{r}^{\alpha}_{1j}$ and $\underline{r}^{\beta}_{1j}$. The choice of these two internuclear vectors depends on whether the molecular motions are correlated or uncorrelated. For example, referring to figure 4.21, if the molecular motion is correlated the two vectors between proton 1 and proton jA would be the vectors between 1 and jA, and between 2 and jB; for uncorrelated motion the two possible vectors are those between 1 and jA and between 1 and jB. It is thus possible to find the angle $2\psi_{1j}$ between the two vectors and the magnitudes of these vectors for the cases of correlated and uncorrelated motion. For both types of motion a computer programme was constructed to calculate the values of $\underline{r}^{\alpha}_{1j}$, $\underline{r}^{\beta}_{1j}$ and ψ_{1j} from the Cartesian coordinates of the protons. The auto correlation functions, which have been expressed as functions of the field coordinates Θ and Φ by the technique of section 4.3, are then integrated over all Θ and Φ with the aid of a separate programme (programme 5, Appendix 1). This integration produces a set of averages of the type $\langle C^{*}_{1j} C_{1j} \rangle$ and $\langle E^{*}_{1j} E_{1j} \rangle$ as in section 4.3, which are then summed and inserted into equation 7.8. This equation for $1/T_1$ is then differentiated with respect to τ_c to calculate the $T^{inter}_{1(min)}$. These calculations are performed separately for correlated

and uncorrelated motions, producing two values of $T_{1(min)}$ denoted by $T^{inter}_{1(min)}$ (corr) and $T^{inter}_{1(min)}$ (uncorr); $T^{intra}_{1(min)}$ will have the same value for correlated and uncorrelated motion. We then assume that the $T_{1(min)}$ which results from the intramolecular interactions is given by

$$\frac{1}{T_{1(min)}} = \frac{1}{T^{intra}_{1(min)}} + \frac{1}{T^{inter}_{1(min)}} \quad . \qquad 7.18$$

The intermolecular relaxation has also to be calculated for both possible crystal structures of ethylene. The table below shows the values of $T_{1(min)}$ calculated using the $T^{intra}_{1(min)}$ value of 759 msec calculated previously.

Table 7.1

	$P_{21}/n(C^5_{2h})$	$P_{nnm}(D^{12}_{2h})$
$T^{inter}_{1(min)}$ (corr)	117 msec	62 msec
$T^{inter}_{1(min)}$ (uncorr)	176 msec	94.5 msec
$T_{1(min)}$ (corr)	101 msec	69 msec
$T_{1(min)}$ (uncorr)	143 msec	84 msec

Before discussing these results, an outline of the second method

of averaging will be given.

In method (B), suggested by Jeener[99], the assumption is made that the sample is composed of a number of crystallites each having a different orientation with respect to the steady magnetic field. In each crystallite we consider only protons within 10 Å of the proton selected as proton 1, and find their coordinates with respect to the crystal axes. A field direction is then chosen and the coordinates of the protons of the crystallite transformed into a coordinate frame in which the field direction is the Z axis. The auto correlation averages $\overline{< c^{*}_{1j}(0)c_{1j}(\tau) >}$ and $\overline{< e^{*}_{1j}(0)e_{1j}(\tau) >}$ for all protons j in the crystallite are calculated for correlated and uncorrelated motion. These averages are then summed and inserted into equation 7.8 to find $T_{1(min)}$ (corr) and $T_{1(min)}$ (uncorr) as before. The calculations are repeated for different field directions to yield a set of values of $T_{1(min)}$ (corr) and $T_{1(min)}$ (uncorr) corresponding to the values of θ and Φ. Note that in this method the intramolecular interaction must be calculated at the same time as the intermolecular interaction.

These calculations were performed using the I.B.M. 1620 digital computer, but because of the long computing time required for the calculations, only the high temperature ethylene lattice $P_{21}/n(C^{5}_{2h})$ was considered. However, because the experimental $T_{1(min)}$ occurs at 90°K,

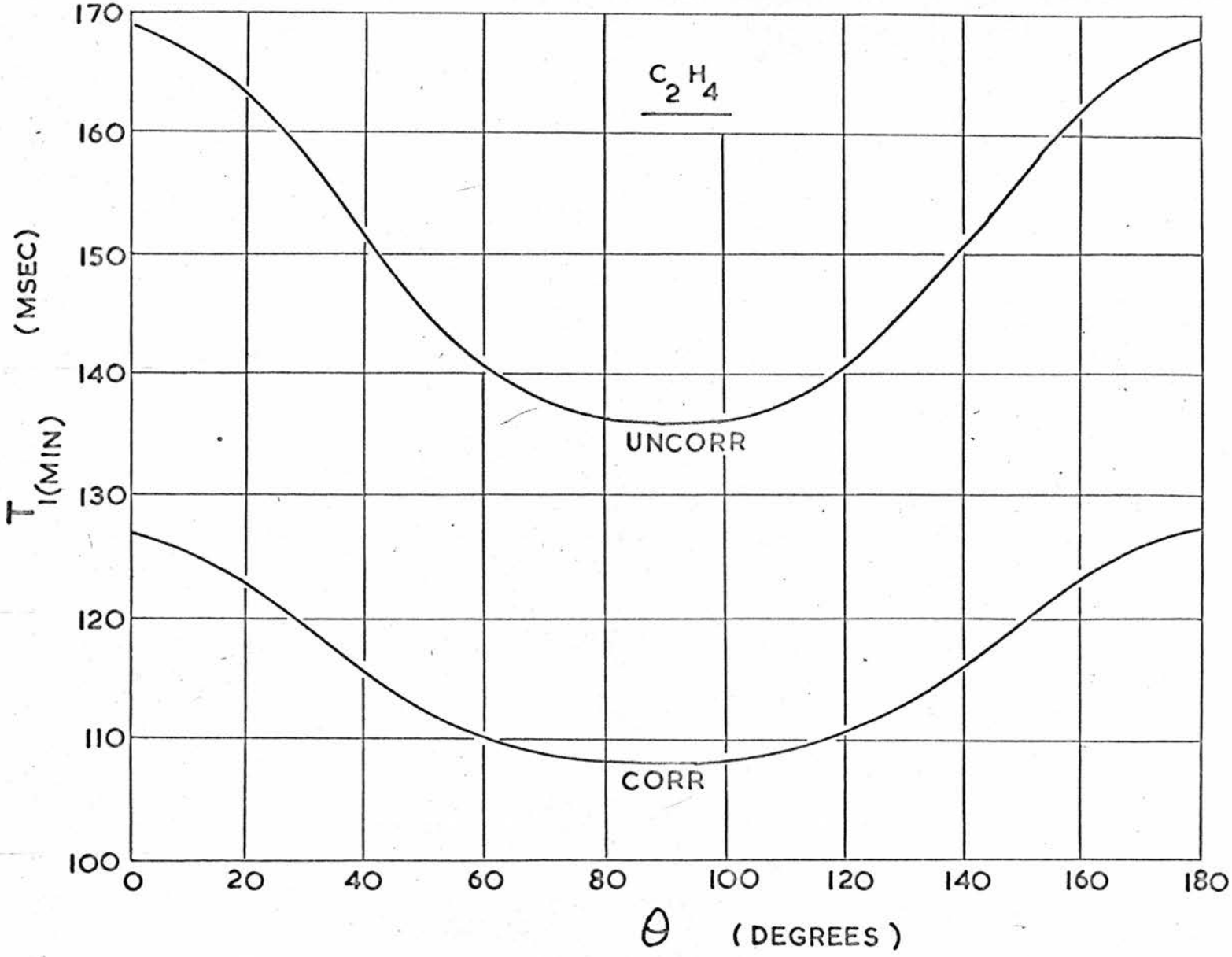
C_2H_4
UNCORR
CORR
$T_{I(MIN)}$ (MSEC)
170
160
150
140
130
120
110
100
0
20
40
60
80
100
120
140
160
180
θ (DEGREES)

FIGURE 22

at which temperature the lattice is assumed to have this symmetry, it is valid to correlate the theoretical and experimental values of $T_{1(min)}$.

To attempt to find the theoretical value of $T_{1(min)}$ which corresponds to the measured value, two methods of averaging the set of $T_{1(min)}$ were used. The first method consists of averaging the reciprocals of the various $T_{1(min)}$ values as below,

$$\left\langle \frac{1}{T_{1(min)}} \right\rangle_1 = \frac{\sum_{k,l} \left[\sin\theta_k / T_{1(min)}(\theta_k, \bar{\theta}_l) \right]}{\sum_{k,l} \sin\theta_k} \qquad 7.19$$

and hence the average $T_{1(min)}$ value denoted $\langle T_{1(min)} \rangle_1$ can be calculated. Figure 22 shows a plot of $T_{1(min)}$ (corr) and $T_{1(min)}$ (uncorr) as a function of θ for the $P_{21}/n(C_{2h}^5)$ ethylene space group. The symmetry of the plot about $\theta = 90^\circ$ follows directly from the model and it is interesting to note that there is a larger distribution of $T_{1(min)}$ (uncorr) values than $T_{1(min)}$ (corr) values. This method assumes that the polycrystallites will have a common rate of relaxation. This is not strictly correct because spin diffusion, the process which would enable this to happen, does not cross grain boundaries[100].

The second method of averaging is perhaps closer to the true experimental situation since it assumes that the magnetization of a crystallite decays with the time constant appropriate to that particular crystallite, and hence what we observe is a sum of exponentials. This sum can be approximated by a single exponential if the decay rates of the individual exponentials in the sum are not vastly different. We then require to know what the experimentally observed value of $T_{1(min)}$ will be if the decay rate is measured at time t. This value denoted $<T_{1(min)}>2$ is given by

$$<T_{1(min)}>2 = t/\ln(1/k) \qquad 7.20$$

where

$$K = \exp\left(-\frac{t}{<T_{1(min)}>2}\right) = \frac{\sum_{k,l} \exp\left[-t/T_{1(min)}(\theta_k, \Phi_l)\right]\sin\theta_k}{\sum_{k,l} \sin\theta_k} .$$

The variation of $<T_{1(min)}>2$ with t determines the validity of the assumption made in approximating the sum of exponentials by an exponential.

Table 7.2 shows the values obtained for $T_{1(min)}$ for correlated and uncorrelated motion in ethylene lattice of type $P_{21}/n(C_{2h}^5)$ assuming t equal to 70 msec which is a reasonable value of pulse spacing to use in the measurement of a T_1 of the order of 120 msec.

Table 7.2

	correlated motion	uncorrelated motion
$<T_{1(min)}>1$	112.4 msec	143.8 msec
$<T_{1(min)}>2$	112.5 msec	144.2 msec

Method (B) produces results of the same order of magnitude for $T_{1(min)}$ (corr) and $T_{1(min)}$ (uncorr) as method (A), while in both cases the results for correlated molecular motion are closer to the experimental value of 85 msec.

We have not so far included in the discussion of relaxation the effect of molecular vibration which by comparison with other molecules could have, at 90°K, an r.m.s. magnitude of between 0.1 Å and 0.15 Å with a greater probability of being closer to 0.1 Å. Although in the intramolecular relaxation calculations we have ruled out the possibility of a relaxation effect between proton number 1 and proton number 2 (as in figure 21) the relaxation caused by molecular vibration will come mainly from this interaction; proton 2 being the closest neighbour to proton 1. A rough calculation based on the techniques of method (A) gives the vibrational contribution to $T_{1(min)}$ as between 700 msec, which when added to the

contributions from the 180° flipping motion for the $P_{21}/n(C_{2h}^5)$ space group give the values in the table below, where we have ignored the small difference between $<T_{1(min)}>_1$ and $<T_{1(min)}>_2$

Table 7.3

	Method	Lower Limit
$T_{1(min)}$ (corr)	(A)	96.5 msec
$T_{1(min)}$ (uncorr)	(A)	118 msec
$T_{1(min)}$ (corr)	(B)	97 msec
$T_{1(min)}$ (uncorr)	(B)	119 msec

The experimental value of 85 ± 9 msec for $T_{1(min)}$ would therefore seem to point in favour of predicting correlated motion of the ethylene molecules.

A similar type of correlated molecular motion in benzene has been reported by Anderson[101] from T_1 measurements. His conclusions however are reached using a different theory to that used here for ethylene.

It is also possible to estimate the activation energy for molecular flipping from the spin-lattice relaxation results. This is

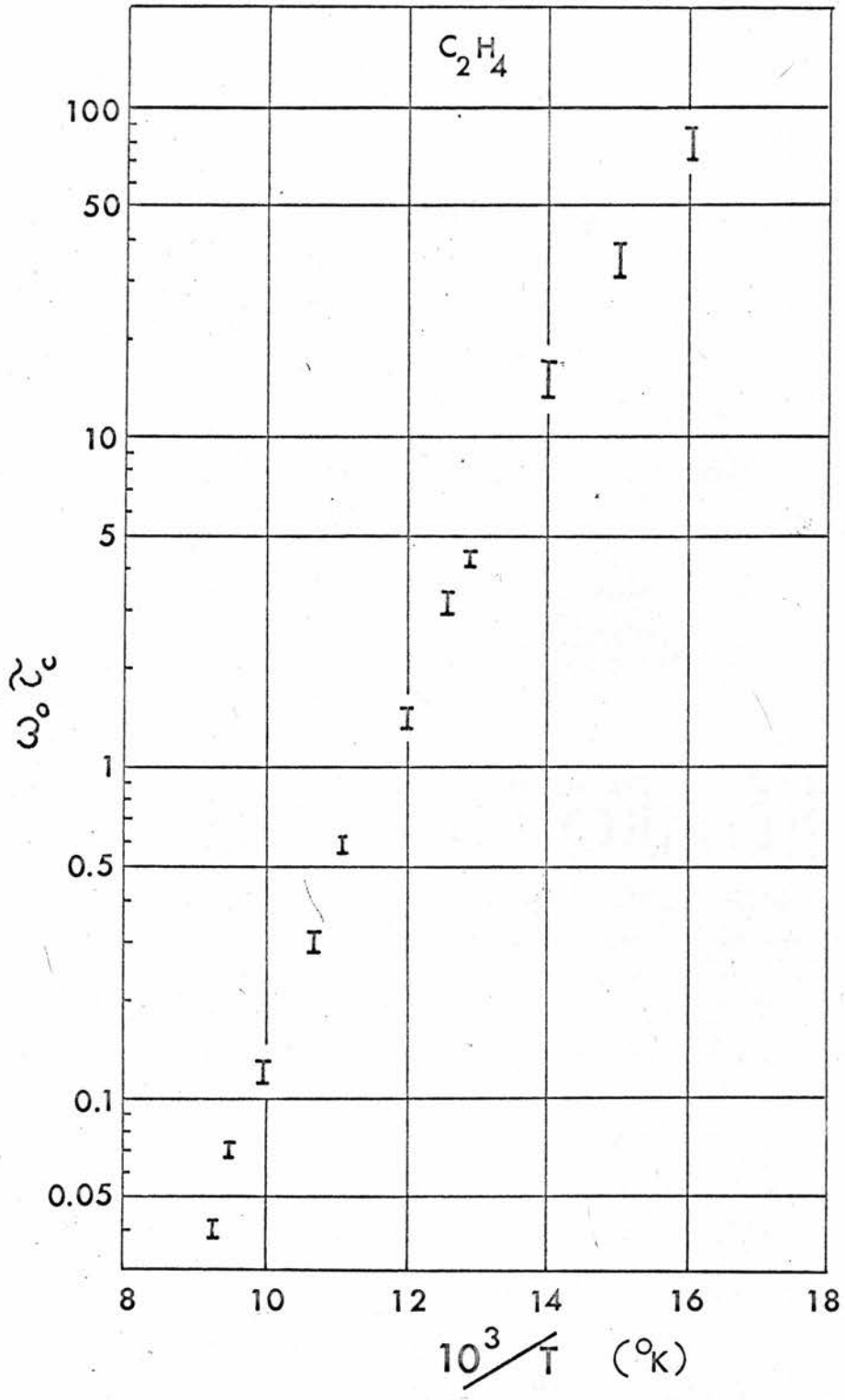

FIGURE 23

done by first differentiating equation 7.8 to find $T_{1(min)}$ in terms of the constant C, the finding the value of C from the experimental $T_{1(min)}$. Hence values of $\omega_o\tau_c$ can be found for all the experimental T_1 results, and we assume that the correlation time will have a temperature dependence given by

$$\tau_c = \tau_o \exp(E_a/RT) \qquad 7.21$$

where τ_o is a constant, E_a is the activation energy of the process R is the gas constant, and T is the temperature in degrees absolute. Thus from 7.21

$$\ln \omega_o\tau_c = \frac{E_a}{RT} + \ln \omega_o\tau_o \qquad 7.22$$

and hence the gradient from a plot of $\ln \omega_o\tau_c$ against $1/T$ will yield a value for the activation energy. Figure 23 shows a plot of $\omega_o\tau_o$ against $10^3/T$ for ethylene, where the T_1 results obtained by pulse techniques have been used. From the slope of the best straight line through these points an activation energy of 2.4 ± 0.3 kcal/mole is predicted for the slipping of an ethylene molecule. Considering the zero point energy of 0.2 kcal/mole this yields a total activation energy of 2.6 ± 0.3 kcal/mole. This value is 0.4 kcal/mole higher than that predicted by Hoch from his T_1 measurements, but is in agreement with the lower limit of 2.2 kcal/mole predicted by Todireanu (see section 7.2.3) from neutron scattering studies. The fact that the points on the graph of figure 23 do not lie exactly on

a straight line could be attributed to an incorrect description of the Fourier spectrum of the lattice motions.

The possibility of a tunnelling effect to explain the levelling off in the T_1 results by C.W. techniques has already been ruled out on theoretical grounds in section 4.4. It has also been observed that T_1 measurements, using the C.W. apparatus, made on other samples, which have no possibility of possessing a tunnelling mode, also exhibit a levelling off in the low temperature region. This would seem to imply that the sample is being saturated to some degree. However in ethylene, this turning over of the T_1 results at about 50°K could be caused by the lattice structure changing from $P_{21}/n(C_{2h}^5)$ to $P_{nnm}(D_{2h}^{12})$ as the temperature is lowered. As discussed previously, method (A) gives $T_{1(min)}$ (corr) equal to 69 msec for the $P_{nnm}(D_{2h}^{12})$ structure and 101 msec for the $P_{21}/n(C_{2h}^5)$ high temperature lattice, without considering vibrational effects. This means that at the temperature giving T_1 equal to 300 sec for the $P_{21}/n(C_{2h}^5)$ lattice T_1 will be 95 sec for the $P_{nnm}(D_{2h}^{12})$ lattice. This is approximately equal to the reduction in T_1 in the region of 50°K as measured in the C.W. experiment.

This levelling off in T_1 has not yet been checked by pulse techniques because of the unavailability of liquid hydrogen, and because it was felt that to increase the accuracy of long T_1 measurements, an r.f. comb technique (section 5.1) should be used to avoid

the long delay between pulse sequences. The apparatus is at present being modified to incorporate a helium cryostat and a new pulsing unit to enable the use of an r.f. comb technique. Also because of the predicted relative magnitudes of the intramolecular and intermolecular effects in ethylene it would be interesting to perform T_1 measurements on samples of ethylene diluted with various amounts of deuterated ethylene. This would enable the magnitudes of T_1^{inter} and T_1^{intra} to be checked.

7.4.2 Absorption Spectra

Hoch, assuming the structure of ethylene to be $P_{21}/n(C_{2h}^5)$ and using the revised molecular structure values of Bartell et al.[89], calculated the rigid lattice intramolecular contribution M_2' to be 11.39^2 while the intermolecular contribution M_2'' was 6.29^2 at 98°K. This gave a total second moment of 17.59^2 for the rigid lattice.

A correction for lattice contraction with decreasing temperature increased M_2'' to 6.69^2 in the region of 20°K to 30°K. In addition, a formula derived by Das[20], corrected by Hoch[40], was used to estimate the reduction in the intermolecular contribution caused by large amplitude zero-point vibrations. Hoch calculated that these corrections predicted a total rigid lattice second moment of 16.89^2 in the temperature range 20° to 30°K. This was in agreement with his experimental results.

The narrowing of the absorption spectrum between 50°K and 70°K

requires that some form of motion is occurring at a rate faster than the rigid lattice line width expressed in frequency units i.e. in this case faster than 5×10^4 Hz. A steady second moment value of 10.6 G^2 was reached between 70°K and the melting point as against the 13.1 G^2 obtained at a temperature of 90°K by Gutowsky, Kistiakowsky, Pake and Purcell[102]. Hoch states that the difference in the experimental results could be ascribed to a lack of true polycrystallinity in his sample because the occurrence of large single crystals could result in either a higher or lower second moment than would be measured in a polycrystalline sample. However on comparing the cooling techniques used in both experiments it is more likely that large single crystals would be formed in the sample of Gutowsky et al.

Classical rotation of the molecules about the C = C bond may be ruled out as a cause of this second moment reduction because this type of motion would produce a reduced value of less than 7.9 G^2.

To attempt to explain the reduction Hoch calculated the effect of 180° molecular flips, about the C = C bond, on the second moment by using the reduction factors of Eades[18] and Andrew and Eades[103]. The reduced second moment for this type of motion was calculated to be 13.9 ± 1 G^2 at 98°K. This is considerably higher than the experimental value obtained by Hoch, but quite close to the value obtained

by Gutowsky et al., which we have rejected. On the grounds of these results Hoch proposed that the effect of the molecular motion had been underestimated and that the second moment results could not provide unambiguous evidence on the type of motion present.

If we assume the truth of the conclusions drawn from the T_1 measurements that the experimental T_1 values could be predicted from 180° flips of the molecule, then it is justified to postulate that at least some of the reduction in second moment is caused by 180° molecular flips. To show this we use the fact that at the T_1 minimum, which occurs at 90°K, the correlation time is related to the resonance frequency by $\omega_o \tau_c \simeq 0.61$ and the Arhennius relationship $\tau_c = \tau_o \exp(E_a/RT)$. It is then calculated that $1/\tau_c$ will be of the order of 5×10^4 Hz i.e. the frequency for narrowing of the absorption spectrum, at a temperature of about 60°K. Also from the T_1 results there is some evidence in favour of correlated motion which would require small change in the reduction formula of Andrew and Eades which was used to find the intermolecular contribution.

Because of the discovery of the change from the $P_{nnm}(D_{2h}^{12})$ low temperature structure to the $P_{21}/n(C_{2h}^{5})$ high temperature structure at a temperature somewhere above 53°K, the former space group must be used to find the rigid lattice second moment while the latter structure is used for the reduced moment. Computer calculations

were performed and it was found that the low temperature structure produced a second moment value 3.3 G^2 higher than the rigid second moment calculated using the high temperature lattice parameters.

The combined effect of the 180° molecular flipping and the change of space group is to reduce the second moment by 6.2 G^2 which is approximately equal to the reduction observed by Hoch. We cannot however explain the absolute values of the second moment. Finally it can only be said that the experimental second moment reduction could be predicted by assuming 180° molecular flips and a change in the crystal structure, but that without a more accurate value for the temperature at which the crystal structure changes, the findings are by no means conclusive.

8. CHLORINATED ETHYLENE COMPOUNDS

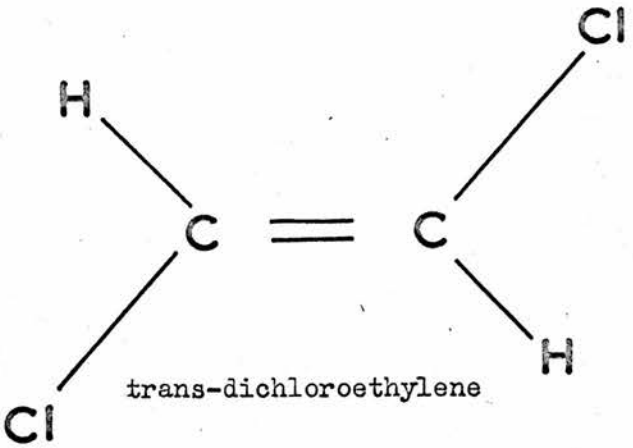

trans-dichloroethylene

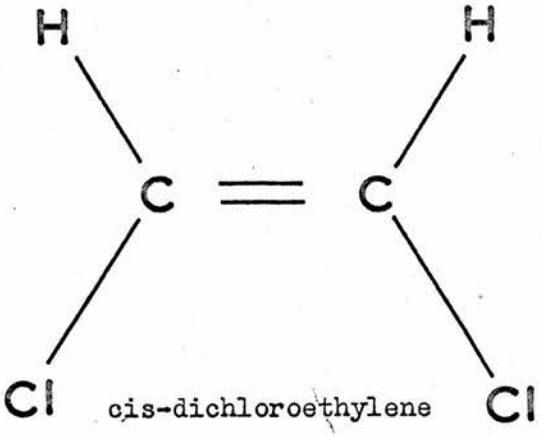

cis-dichloroethylene

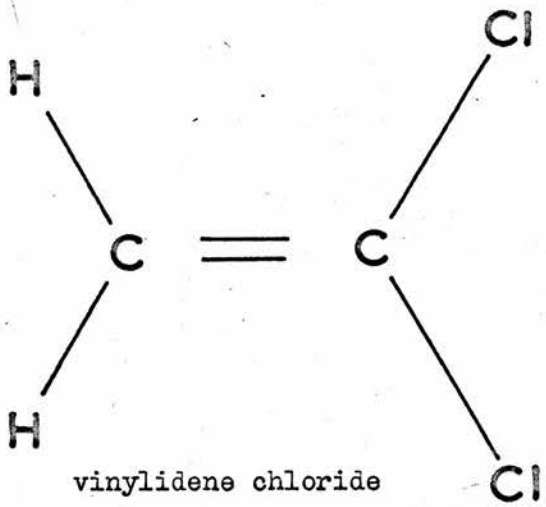

vinylidene chloride

FIGURE 24

8. CHLORINATED ETHYLENE COMPOUNDS

This chapter contains the results and conclusions of spin-lattice relaxation measurements on samples of trans-dichloroethylene, cis-dichloroethylene, vinylidene chloride and mixtures of trans-dichloroethylene (figure 24) with various amounts of tetrachloroethylene.

8.1 Samples

Samples of trans-dichloroethylene were obtained from the Aldrich Chemical Company (sample 1) and Kodak Ltd. (sample 2). Sample 1 was found by gas liquid chromatography (G.L.C.) to contain 6% cis-dichloroethylene as an impurity whereas sample 2 contained no detectable amount of cis-dichloroethylene. Similarly, no impurity was detected in the samples of cis-dichloroethylene, supplied by the Aldrich Company, or in the vinylidene chloride supplied by the Fluka Chemical Company. The university's chemistry department kindly gifted supplies of spectroscopically pure tetrachloroethylene manufactured by Kodak Ltd.

The removal of oxygen from the samples is important since if it were present it would cause relaxation of the type discussed in section 4.6. The samples, which were all liquids at room temperature, were degassed by solidifying them with liquid nitrogen in a vacuum system and pumping on the solid. After the degassing process the samples were transferred into the glass sample tubes used in the

n.m.r. probe; the initial fraction of the liquid distilled being rejected. Because of the reproducibility of the T_1 measurements on different distillates of trans-dichloroethylene it was considered unnecessary to adopt a gettering technique such as used by Sandu et al.[104,105] for the removal of oxygen from the sample.

Experiments were performed on two mixtures of trans-dichloroethylene with tetrachloroethylene. Mixture 1 contained approximately 2/3 by volume of trans-dichloroethylene and 1/3 tetra-chloroethylene, while mixture 2 contained equal amounts of both liquids. To ensure a homogeneous mixture of the liquids the sealed sample tubes were placed, prior to each run, in an ultrasonic bath, then rapidly cooled after removal from the bath.

8.2 Molecular and Crystal Structures

No reference could be found to any determination of the crystal structure of any of the chlorinated ethylenes.

The molecule of trans-dichloroethylene is planar with the following parameters as determined by Kaplan[106] from electron diffraction experiments in the gas phase:

C = C	1.343 ± 0.015 Å
C-Cl	1.721 ± 0.010 Å
∠Cl-C-H	$123.0^\circ \pm 1^\circ$

Unfortunately the C-H bond length could not be determined and was

assumed[107] to be 1.09 Å.

Cis-dichloroethylene is a planar molecule with mm(C_{2v}) symmetry. The molecular parameters as determined by Hoffman[108], are

C = C	1.336 ± 0.016 Å
C-Cl	1.722 ± 0.010 Å
∠Cl-C-C	123° ± 1.5°

and again the C-H bond length has been assessed[107] at 1.09 Å.

The molecular configuration of vinylidene chloride has been determined by microwave experiments[109] and by electron diffraction experiments[106], and there is reasonable agreement between the results, with again a value having to be assumed for the C-H bond length. The molecule was found to be planar with the following parameters[106]

C = C	1.325 ± 0.020 Å
C-Cl	1.707 ± 0.012 Å
∠Cl-C-Cl	122.7° ± 0.5°

Tetra-chloroethylene is planar with mmm(D_{2h}) symmetry and the following parameters determined by Karle and Karle[110] by electron diffraction:

C = C	1.32 Å
C-Cl	1.72 Å
∠Cl-C-Cl	113° 18'

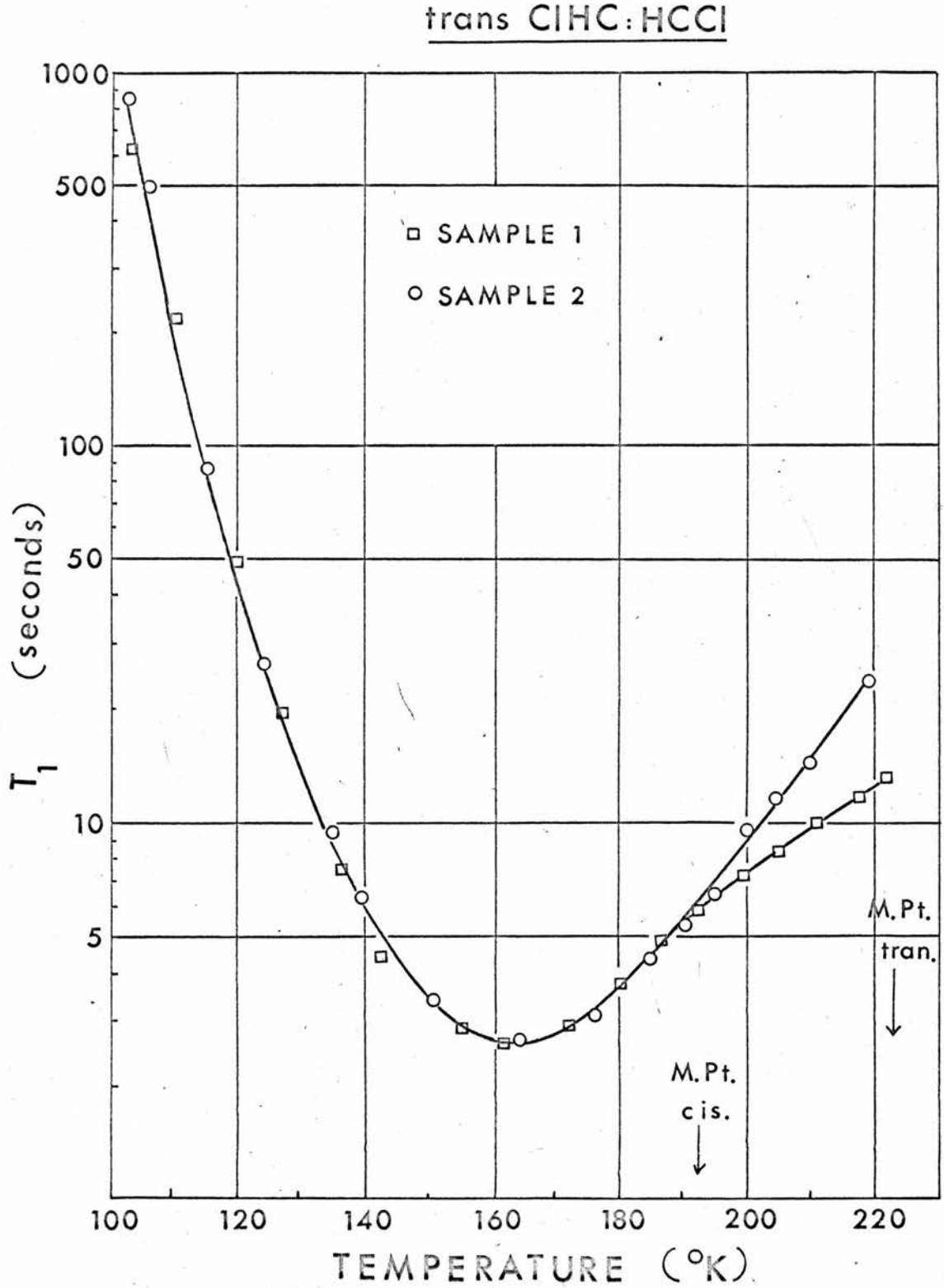
trans ClHC:HCCl
1000
500
100
50
10
5
T_1 (seconds)
SAMPLE 1
SAMPLE 2
M.Pt.
tran.
M.Pt.
cis.
100
120
140
160
180
200
220
TEMPERATURE (°K)

FIGURE 25

8.3 Thermal Data

The following melting point temperatures have been recorded for the chlorinated ethylenes:

trans-dichloroethylene[111,112]	223.42°K
cis-dichloroethylene[111,112]	191.49°K
vinylidene chloride[113,114]	150.9°K
tetra-chloroethylene[111]	251°K

The only specific heat measurements published[113] are those made on vinylidene chloride from 12°K to the melting point. No specific heat anomalies occurred in the temperature range investigated.

8.4 Results

The pulse techniques of section 5.1 were used to obtain the variation of T_1 with temperature (figure 25) of samples 1 and 2 of trans-dichloroethylene. A minimum value of T_1 of 2.7 ± 0.3 sec was observed at a temperature of 162°K. The results from sample 1 are identical to those from sample 2 except in the temperature region above approximately 190°K. Above 190°K the slope of the T_1 against temperature curve is less for sample 1 than for sample 2.

In the case of cis-dichloroethylene and vinylidene chloride no free induction decays could be observed although pulse experiments were performed from 77°K to the melting points of the sub-

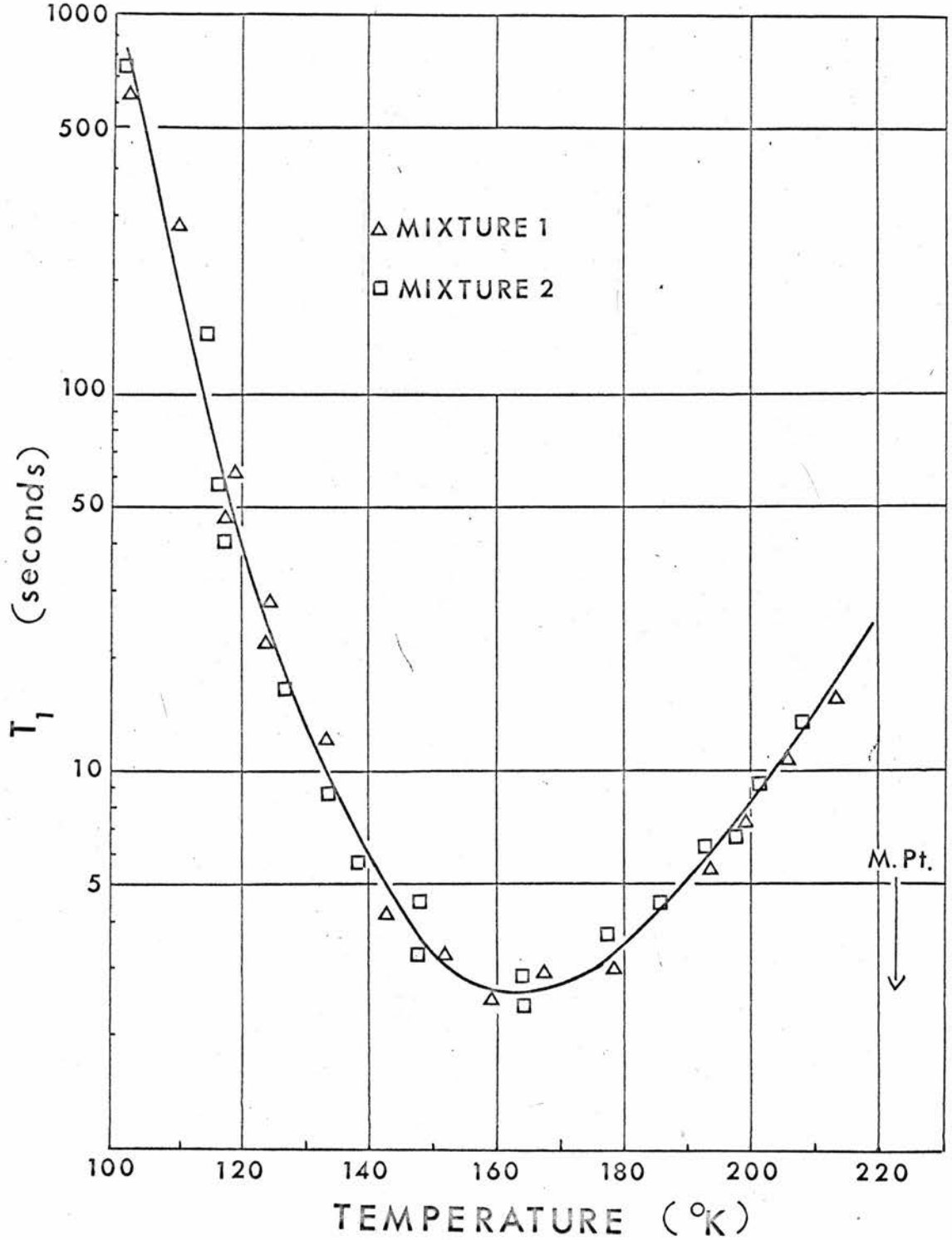
1000
500
100
50
10
5
T_1 (seconds)
△ MIXTURE 1
□ MIXTURE 2
M. Pt.
100
120
140
160
180
200
220
TEMPERATURE (°K)

FIGURE 26

stances.

The results of T_1 measurements on the mixtures of trans-dichloroethylene with tetra-chloroethylene are shown in figure 26. These curves are almost identical with that obtained from pure trans-dichloroethylene sample 2 of figure 25 with the $T_{1(min)}$ occurring at the same temperature and having the same value in both cases.

8.5 Discussion

8.5.1 Cis-dichloroethylene and Vinylidene Chloride

In order to discuss probable reasons for the lack of observation of nuclear free induction decays from cis-dichloroethylene and vinylidene dichloride, the techniques used will be described. The first method was to use a $\pi/2$ τ $\pi/2$ sequence with τ fixed at 100 seconds and to allow the temperature of the sample to increase slowly from 77°K. The second method, which also proved unsuccessful in the observation of a decay, was to estimate, from the trans-dichloroethylene results, the temperature at which the minimum value of T_1 would occur and then to attempt to find an induction decay at that temperature. In both substances the signals obtained from the liquid samples just above their melting points were strong, thus indicating a good filling factor at these temperatures. On cooling, no phenomenon such as "vapour snake" formation[115] occurred to reduce this filling factor. Also because the spin-spin

relaxation time T_2 of ethylene is likely to be shorter than the value of T_2 of either cis-dichloroethylene or vinylidene chloride, it is unlikely that the rapid decay of the free induction signal, which would then be obscured by the receiver recovery time, could account for the lack of observation of a signal. We can therefore conclude that it is a long T_1 which inhibits the observation and place a lower limit of at least a 100 seconds on the value of $T_{1(min)}$.

Because of the lack of information on the crystal structures of these two substances the most likely axis of molecular reorientation is uncertain. However Sekino and Nishikawa[109] in their paper on the microwave rotation spectrum of vinylidene chloride give the most probable axis of molecular reorientation as being perpendicular to the C = C bond and passing between the chlorine atoms and the nearest carbon atom to them. The second most probable axis for reorientation is the C = C bond.

If we now consider the effect that 180° reorientation about either of these axes would have on the proton relaxation in the molecule, we see that for the first axis the interproton vector in its second position is parallel to its direction in the first molecular position and hence as discussed in section 4.3.3, this motion has no effect on the spin-lattice relaxation time T_1 of the protons. In the case of reorientation about the C = C bond the protons merely

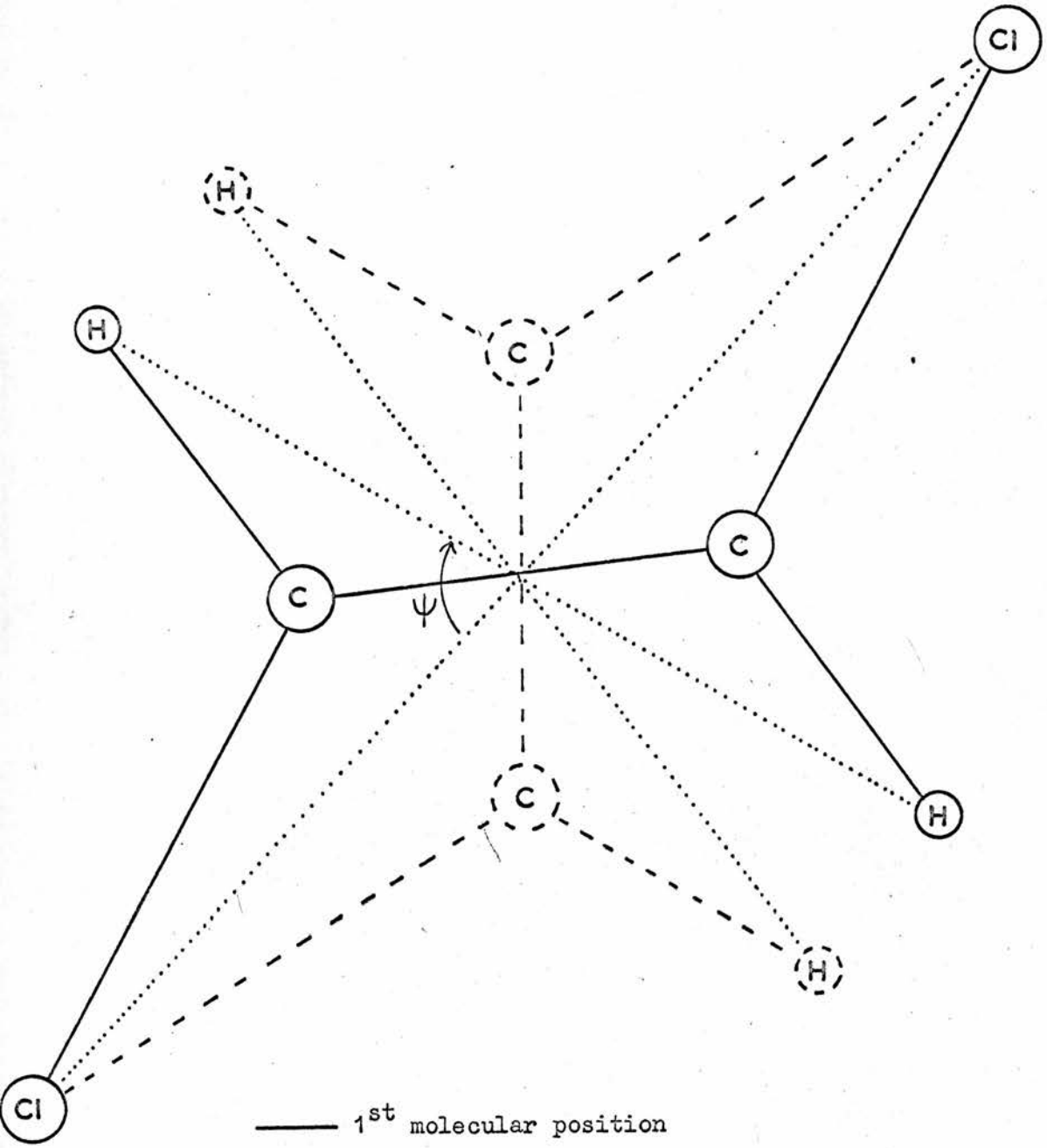
Cl
H
H
C
C
C
ψ
C
H
H
Cl
1st molecular position
2nd molecular position

FIGURE 27

interchange position and as shown in section 4.3.3 this again leads to zero effect on the proton spin-lattice relaxation time.

From infrared spectra by Bernstein and Ramsay[116] and microwave spectra by Shimizu and Takuma[117] and Flygare and Howe[118] the preferred axis of rotation in cis-dichloroethylene is parallel to the C = C bond, and between the C = C bond and the line joining the chlorine atoms. If 180° flips take place about this axis then the contribution to the proton spin-lattice relaxation is zero, as discussed in section 4.3.3, because the two possible interproton vectors are parallel.

In vinylidene chloride and cis-dichloroethylene the only contribution to spin-lattice relaxation come from vibrational and intermolecular effects which cannot be estimated without more knowledge of the crystal structures. It is however reasonable to assume that the intermolecular interactions in trans-dichloroethylene and vinylidene chloride will be smaller than in ethylene because of the smaller number of protons per molecule. The n.m.r. experimental work described previously would seem to indicate that the intermolecular and vibrational interactions in vinylidene chloride and cis-dichloroethylene are very small.

8.5.2 Trans-dichloroethylene

The divergence of the T_1 trans-dichloroethylene results above 190°K in figure 25 was found to be caused by the presence of approxi-

mately 6% of cis-dichloroethylene in sample 1. The cis-dichloroethylene liquified at 191.5°K and reduced the measured T_1 of the trans-dichloroethylene sample. The discussions below will be limited to sample 2 of trans-dichloroethylene whose purity was discussed in section 8.1.

Before the discussion of the spin-lattice results of trans-dichloroethylene it is interesting to review the results of measurements made on trans-dichloroethane. In this substance hindered rotation about the long axis passing through the two chlorine atoms has revealed itself through anomalies in heat capacity[119], dielectric constant[120], Raman spectrum[121] and proton magnetic resonance[16,122]. Dodgen and Ragle[123], Ragle[124] and Tokuhiro[125] have measured the quadrupole resonance frequency and line width as a function of temperature and find a strong correlation between their results and a theory predicting random jumping motions of the molecule around the axis passing through the two chlorine atoms. It follows from this that the shape of the trans-dichloroethane molecule is such that when packed in the crystal lattice oscillation or rotation about this axis is less hindered than motions about axes perpendicular to this.

Because of the similarity in general shape of trans-dichloroethylene and trans-dichloroethane it would seem reasonable to predict, for trans-dichloroethylene a similar type of random jumping motion

around the long Cl-Cl axis. Another point in favour of the assumption of this particular axis of reorientation is an infrared study by Bernstein and Ramsay[116], who find that the moment of inertia about this axis is 15.8×10^{-40} g cm^2, while the moment of inertia about the C = C axis is 548×10^{-40} g cm^2. The first of these values can be contrasted with the value of 70.3×10^{-40} g cm^2 found by the same authors for rotation of cis-dichloroethylene about its favoured axis.

Having specified the axis of reorientation of the molecule it is now possible to apply the theories of chapter 4 to the estimation of a theoretical value of $T_{1(min)}$ to be compared with the experimental $T_{1(min)}$ of 2.7 seconds from figure 25. The B.P.P. theory of random motion, of course, predicts the same value for the $T_{1(min)}$ of trans-dichloroethylene as it does for the relaxation between protons 1 and 4 (figure 21) of the ethylene molecule, namely 550 msec, and therefore this type of interaction is too strong to account for the observed relaxation. The theory of section 4.3 for reorientation between two equilibrium positions of the molecule will now be applied in two ways.

Method (A) uses the computational work of section 4.3.3 which gives $T_{1(min)}$ as a function of the angle ψ, where 2ψ is the angle between the two possible positions of the internuclear vector. Figure 27 illustrates the two equilibrium positions of the trans-

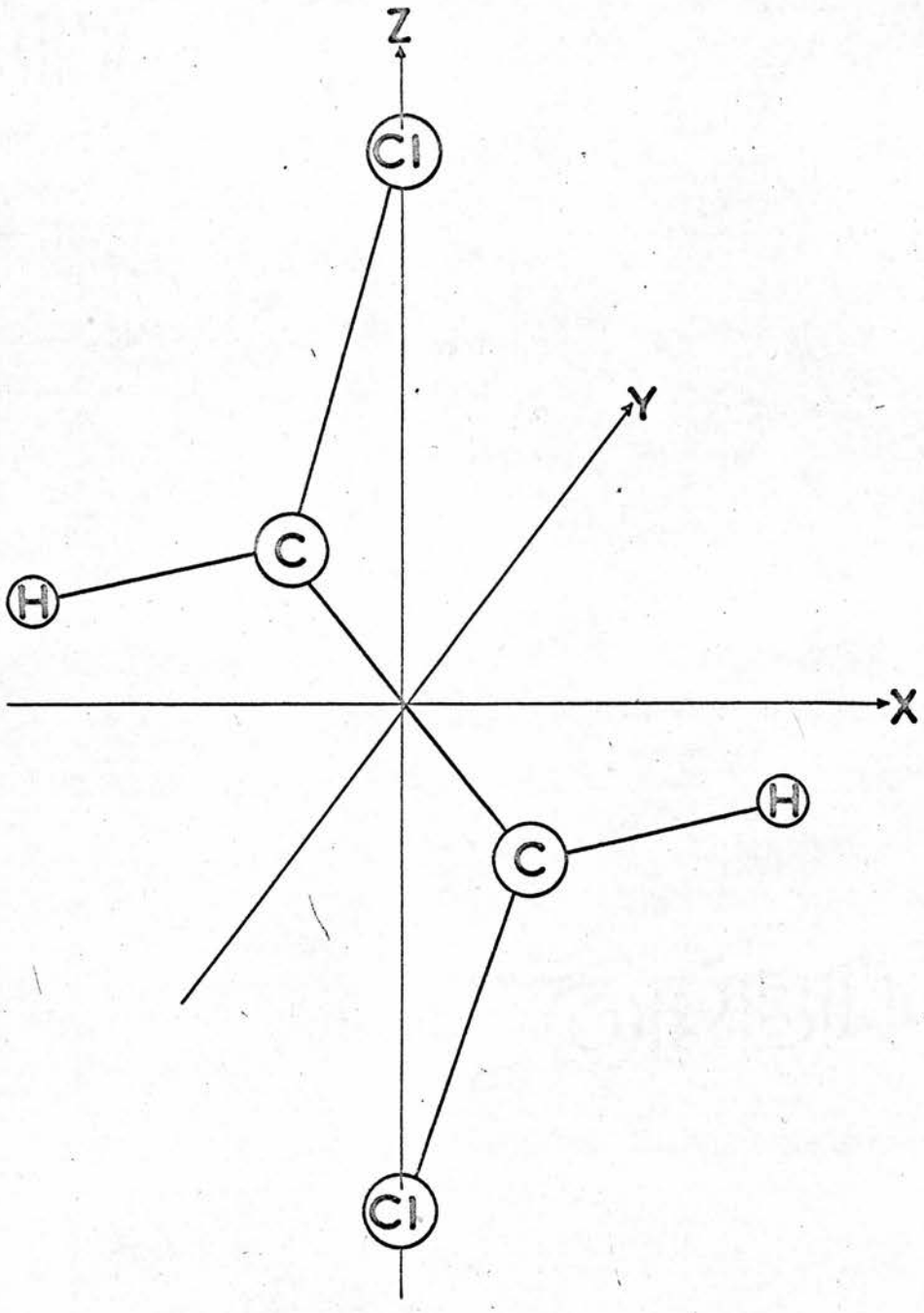

FIGURE 28

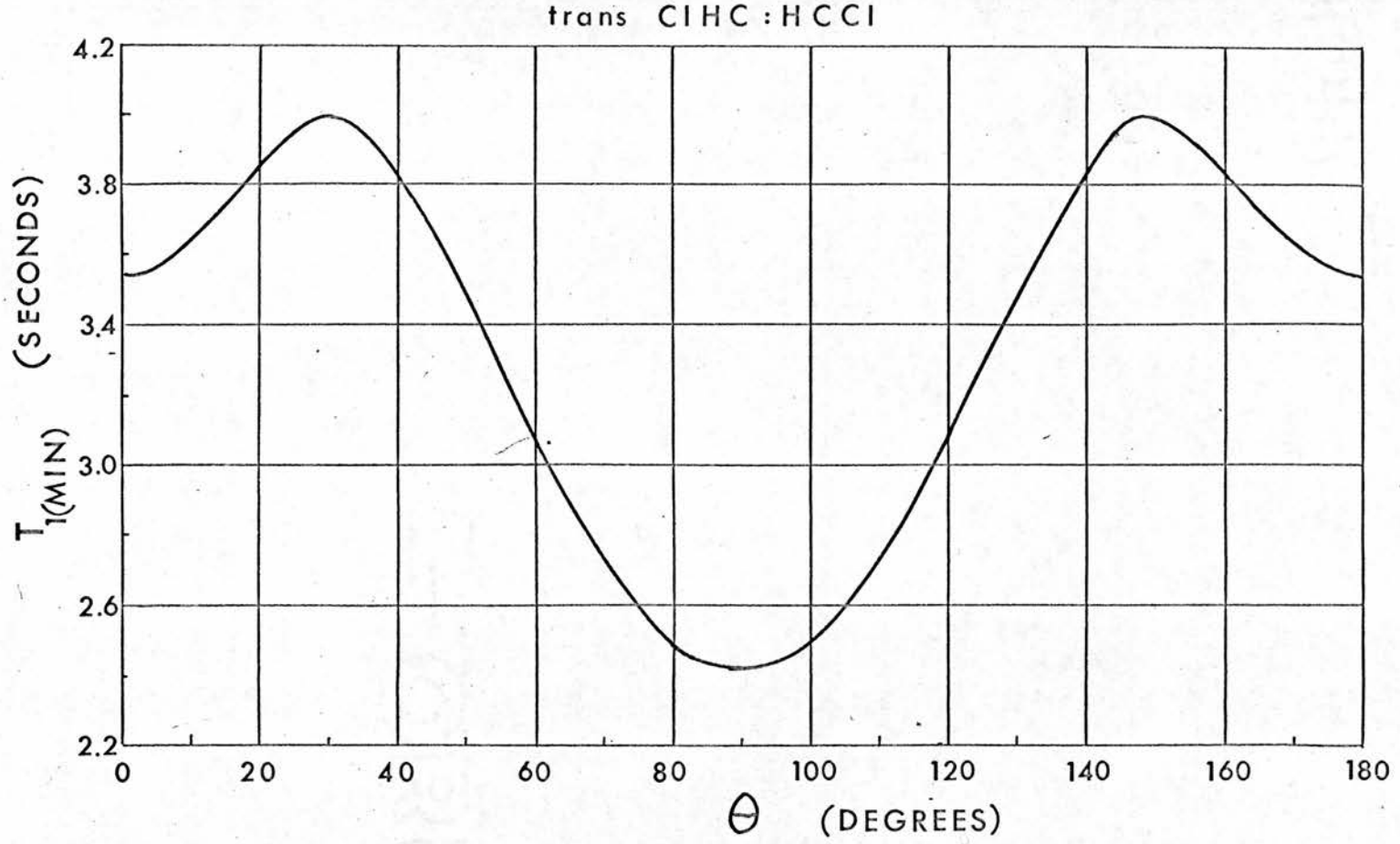
trans ClHC : HCCl
4.2
3.8
3.4
3.0
2.6
2.2
$T_{1(MIN)}$ (SECONDS)
0
20
40
60
80
100
120
140
160
180
θ (DEGREES)

FIGURE 29

dichloroethylene molecule for reorientation about the long Cl-Cl axis, and hence defines the angle ψ. Because of the uncertainties in the molecular parameters, mainly in the length of the C-H bond, the angle ψ can only be estimated as in the region between 75° and 77°. Unfortunately this range of ψ corresponds to the steep part of the curve of figure 3 and $T_{1(min)}$ can only be predicted as being between 2.5 seconds and 3.3 seconds. These results in conjunction with the experimental $T_{1(min)}$ of 2.7 seconds imply that the intermolecular contribution to spin-lattice relaxation is small.

Method (B) is identical with method (B) of chapter 7. We select a set of coordinate axes with respect to a fixed molecule of trans-dichloroethylene (figure 28) with the Z axis along the line joining the chlorine atoms, and with the molecule in the XZ plane. The magnetic field H_o is then given a direction specified by the polar and azimuthal angles θ and ϕ. Then using an identical method to that used in section 7.4.1 we can find $T_{1(min)}$ of the intramolecular effect as a function of θ and ϕ. The computer programmes used to perform these calculations are not given for the corresponding calculations on ethylene. Figure 29 shows a plot of $T_{1(min)}$ as a function of θ after having averaged over ϕ. The averaging techniques of equation 7.18 and 7.19 then yield values of $T_{1(min)}$ of 3.02 seconds and 3.13 seconds respectively; the value of t in equation 7.19 being chosen as 2 seconds. These results are in good

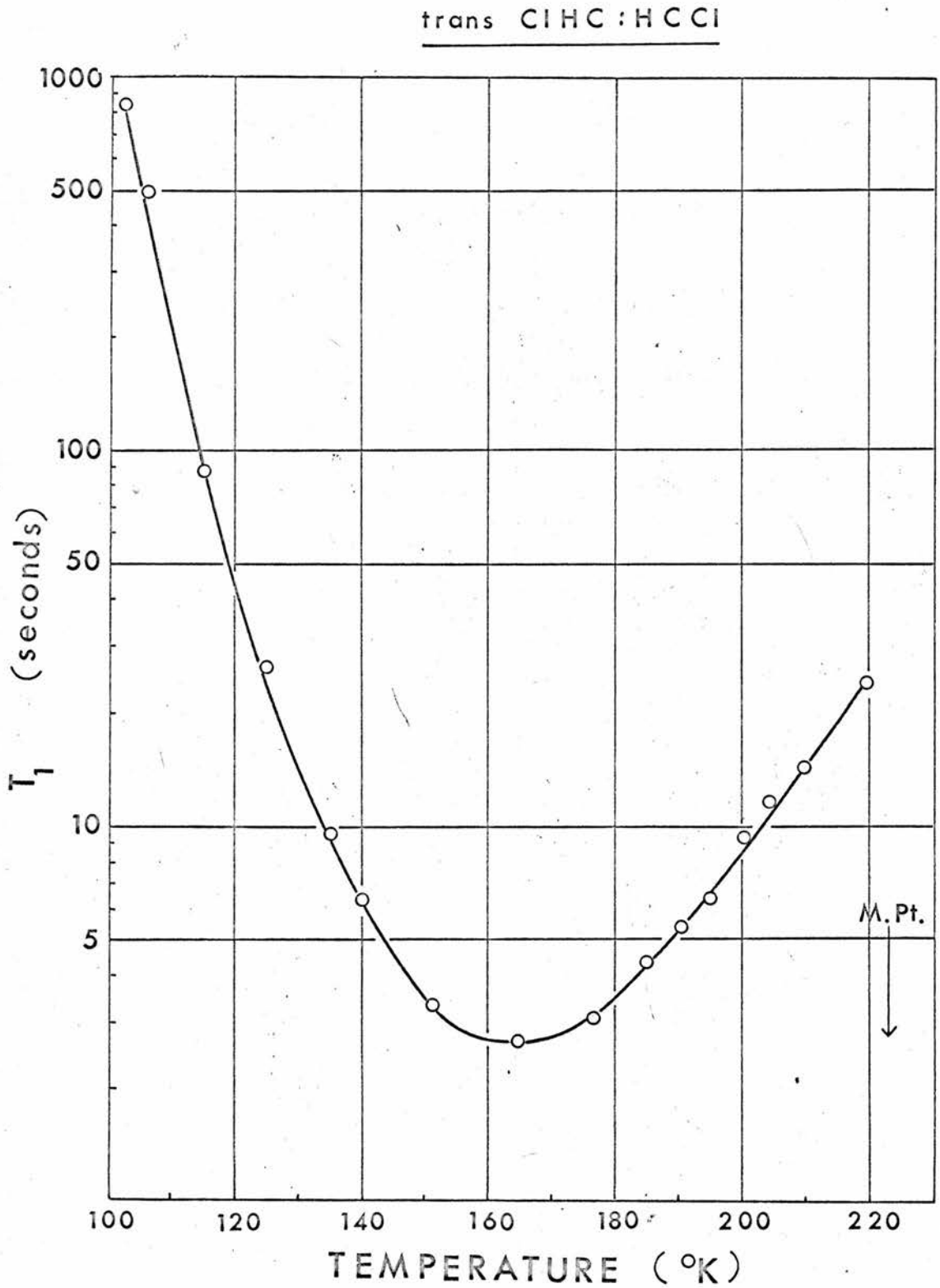
trans ClHC : HCCl
1000
500
100
50
10
5
T_1 (seconds)
M. Pt.
100
120
140
160
180
200
220
TEMPERATURE (°K)

FIGURE 30

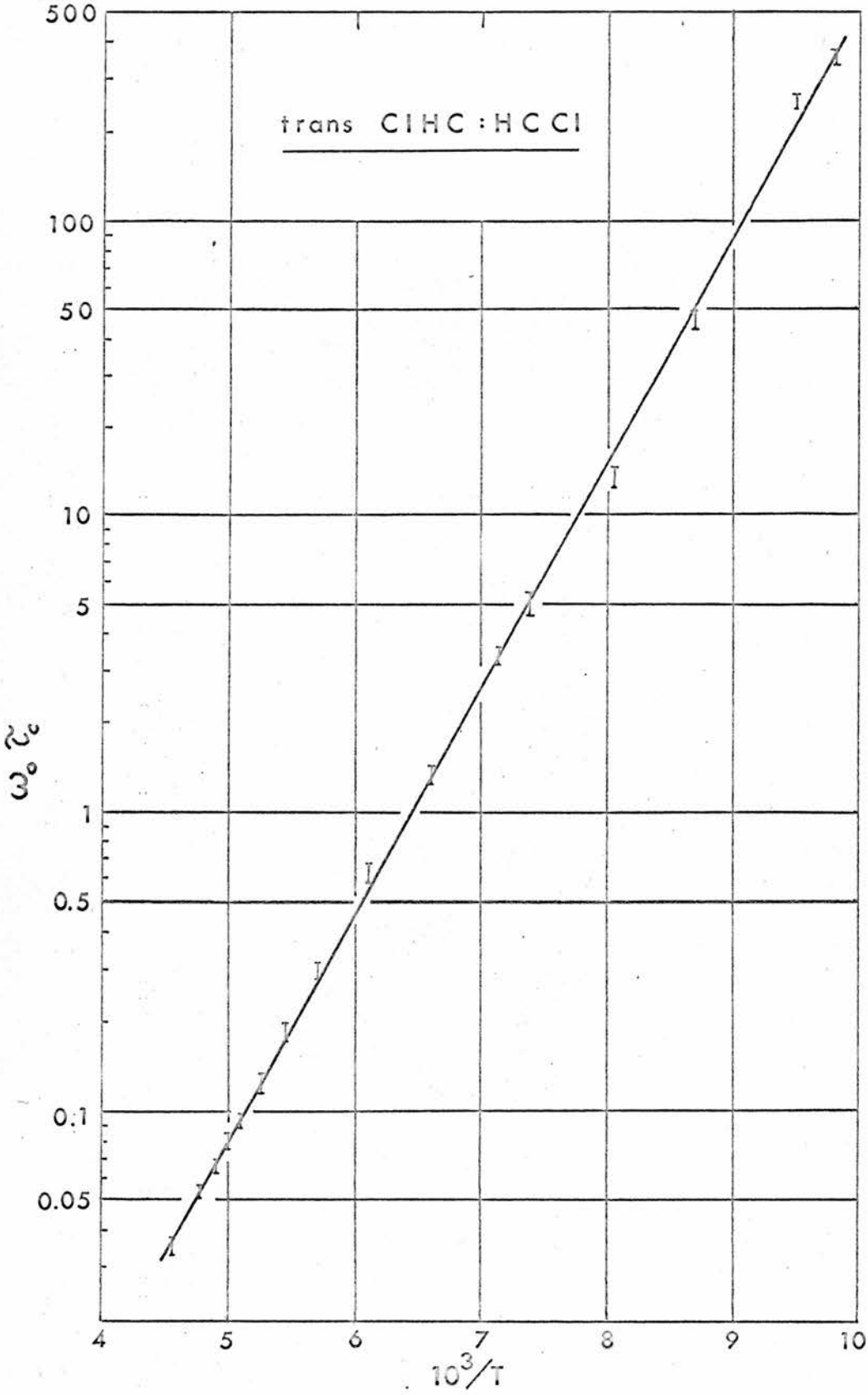
trans ClHC:HCCl
500
100
50
10
5
1
0.5
0.1
0.05
$\omega_o \tau_c$
4
5
6
7
8
9
10
$10^3/T$

FIGURE 31

agreement with the results of method (A), taking into account the inaccuracies in the molecular parameters. The close agreement between experiment and theory adds a point in favour of correctness of the theory developed in section 4.3, if we can assume that the intermolecular relaxation interactions are small.

Applying the same techniques as used in ethylene we can arrive at an estimate to the energy barrier to hindered reorientation around the Cl-Cl axis. Values of $\omega_o \tau_c$ are calculated from the experimental T_1 values of sample 2 (figure 30) of trans-dichloroethylene using equation 4.25. The gradient of a plot of $\ln \omega_o \tau_c$ against 1/T then yields a value for the activation energy, as shown by equation 7.22. The energy calculated from such a plot (figure 31) is found to be 3.5 $\pm$ 0.2 kcal/mole which together with a zero point energy of 0.1 kcal/mole gives a total activation energy of 3.6 $\pm$ 0.2 kcal/mole. The close fit of the points on figure 31 to a straight line might be the direct result of the occurrence of only an intramolecular interaction in the spin-lattice relaxation.

8.5.3 Trans-dichloroethylene diluted with tetra-chloroethylene

Dilution experiments performed on liquid samples of methane[126], benzene[127], acetone[127] and bromobenzene[128] in their respective deuterated analogs have enabled the separation of the inter- and intramolecular relaxation interactions. Anderson[101] has also pub-

lished a report on this separation of interactions in solid solutions of benzene and C_6D_6. The basis of these experiments is the assumption that T_1 or in particular, $T_{1(min)}$ follows the relation

$$\frac{1}{T_{1(min)}} = A + Bx \qquad 8.1$$

where A and B refer to the contributions from the intra- and intermolecular local fields, and x is the mole fraction of the substance containing the spins under observation. A plot of $T_{1(min)}$ against mole fraction x then yields values of A and B. As discussed by Bonera and Rigamonti[127], care must be taken when choosing the solvent substance or the information from the measurements might be pertinent to the molecular motions in the solvent, and hence not correspond to the pure solute motions. It is interesting to note that this separation of relaxation interactions has also been performed on certain solids by measurement of T_1 at varying temperature and pressure[129,130].

In an attempt to separate the inter- and intramolecular effects on spin-lattice relaxation, experiments were performed on two mixtures of trans-dichloroethylene in tetra-chloroethylene. The results of these measurements are shown in figure 26 where mixture 1 contains 2/3 by volume of trans-dichloroethylene and 1/3 of tetra-chloroethylene, while mixture 2 contains equal amounts of both. The

solid curve drawn through these points is the curve of T_1 obtained from the measurements on pure trans-dichloroethylene (figure 30).

We must now examine the possible reasons for the lack of resolution of the inter- and intramolecular effects. Tetrachloroethylene would seem to be a reasonable choice of solvent because of its planar structure, similar to that of trans-dichloroethylene, and because the local fields generated by the Cl nuclei are smaller than the corresponding proton fields by $(\gamma_{Cl}/\gamma_H)^2 = 0.01$ and can thus be ignored. One possible reason for the lack of separation of the interactions is that a homogeneous mixture of the solids might not have been obtained. This reason can be ruled out because of the method of sample preparation and because of the lower signal to noise ratios in the measurements on the mixtures than in the measurements on pure trans-dichloroethylene. The only conclusion therefore is that the T_1 of the intermolecular relaxation is long and cannot be separated from the intramolecular relaxation in the limit of the accuracy obtained in these experiments.

If the energy barrier to reorientation is intermolecular in origin, which it must be for this sample, one would expect the height of the energy barrier and thus the temperature of the minimum T_1 value and the slope of the T_1 versus temperature curve to change on dilution. This does not occur in the measurements recorded and hence we can postulate that the main contribution to the energy barrier to

reorientation comes from the chlorine atoms on neighbouring molecules.

8.6 Summary of results on chlorinated ethylene

The experiments performed on the chlorinated ethylenes are evidence for the correctness of the spin-lattice relaxation theories developed in chapter 4. The results from vinylidene chloride, cis-dichloroethylene and diluted trans-dichloroethylene are in favour of the assumption of a very small intermolecular contribution to the spin-lattice relaxation.

9. SUMMARY

9. SUMMARY

The purpose of the investigations reported in this thesis was to establish a connection between the observed proton spin-lattice relaxation times and the types of motion occurring in certain solids. The theory necessary to obtain estimates of T_1 has been developed in chapter 4 from existing theories by considering a molecule with two equilibrium positions and assuming that the predominant motion is a flipping process between these two positions.

The experimental work consisted of building an apparatus to give reliable values of T_1 in solids as a function of temperature down to $20^{\circ}K$. For the reasons given in chapter 5 it was considered that the C.W. apparatus already existing in the laboratory was unsuitable for the measurement of T_1. Hence the pulse spectrometer described in chapter 6 was built and used.

Spin-lattice relaxation measurements were recorded from a sample of solid ethylene and it was found that the results differed from those previously recorded by C.W. techniques. The theory of relaxation developed in chapter 4 was then applied to ethylene, as this molecule possesses a diad axis. Good agreement was obtained between experiment and theory and a strong intermolecular contribution to the spin-lattice relaxation interaction was predicted. Evidence in favour of correlated motion of the ethylene molecules is also presented in chapter 7.

Examination of the molecular motion occurring in the chlorinated ethylenes provided further evidence for the correctness of the theory developed in chapter 4. From the measurements on pure samples and diluted samples a weak intermolecular contribution to the proton spin-lattice relaxation interaction is predicted for the chlorinated ethylenes.

10. APPENDICES

```
C          PROGRAMME 1
           SUBROUTINE PPQAD(A,XR1,XR2,XI)
C          SOLUTION OF THE QUADRATIC EQUATION
C          A(1)*X*X+A(2)*X+A(3)=0.
C
           DIMENSION A(3)
           X1 = -A(2)/(2.*A(1))
           DISC = X1*X1-A(3)/A(1)
           IF(DISC)   10,20,20
        10 X2=SQRTF(-DISC)
           XR1=X1
           XR2=X1
           XI=X2
           GO TO 30
        20 X2=SQRTF(DISC)
           XR1=X1+X2
           XR2=X1-X2
           XI=0
        30 RETURN
           END
```

```
C         PROGRAMME 2
          SUBROUTINE PPCUB(A,XR,XI)
C         SOLUTION OF CUBIC EQUATION
C         A(1)*X**3+A(2)*X**2+A(3)*X+A(4)=0.
C
          DIMENSION A(4),XR(3),AQ(3)
          IPATH=2
          EX=1./3.
          IF (A(4)) 1006,1004,1006
     1004 XR(1)=0.
          GO TO 1034
     1006 A2=A(1)*A(1)
          Q=(27.*A2*A(4)-9.*A(1)*A(2)*A(3)+2.*A(2)**3)/(54.*A2*A(1))
          IF (Q) 1010,1008,1014
     1008 Z=0
          GO TO 1032
     1010 Q=-Q
          IPATH=1
     1014 P=(3.*A(1)*A(3)-A(2)*A(2))/(9.*A2)
          ARG=P*P*P+Q*Q
          IF (ARG) 1016,1018,1020
     1016 Z=-2.*Q**EX
          GO TO 1028
     1020 SARG=SQRTF(ARG)
          IF (P) 1022,1024,1026
     1022 Z=-(Q+SARG)**EX-(Q-SARG)**EX
          GO TO 1028
     1024 Z=-(2.*Q)**EX
          GO TO 1028
     1026 Z=(SARG-Q)**EX-(SARG+Q)**EX
     1028 GO TO (1030,1032), IPATH
     1030 Z=-Z
     1032 XR(1)=(3.*A(1)*Z-A(2))/(3.*A(1))
     1034 AQ(1)=A(1)
          AQ(2)=A(2)+XR(1)*A(1)
          AQ(3)=A(3)+XR(1)*AQ(2)
          CALL PPQAD(AQ,XR(2),XR(3),XI)
          RETURN
          END
```

APPENDIX 1 - COMPUTER PROGRAMMES

The completion of the theoretical calculations in this thesis would have been impossible without the aid of the I.B.M. 1620 digital computer at the University's Computing Laboratory. The input to this computer is by means of either punched card decks or discs, and the output can be punched on to cards, printed, or plotted using an X-Y recorder. A few of the programmes used are listed below in Fortran IID language together with a brief description of each programme. The programmes listed are confined to those required for the spin-lattice relaxation calculations described in previous chapters.

Programmes 1 and 2

A number of basic subroutines are compiled automatically by the computer, when called by a statement containing the name of the function e.g. SQRTF(DELTA) is the statement to calculate the square root of the quantity DELTA. These are called relocatable subroutines. Two non-relocatable subroutines which are required in later programmes are listed here for completeness although they are not original work[131].

Programme 1 is a subroutine to compute the roots of a quadratic equation, while programme 2 computes the roots of a cubic equation. Full details of these programmes can be found in reference[131].

```
C         PROGRAMME 3
*FANDK    1105
C         J.PAGE   TUNNELING CALCULATIONS   ETHYLENE
          PRINT 92
          DIMENSION EF0(32),D04(32),EF1(32),D12(32),
         1 D14(32),D(32),E2(32),F2(32),E4(32),F4(32),A(32),BE(17),
         2B(34),B0(17),DB(17),F(17),EAV(17),EAVK(17)
          H=6.62554/10.**27
          PHI=3.14159265
          PHIQ=SQRTF(PHI)
          BK=1.38054/10.**16
          PHI2=PHI**2
          HB=H/(2.*PHI)
          HB2=HB**2
        1 READ 91,BAR
          ERT=5.644/10.**40
          S=2.*ERT*BAR/HB2
          RTS=SQRTF(S)
          XP=EXPF(-2.*RTS)
          A1=H/(4.*PHI2*ERT)
          S1=A1*XP/PHIQ
          B1=HB2/(4.*ERT)
          PRINT 93, BAR
          DO 10 I=1,31
          READ 95,EF0(I)D02(I),D04(I),EF1(I),D12(I),D14(I),
         1D(I),E2(I),F2(I),E4(I),F4(I)
       10 CONTINUE
          PRINT 97
          DO 20 I=1,31
          A(I)=1.-D(I)
          B(I)=A(I)*EF0(I)+D(I)*EF1(I)+E2(I)*D02(I)+F2(I)*D12(I)+
         1E4(I)*D04(I)+F4(I)*D14(I)
         C*D04(I)+F4(I)*D14(I)
       20 CONTINUE
          B0(1)=0.00
          DO 30  I=1.16
       30 BE(I)=B(I)
          DO 40  I=2,17,1
       40 B0(I)=B(I+15)
          DO 50  I=1,15
          DB(I)=B0(I+1)-BE(I)
          F(I)=DB(I)*A1
          P=2*I-1
          C=2.*P*RTS
          EAV(I)=(B0(I+1)+BE(I)+C)*B1
          EAVK(I)=EAV(I)/BK
       50 PRINT 94,BE(I),B0(I),F(I),EAV(I),EAVK(I)
          PRINT 94,BE(16),B0(16)
C         CONTINUED
```

```
C       PROGRAMME 3 CONTINUED -
        F(1)=0016.*S1*(S**0.75)*(1.-(0.43/RTS)-(0.19/S))
        F(2)=0128.*S1*(S**1.25)*(1.-(1.58/RTS)-(0.86/S))
        F(3)=00512.*S1*(S**1.75)*(1.-(3.55/RTS)+(0.65/S))
        F(4)=4096.*S1*(S**2.25)*(1.-(6.30/RTS)+(7.50/S))/3.
        PRINT 98
        DO 60 I=1,4
   60   PRINT 99.F(I)
        PRINT 97
        T1=5.
   80   SNUM=0
        SDEN=0
        T=1000./T1
        DO 70 I=1,15
        EAV(I)=EAVK(I)/T
        X=EAV(I)
        IF (X-227.) 159,160,160
  159   Y=EXPF(X)
        GO TO 162
  160   X=EAV(I)/10.
        IF (X-227.) 163,70,70
  163   W=EXPF(X)
        U=W*W*W
        Y=U*U*U*W
  162   SNUM=SNUM+F(I)/Y
        SDEN=SDEN +1./Y
   70   CONTINUE
        TUNF=SNUM/SDEN
        TUNF1=0.4343*LOGF(TUNF)
        PRINT 101,T1,T,TUNF,TUNF1
        T1=T1+2.5
        IF (100.-T1) 81,81,80
   81   CONTINUE
        PRINT 97
        GO TO 1
   91   FORMAT(E13.7)
   92   FORMAT (5X,42HJ.PAGE    TUNNELING CALCULATIONS  ETHYLENE)
   93   FORMAT (/10X,17HBARRIER HEIGHT = ,E14.7/)
   94   FORMAT (3X,F13.8,5X,F13.8,5X,E10.3,5X,E12.5,5X,E12.5)
   95   FORMAT (F13.8,2F10.8/F13.8,2F10.8/F4.2,4F12.10)
   96   FORMAT (8X,F13.8,2F10.8/8X,F13.8,2F10.8/8X,F4.2,4F12.10)
   97   FORMAT (///)
   98   FORMAT (//8X,20HGOLDSTEIN SPLITTINGS/)
   99   FORMAT (8X,E10.3)
  101   FORMAT (5X,F6.1,3X,F7.2,3X,E12.3,3X,F8.4)
    2   CALL EXIT
        END
```

Programme 3

The theory of section 4.4 is used in this programme to evaluate the quantum mechanical tunnelling frequency as a function of temperature, for ethylene, at different barrier heights.

The input includes the value of the barrier height together with the corresponding $B_{em}(S)$ and $B_{om}(S)$ values (related to $b_{em}(S)$ and $b_{om}(S)$ of equation 4.29) from tables[47] of Mathieu functions. Second and fourth differences are used in interpolation calculations to calculate the required set of $b_{em}(S)$ and $b_{om}(S)$ and hence the energy EAV(I) of each level, and the energy difference F(I) in frequency units between levels. For the first three sets of levels the Goldstein equation 4.30 is used to find the splittings because the accuracy of the tables is insufficient. The average tunnelling frequency $\bar{\nu}_t$ (represented by TUNF in the computer programme) of equation 4.31 is then calculated and printed for temperatures from 200°K to approximately 6°K. A point worth noting in this part of the calculations is the inclusion of IF statements to avoid overload in the exponential term. A new set of input data for a different barrier height is then read and the calculations repeated.

The computations were performed for barrier heights of 2, 2.5 and 3 kcal/mole and the results used to plot figure 4.

Programmes 4 and 5

Programme 5, which requires programme 4 as a function subroutine,

```
C       PROGRAMME 4
C       SUBROUTINE PPF(X,Y)
        FUNCTION PPF(X,Y)
        COMMON JBRAN,PSI,R1,R2
        R13=R1**3
        R23=R2**3
        R16=R13*R13
        R26=R23*R23
        R123=R13*R23
        S=SINF(PSI)
        S2=S*S
        C=COSF(PSI)
        C2=C*C
        X2=X*X
        Z=COSF(Y)
        Z2=Z*Z
        V=SINF(Y)
        V2=V*V
        SX2=1.-X2
        SX=SQRTF(SX2)
        A=X2*V2*S2
        B=SX2*C2
        C1=Z2*S2
        SNUM=-A+B-C1
        D=A+B+C1
        E=2.*SX*X*V*S*C
        DEN=SQRTF((D-E)*(D+E))
        CPHI=SNUM/DEN
        A1=SX*V*S
        B1=X*C
        CETA1=A1+B1
        CETA2=-A1+B1
        GO TO (100,200),JBRAN
  100   SETA1=SQRTF(1.-CETA1*CETA1)
        SETA2=SQRTF(1.-CETA2*CETA2)
        SC1=SETA1*CETA1
        SC2=SETA2*CETA2
        SC12=(SC1*SC1)/R16
        SC22=(SC2*SC2)/R26
        G=2.*SC1*SC2*CPHI/R123
        PPF=(SC12+SC22-G)*0.25
        RETURN
  200   A3=1.-CETA1*CETA1
        A4=1.-CETA2*CETA2
        A5=A3*A3/R16
        A6=A4*A4/R26
        CPHI2=CPHI*CPHI
        A7=2.*CPHI2-1.
        A34=2.*A3*A4/R123
        A8=A34*A7
        PPF=(A5+A6-A8)*0.25
        RETURN
        END
```

```
C       PROGRAMME 5
C       AVERAGE OF RELAXATION POSITION FUNCTIONS
C             OVER A SPHERE
        DIMENSION SUMM(3)
        COMMON JBRAN,PSI,R1,R2
      5 PRINT 990
        READ 999, NUMX, NUMY, XA, XB, YA, YB
        PRINT 998,            XA, XB, YA, YB
        PRINT 993
        JBRAN=1
      6 READ 995,R1,R2
      1 PRINT 994,R1,R2,PSI
      4 DO 200 K = 1,3
        GO TO (2,7,7),K
      2 PRINT 989
      7 NUMMX=NUMX*K
        NUMMX = NUMX*K
        NUMMY = NUMY*K
        XSTRIP = 2*NUMMX
        YSTRIP = 2*NUMMY
        XH = (XB - XA)/XSTRIP
        YH = (YB - YA)/YSTRIP
        SUM = 0.
        X1 = XA
        X2 = X1 + XH
        X3 = X2 + XH
        DO 100 I = 1,NUMMX
        Y1 = YA
        Y2 = Y1 + YH
        Y3 = Y2 + YH
        F1=PPF(X1,Y1)
        F2=PPF(X2,Y1)
        F3=PPF(X3,Y1)
        DO 80 J = 1,NUMMY
        F4=PPF(X1,Y2)
        F5=PPF(X2,Y2)
        F6=PPF(X3,Y2)
        F7=PPF(X1,Y3)
        F8=PPF(X2,Y3)
        F9=PPF(X3,Y3)
        SUM=SUM+XH*YH/9.*(F1+F3+F7+F9+4.*(F2+F4+F6+F8)+16.*F5)
C       CONTINUED
```

```
C         PROGRAMME 5 CONTINUED
          F1 = F7
          F2 = F8
          F3 = F9
          Y2 = Y3 + YH
       80 Y3 = Y2 + YH
          X1 = X3
          X2 = X1 + XH
      100 X3 = X2 + XH
          PRINT 997, K, XH, YH, SUM
      200 SUMM(K) = SUM
C
C         RICHARDSON EXTRAPOLATIONS
          EXTR21 = (16.*SUMM(2) - SUMM(1))/15.
          EXTR31 = (81.*SUMM(3) - SUMM(1))/80.
          EXTR32 = (81.*SUMM(3) - 16.*SUMM(2))/65.
          TIN=EXTR32/(4.*3.14159)
          PRINT 996, EXTR21, EXTR31, EXTR32
          PRINT 992,JBRAN,TIN
          GO TO 6
          PRINT 993
      989 FORMAT (17X,1HK 6X, 2HXH 8X, 2HYH 8X,8HINTEGRAL)
      990 FORMAT(5X,38HJ.L.PAGE  RELAXATION FUNCTION AVERAGES)
      992 FORMAT(5X,8HJBRAN = ,I3,6X,10HAVERAGE = ,E14.7)
      993 FORMAT(///)
      994 FORMAT(5X,5HR1 = ,F7.4,10H ANGSTROMS,5X,5HR2 = ,F7.4,
         1 10H ANGSTROMS,5X,6HPSI = ,F7.4,8H RADIANS)
      995 FORMAT (3F7.4)
      996 FORMAT (/ 19X, 19HEXTRAPOLATION 2,1 = E14.7 /
         1 33X, 5H3,1 = E14.7 / 33X, 5H3,2 = E14.7 )
      997 FORMAT (I18, 2F10.5, E17.7)
      998 FORMAT (25X,21HLIMITS OF INTEGRATION/16X,4HXA = E14.7,
         14X,4HXB = E14.7/16X,4HYA = E14.7,4X,4HYB = E14.7)
      999 FORMAT (2I5/4E13.8)
        9 CALL EXIT
          END
```

was used to calculate the average of the relaxation position functions over a sphere using Simpson's rule and a Richardson extrapolation[131]. The value of the parameter JBRAN determines which relaxation position function is to be averaged e.g.

if JBRAN = 1

$$\text{then PPF} = \frac{1}{4}\left[(r_{ij}^{\alpha})^{-6}\sin^2\theta_{ij}^{\alpha}\cos^2\theta_{ij}^{\alpha} + (r_{ij}^{\beta})^{-6}\sin^2\theta_{ij}^{\beta}\cos^2\theta_{ij}^{\beta} - 2(r_{ij}^{\alpha})^{-3}(r_{ij}^{\beta})^{-3}\sin\theta_{ij}^{\alpha}\cos\theta_{ij}^{\alpha}\sin\theta_{ij}^{\beta}\cos\theta_{ij}^{\beta}\cos(\Phi_{ij}^{\alpha} - \Phi_{ij}^{\beta})\right]$$

if JBRAN = 2

$$\text{then PPF} = \frac{1}{4}\left[(r_{ij}^{\alpha})^{-6}\sin^4\theta_{ij}^{\alpha} + (r_{ij}^{\beta})^{-6}\sin^4\theta_{ij}^{\beta} - 2(r_{ij}^{\alpha})^{-3}(r_{ij}^{\beta})^{-3} \times \sin^2\theta_{ij}^{\alpha}\sin^2\theta_{ij}^{\beta}\cos 2(\Phi_{ij}^{\alpha} - \Phi_{ij}^{\beta})\right]$$

where θ_{ij} and Φ_{ij} are the polar and azimuthal angles with respect to H_o as the Z axis, of the internuclear vector between nuclei i and j. These functions are expressed in terms of ψ_{ij}, see figure 1, and the variables X and Y where X equals $\cos\theta$ and Y equals Φ using

$$\cos\theta_{ij}^{\alpha} = \sin\theta\sin\Phi\sin\psi_{ij} + \cos\theta\cos\psi_{ij}$$

$$\cos\theta_{ij}^{\beta} = -\sin\theta\sin\Phi\sin\psi_{ij} + \cos\theta\cos\psi_{ij}$$

where θ and Φ are the spherical coordinates of the magnetic field H_o with respect to the crystal axes. The values of r_{ij}^{α}, r_{ij}^{β} and ψ_{ij} calculated from the lattice structure by means of a separate computer

```
C       PROGRAMME 6
C       J.L.PAGE  CALCULATION OF T1 BY 2ND METHOD
        DIMENSION XA(150),YA(150),ZA(150),XB(150),
       1YB(150),ZB(150),XTA(150),YTA(150),ZTA(150)
       2,XTB(150),YTB(150),ZTB(150)
        PRINT 33
        PRINT 22
        READ 1,N
        DO 4 I=1,N
        READ  2,XA(I),YA(I),ZA(I),XB(I),YB(I),ZB(I)
        PRINT 3,XA(I),YA(I),ZA(I),XB(I),YB(I),ZB(I)
    4 CONTINUE
        PRINT 22
   12 READ 11,THETA
        PHI =0.
   15 A =0.
        B =0.
        AC=0.
        BC=0.
        CA=COSF(THETA)
        CI=COSF(PHI)
        SA=SINF(THETA)
        SI=SINF(PHI)
        SC=SA*CI
        CC=CA*CI
        CS=CA*SI
        SS=SA*SI
        PRINT 13,THETA,PHI
        CON=180./3.1416
        HP=CON*PHI
        THET=CON*THETA
        PRINT 16,THET,HP
C       TRANSFORMATION TO HO AS Z
        DO 5 I=1,N
        XTA(I)=CC*XA(I)+CS*YA(I)-SA*ZA(I)
        XTB(I)=CC*XB(I)+CS*YB(I)-SA*ZB(I)
        YTA(I)=-SI*XA(I)+CI*YA(I)
        YTB(I)=-SI*XB(I)+CI*YB(I)
        ZTA(I)=SC*XA(I)+SS*YA(I)+CA*ZA(I)
        ZTB(I)=SC*XB(I)+SS*YB(I)+CA*ZB(I)
    5 CONTINUE
C       FINDING INTERPROTON VECTORS
        DO 6 I=3,N
        CALL PPINV(XTA(1),YTA(1),ZTA(1),XTA(I),YTA(I),ZTA(I),
       1XE,YE,ZE)
        CALL PPINV(XTA(1),YTA(1),ZTA(1),XTB(I),YTB(I),ZTB(I),
       1XF,YF,ZF)
        CALL PPINV(XTB(1),YTB(1),ZTB(1),XTB(I),YTB(I),ZTB(I),
       1XC,YC,ZC)
        CALL PPINV(XTB(1),YTB(1),ZTB(1),XTA(I),YTA(I),ZTA(I),
       1XD,YD,ZD)
C       CONTINUED
```

```
C       PROGRAMME 6 CONTINUED
        CALL PPRP(XE,YE,ZE,XF,YF,ZF,A1,B1)
        CALL PPRP(XE,YE,ZE,XC,YC,ZC,A2,B2)
        CALL PPRP(XF,YF,ZF,XD,YD,ZD,A3,B3)
C       NON COHERENT EFFECT
        A=A+A1*2.
        B=B+B1*2.
C       COHERENT EFFECT
        AC=AC+A2+A3
        BC=BC+B2+B3
      6 CONTINUE
        PRINT 9,A,B
        PRINT 9,AC,BC
C       INTRAMOLECULAR CONTRIBUTION
        CALL PPINV(XTA(1),YTA(1),ZTA(1),XTB(2),YTB(2),ZTB(2),
       1X1,Y1,Z1)
        CALL PPINV(XTB(1),YTB(1),ZTB(1),XTA(2),YTA(2),ZTA(2),
       1X2,Y2,Z2)
        CALL PPRP(X1,Y1,Z1,X2,Y2,Z2,A1,B1)
        PRINI 9,A1,B1
        A=A+A1
        B=B+B1
        PRINT 9,A,B
        AC=AC+A1
        BC=BC+B1
        PRINT 9,AC,BC
C       CALCULATION OF T1
        CALL PPTMIN(A,B,TM4)
        PRINT 7,TM4
        CALL PPTMIN(AC,BC,TMC)
        PRINT 7,TMC
        PUNCH 17,THETA,PHI,AC,BC,TM4,TMC
        PRINT 22
     32 PHI=PHI+0.1745
        IF (6.2832-PHI) 12,15,15
      1 FORMAT (I4)
      2 FORMAT (6F7.4)
      3 FORMAT (6F9.4)
      7 FORMAT (2X,E13.3)
      9 FORMAT (3X,E11.4,3X,E11.4)
     11 FORMAT (F7.4)
     13 FORMAT (3X,F6.3,3X,F6.3)
     16 FORMAT (2X,8HTHETA = ,F6.1,5X,6HPHI = ,F6.1)
     17 FORMAT (F7.4,F7.4,E11.4,E11.4,E13.3,E13.3)
     22 FORMAT (//)
     33 FORMAT (3X,32HJ.L.PAGE T1 BY 2ND METHOD JEENER)
     50 FORMAT (1H1)
     51 FORMAT (1H ,9E13.3)
     14 CALL EXIT
        END
```

```
C       PROGRAMME 7
        SUBROUTINE PPINV(X1,Y1,Z1,X2,Y2,Z2,X3,Y3,Z3)
        X3=X2-X1
        Y3=Y2-Y1
        Z3=Z2-Z1
        RETURN
        END


C       PROGRAMME 8
        SUBROUTINE PPTMIN(A,B,TM4)
        DIMENSION C(4),X(3),XI(3)
        C(1)=16.*A+4.*B
        C(2)=-(8.*A-7.*B)
        C(3)=-(7.*A-2.*B)
        C(4)=-(A+B)
        CALL PPCUB(C,X,XI(2))
        D=X(1)
        E1=A/(1.+D)
        E2=B/(1.+4.*D)
        TM=(E1+E2)*SQRTF(D)
        TM3=TM*0.8017*(10.**4)
        TM4=1./TM3
        RETURN
        END
```

```
C       PROGRAMME 9
        SUBROUTINE PPRP(X1,Y1,Z1,X2,Y2,Z2,A,B)
        X12=X1*X1
        X22=X2*X2
        Y12=Y1*Y1
        Y22=Y2*Y2
        Z12=Z1*Z1
        Z22=Z2*Z2
        XY12=X12+Y12
        XY22=X22+Y22
        DEN=SQRTF(XY12*XY22)
C       INTERPROTON DISTANCES
        R12=XY12+Z12
        R22=XY22+Z22
        R1=SQRTF(R12)
        R13=R12*R1
        R16=R13*R13
        R2=SQRTF(R22)
        R23=R22*R2
        R26=R23*R23
        R1323=R13*R23
C       ANGULAR FACTORS
        C1=Z1/R1
        C12=C1*C1
        S12=1.-C12
        S1=SQRTF(S12)
        S14=S12*S12
        C2=Z2/R2
        C22=C2*C2
        S22=1.-C22
        S2=SQRTF(S22)
        S24=S22*S22
        DCPH=(X1*X2+Y1*Y2)/DEN
        DCP2=DCPH*DCPH
        A1=S12*C12/R16
        A2=S22*C22/R26
        A3=2.*S1*C1*S2*C2*DCPH/R1323
        A=(A1+A2-A3)*0.25
        B1=S14/R16
        B2=S24/R26
        B3=2.*S12*S22*(2.*DCP2-1.)/R1323
        B=(B1+B2-B3)*0.25
        RETURN
        END
```

programme, are read into the programme as the parameters R1, R2 and PSII.

The limits of integration are set by XA, XB and YA, YB while the mesh size, which is adjusted for the accuracy required, is determined by NUMX and NUMY. The values of the relaxation function averages thus obtained were then substituted into equation 4.25 and $T_{1(min)}$ calculated.

Programmes 6, 7, 8 and 9

Programmes 6, 7, 8 and 9 were used to compute $T_{1(min)}$ (corr) and $T_{1(min)}$ (uncorr) as a function of the magnetic field direction, $H(\theta,\Phi)$, by method (B) of section 7.4.1 from the coordinates of the protons of the ethylene lattice. After the coordinates of all the proton pairs followed by a value of θ (THETA) have been read into the computer the value of Φ (PHI) is taken as zero, and these values used to transform the proton coordinates into a reference frame which has H_o as the Z axis. Subroutine PPINV (Programme 7) which simply subtracts the appropriate components of two vectors is then used to calculate the components of the two possible internuclear vectors of the intermolecular effect for correlated and uncorrelated motion. Subroutine PPRP (Programme 9) then uses the components of these internuclear vectors to evaluate the averages of the relaxation position functions. These calculations are repeated for all the protons under consideration and the resulting averages added to find

the total contributions to the relaxation position functions averages. The intramolecular effect is then calculated in a similar manner and its contributions added to those of the intermolecular effect and the contributions used by subroutine PPTMIN, (Programme 8) to evaluate $T_{1(min)}$ for correlated and uncorrelated motion. The programme is designed to repeat these calculations for $T_{1(min)}$ values of θ from 0^{o} to 90^{o} in 5^{o} increments and ϕ from 0^{o} to 360^{o} in 10^{o} increments.

APPENDIX 2 - ELECTRONIC COMPONENTS

Figure 6: Pulse Shaper

V1	ECC83	V2	ECC83
D1	OA81		
R1	33KΩ	R2	500KΩ
R3	100KΩ	R4	33KΩ
R5	10KΩ	R6	100KΩ
R7	10KΩ		
C1	50pF	C2	50pF
C3	0.01μF		

Figure 7: Cathode Follower Mixer and Oscillator

V1, V2	ECC82	V3, V4	QQV06-40A
R1	680KΩ	R2	680KΩ
R3	3KΩ	R4	10KΩ
R5	5KΩ	R6	20Ω
R7	67Ω	R8	20Ω
R9	20Ω	R10	67Ω
C1	0.008μF	C2	0.008μF
C3	0.008μF	C4	100pF
C5	4-20pF	C6	4-20pF
C7	0.05μF	C8	100pF

Figure 8: Intermediate Amplifier

V1	QQV06-40A	V2	QQV06-40A
R1	10KΩ 5W	R2	10KΩ 3W
R3	30Ω	R4	30Ω
R5	10Ω	R6	10Ω
R7	100Ω	R8	100Ω
R9	100Ω	R10	100Ω
R11	10Ω	R12	10Ω
R13	20Ω	R14	20Ω
R15	10KΩ		
C1	25-250pF	C2	25-250pF
C3	5-25pF	C4	5-25pF
C5	0.5μF	C6	100pF
C7	3-10pF	C8	3-10pF
C9	0.1μF	C10	6000pF
C11	0.1μF	C12	100pF

Figure 9: Final Amplifier

V1	3E29	V2	3E29
R1	10KΩ 3W	R2	10KΩ 10W
R3	10KΩ 10W	R4	33Ω
R5	33Ω	R6	10Ω
R7	10Ω	R8	10Ω
R9	10Ω	R10	10Ω
R11	10Ω	R12	10Ω
R13	10Ω	R14	10Ω
R15	10Ω	R16	2.9KΩ
C1	10-252pF	C2	10-252pF
C3	5-27pF	C4	0.1μF
C5	450pF	C6	4-13.5pF
C7	4-13.5pF	C8	0.1μF
C9	2500pF	C10	0.1μF
C11	500pF		

Figure 10: Preamplifier

V1	A2599	V2	A2521
D1	OA5	D2	OA5
R1	3.3KΩ	R2	180Ω
R3	68Ω	R4	68Ω
R5	3.3KΩ	R6	180Ω
R7	10KΩ		
C1	2μF electrolytic	C2	1000pF
C3	1000pF	C4	1000pF
C5	1000pF	C6	1000pF
C7	2μF electrolytic	C8	1000pF
C9	1000pF		

Figure 11: Local Oscillator and Mixer

R8	10KΩ	R9	33KΩ
R10	10KΩ	R11	2KΩ
R12	180Ω		
C12	1000pF	C13	2-12pF
C14	6pF	C15	10pF
C16	1.8pF	C17	1000pF
C18	2μF electrolytic	C19	1000pF
C20	240pF	C21	1000pF
C22	2-18pF		

Figure 12: I.F. Amplifier

V1	EF95	V2	EF95
V3	EF95	V4	EF95
V5	EF95	V6	EF95
R1	220Ω	R2	100Ω
R3	1.2KΩ	R4	1.2KΩ
R5	220Ω	R6	100Ω
R7	10KΩ	R8	10KΩ
R9	1KΩ	R10	1.2KΩ
R11	220Ω	R12	100Ω
R13	1.2KΩ	R14	220Ω
R15	100Ω	R16	10Ω
R17	220Ω	R18	1.2KΩ
R19	75Ω	R20	10KΩ
R21	100Ω		
C1	2.2pF	C2	3.5pF
C3	3pF	C4	1000pF
C5	1000pF	C6	1000pF
C7	3pF	C8	1000pF
C9	1000pF	C10	1000pF
C11	1000pF	C12	1000pF
C13	1000pF	C14	1000pF
C15	1000pF	C16	1000pF
C17	1000pF	C18	1000pF
C19	1000pF	C20	1000pF
C21	1000pF	C22	1000pF
C23	1000pF	C24	1000pF
C25	5.6pF	C26	5.6pF

Figure 13: Video Amplifier

V1	ECC88	V2	ECC88
D1	OA81	D2	OAZ207
R1	100Ω	R2	300KΩ
R3	560Ω	R4	1.1KΩ
R5	2.7KΩ	R6	56Ω
R7	750Ω	R8	50KΩ
R9	30KΩ		
C1	200pF	C2	200pF
C3	0.01μF	C4	10μF electrolytic
C5	20pF	C6	10pF
C7	300pF	C8	0.001pF
C9	0.003μF	C10	0.01μF
C11	1μF electrolytic		

REFERENCES

REFERENCES

1. F. Bloch, W. W. Hansen and M. E. Packard (1946) Phys. Rev. 69, 127.

2. E. M. Purcell, H. C. Torrey and R. V. Pound (1946) Phys. Rev. 69, 37.

3. A. Einstein (1917) Phys. Z. 18, 121.

4. E. R. Andrew (1955) Nuclear Magnetic Resonance (Cambridge University Press).

5. G. E. Pake (1956) Solid State Physics 2, 1.

6. A. Abragam (1961) The Principles of Nuclear Magnetism (O.U.P.).

7. C. P. Slichter (1963) Principles of Magnetic Resonance (Harper and Row, New York).

8. F. Bloch (1946) Phys. Rev. 70, 460.

9. A. G. Redfield (1955) Phys. Rev. 98, 1787.

10. G. E. Pake (1948) J. Chem. Phys. 16, 327.

11. E. R. Andrew and R. Bersohn (1950) J. Chem. Phys. 18, 159; 20, 924.

12. E. R. Andrew and N. D. Finch (1957) Proc. Phys. Soc. 70, 980.

13. J. Itoh, R. Kusaka, Y. Yamagata, R. Kiriyama and H. Ibamato (1953) J. Phys. Soc. Japan 8, 293.

14. R. Bersohn and H. S. Gutowsky (1954) J. Chem. Phys. 22, 651.

15. J. H. Van Vleck (1948) Phys. Rev. 74, 1168.

16. H. S. Gutowsky and G. E. Pake (1950) J. Chem. Phys. 18, 162.

17. Reference 6, p. 453.

18. R. G. Eades (1952) Thesis, St. Andrews University.

19. E. R. Andrew (1950) J. Chem. Phys. 18, 607.

20. T. P. Das (1957) J. Chem. Phys. 27, 763.

21. J. Jeener and P. Broekaert (1967) Phys. Rev. 157, 232.

22. L. C. Hebel and C. P. Slichter (1959) Phys. Rev. 113, 1504.

23. D. C. Look and I. J. Lowe (1966) J. Chem. Phys. 44, 2995.

24. C. J. Gorter (1940) Phys. Rev. 57, 426.

25. D. F. Holcomb and B. Pedersen (1962) J. Chem. Phys. 36, 3270.

26. Reference 6, p. 272.

27. Reference 7, p. 136.

28. Reference 7, p. 52.

29. E. Ambler, J. C. Einstein and J. F. Schooley (1962) J. Math. Phys. 3, 118, 760.

30. A. G. Redfield (1957) I.B.M. Journal 1, 19.

31. Reference 7, p. 148.

32. R. L. Hilt and P. S. Hubbard (1964) Phys. Rev. 134, A392.

33. Reference 6, p. 271.

34. R. Kubo and K. Tomita (1954) J. Phys. Soc. Japan 9, 888.

35. I. Solomon (1955) Phys. Rev. 99, 559.

36. N. Bloembergen, E. M. Purcell and R. V. Pound (1948) Phys. Rev. 73, 679.

37. Reference 7, p. 230.

38. Reference 6, p. 297.

39. M. J. R. Hoch and F. A. Rushworth (1964) Phys. Letters 12, 292.

40. M. J. R. Hoch (1963) Thesis, St. Andrews University.

41. J. G. Powles and H. S. Gutowsky (1955) J. Chem. Phys. 23, 1692.

42. E. O. Stejskal and H. S. Gutowsky (1958) J. Chem. Phys. 28, 388.

43. T. P. Das (1956) J. Chem. Phys. 25, 896.

44. G. Herzberg (1945) Infrared and Raman Spectra of Polyatomic Molecules (D. Van Nostrand).

45. K. S. Pitzer and J. L. Hollenberg (1953) J. Am. Chem. Soc. 75, 2219.

46. Tables Relating to Mathieu Functions (1951) (Columbia University Press, N.Y.).

47. G. Blanch and I. Rhodes (1955) J. Wash. Acad. Sci. 45, 166.

48. H. Eyring, J. Walter and G. E. Kimball (1944) Quantum Chemistry (Wiley).

49. S. Goldstein (1929) Proc. Roy. Soc. Edin. 49, 210.

50. J. H. Freed (1965) J. Chem. Phys. 43, 1710.

51. E. O. Stejskal, D. E. Woessner, T. C. Farrar and H. S. Gutowsky (1959) J. Chem. Phys. 31, 55.

52. J. G. Powles and H. S. Gutowsky (1953) J. Chem. Phys. 21, 1695.

53. R. G. Eades, N. D. Finch and Z. M. El Saffar (1959) Archives des Sciences 12, 109.

54. E. R. Andrew, R. G. Eades, Z. M. El Saffar and J. P. Llewellyn (1960) Bulletin Ampere 9e, 379.

55. E. R. Andrew and P. S. Allen (1966) J. Chim. Phys. 1, 85.

56. R. G. Eades, G. P. Jones, J. P. Llewellyn and K. W. Terry (1967) Proc. Phys. Soc. 91, 124.

57. R. G. Eades, T. A. Jones and J. P. Llewellyn (1967) Proc. Phys. Soc. 91, 632.

58. J. S. Waugh and E. I. Fedin (1963) Soviet Physics - Solid State, 4, 1633.

59. R. G. Eades (1965) Private communication.

60. E. R. Andrew (1967) Private communication.

61. N. Bloembergen (1949) Physica 15, 386.

62. C. M. Verber, H. P. Mahon and W. H. Tantilla (1962) Phys. Rev. 125, 1149.

63. S. M. Day, G. B. Grimes and W. Weatherford (1965) Phys. Rev. 139, A515.

64. J. G. Powles and K. Luszczuski (1959) Physica 25, 455.

65. T. M. Connor (1964) Trans. Faraday Soc. 60, 1574.

66. D. W. McCall, D. C. Douglass and E. W. Anderson (1959) J. Chem. Phys. 30, 1272.

67. E. L. Hahn (1950) Phys. Rev. 80, 580.

68. Reference 6, p. 21.

69. Reference 6, p. 33.

70. A. Narath and D. W. Alderman (1966) Phys. Rev. 143, 328.

71. W. W. Simmons, W. J. O'Sullivan and W. A. Robinson (1962) Phys. Rev. 127, 1168.

72. Reference 4, p. 20.

73. E. R. Andrew, K. M. Swanson and B. R. Williams (1961) Proc. Phys. Soc. 77, 36.

74. J. E. Anderson and K. J. Liu (1966) J. Chem. Phys. 4744.

75. N. Bloembergen (1948) Nuclear Magnetic Relaxation (M. Nijhoff, The Hague).

76. M. Goldman (1964) Le Journal de Physique 25, 843.

77. G. P. Jones (1963) Thesis, University College of North Wales, Bangor.

78. P. Mansfield and J. G. Powles (1963) J. Sci. Inst. 40, 232.

79. W. G. Clark (1964) Rev. Sci. Inst. 35, 316.

80. R. K. Mazitov and V. I. Ionov (1965) Pribory i Teknika Exsperimenta 3, 142.

81. J. Czech (1965) Oscilloscope Measuring Technique (Philips Technical Library).

82. G. P. Jones, D. C. Douglass and D. W. McCall (1965) Rev. Sci. Inst. 36, 1460.

83. G. E. Wallman, M.I.T. Vacuum Tube Amplifiers, Radiation Lab. Series 18, 329.

84. M.O. Valve Company G.E.C. Design of Low Noise Amplifier using Triode Valves.

85. E. R. Andrew and F. A. Rushworth (1952) Proc. Phys. Soc. B65, 801.

86. F. A. Rushworth (1953) Thesis, St. Andrews University.

87. J. M. Dowling and B. P. Stoicheff (1958) Bull. Am. Phys. Soc. 3, 313; (1959) Can J. Phys. 37, 703.

88. H. C. Allen and E. K. Plyler (1958) J. Am. Chem. Soc. 80, 2673.

89. L. S. Bartell and R. A. Bonham (1957) J. Chem. Phys. 27, 1414.

90. L. S. Bartell, E. A. Roth, C. D. Hollowell, K. Kuchitsu and J. E. Young (1965) J. Chem. Phys. 42, 2683.

91. C. W. Bunn (1944) Trans. Faraday Soc. 40, 23.

92. W. H. Keesom and K. W. Taconis (1935) Physica 2, 463.

93. C. I. Brecher (1959) Thesis, Columbia University.

94. C. I. Brecher and R. S. Halford (1961) J. Chem. Phys. 35, 1109.

95. M. E. Jacox (1962) J. Chem. Phys. 36, 140.

96. C. J. Egan and J. D. Kemp (1937) J. Am. Chem. Soc. 59, 1264.

97. S. Todireanu (1967) Phys. Letters 24A, 554.

98. J. G. Powles and R. Figgins (1967) Annalen der Physik 19, 84.

99. J. Jeener (1967) Private communication.

100. D. A. Jennings and W. H. Tantilla (1962) J. Chem. Phys. 37, 1874.

101. J. E. Anderson (1965) J. Chem. Phys. 43, 3575.

102. H. S. Gutowsky, G. B. Kistiakowsky, G. B. Pake and E. M. Purcell (1949) J. Chem. Phys. 17, 972.

103. E. R. Andrew and R. G. Eades (1953) Proc. Roy. Soc. A216, 398; (1953) Proc. Roy. Soc. A218, 537.

104. H. S. Sandu, J. Lees and M. Bloom (1960) J. Chem. 38, 493.

105. J. Lees, B. H. Muller and J. D. Noble (1961) J. Chem. Phys. 34, 341.

106. L. H. Kaplan (1959) Dissertation Abstracts 19, 3130.

107. Interatomic Distances Supplement (1965) (The Chemical Society, London).

108. C. W. W. Hoffman (1958) Dissertation Abstracts 18, 420.

109. S. Sekino and T. Nishikawa (1957) J. Phys. Soc. Japan 12, 43.

110. I. L. Karle and J. Karle (1952) J. Chem. Phys. 20, 63.

111. J. Timmermans (1965) Physico-Chemical Constants of Pure Organic Compounds (Elsevier, Amsterdam).

112. S. E. J. Johnsen and J. W. Fitzpatrick (1951) Rec. Trav. Chim. 70, 823.

113. D. L. Hildenbrand, R. A. McDonald, W. R. Kramer and D. R. Stull (1959) J. Chem. Phys. 30, 930.

114. Handbook of Chemistry and Physics (1966) (The Chemical Rubber Co.)

115. J. G. Powles (1966) B.R.S.G. Conference, University of Kent.

116. H. J. Bernstein and D. A. Ramsay (1949) J. Chem. Phys. 17, 556.

117. T. Shimizu and H. Takuma (1960) J. Phys. Soc. Japan 15, 646.

118. W. H. Flygare and J. A. Howe (1962) J. Chem. Phys. 36, 440.

119. K. S. Pitzer (1940) J. Am. Chem. Soc. 62, 331.

120. A. H. White and S. O. Morgan (1937) J. Chem. Phys. 5, 655.

121. I. Ichishima (1950) J. Chem. Soc. Japan, Pure Chem. Sec. 71, 44.

122. S. Linder (1957) J. Chem. Phys. 26, 900.

123. H. W. Dodgen and J. L. Ragle (1956) J. Chem. Phys. 25, 376.

124. J. L. Ragle (1959) J. Chem. Phys. 63, 1395.

125. T. Tokuhiro (1964) J. Chem. Phys. 41, 438.

126. B. H. Muller and J. F. Harmon (1965) J. Chem. Phys. 43, 18.

127. G. Bonera and A. Rigamonti (1965) J. Chem. Phys. 42, 171.

128. J. G. Powles and R. Figgins (1967) Molecular Physics 13, 253.

129. J. E. Anderson and W. P. Slichter (1966) J. Chem. Phys. 44, 1797.

130. J. E. Anderson and W. P. Slichter (1966) J. Chem. Phys. 44, 3647.

131. J. M. McCormack and M. G. Salvadori (1964) Numerical Methods in Fortan (Prentice-Hall).